UNIVERSIDADE ESTADUAL DE CAMPINAS

INSTITUTO DE BIOLOGIA

JOSE EDWIN NECIOSUP QUESÑAY

“PRODUÇÃO HETERÓLOGA, PURIFICAÇÃO, CARACTERIZAÇÃO FUNCIONAL E PREDIÇÃO ESTRUTURAL DO CARREADOR MITOCONDRIAL DE PIRUVATO HUMANO.”

“HETEROLOGOUS PRODUCTION, PURIFICATION, FUNCTIONAL CHARACTERIZATION, AND STRUCTURAL PREDICTION OF THE HUMAN MITOCHONDRIAL PYRUVATE CARRIER.”

CAMPINAS

2020

JOSE EDWIN NECIOSUP QUESÑAY

“HETEROLOGOUS PRODUCTION, PURIFICATION, FUNCTIONAL CHARACTERIZATION, AND STRUCTURAL PREDICTION OF THE HUMAN MITOCHONDRIAL PYRUVATE CARRIER.”

“PRODUÇÃO HETERÓLOGA, PURIFICAÇÃO, CARACTERIZAÇÃO FUNCIONAL E PREDIÇÃO ESTRUTURAL DO CARREADOR MITOCONDRIAL DE PIRUVATO HUMANO.”

Tese apresentada ao Instituto de Biologia da Universidade Estadual de Campinas como parte dos requisitos exigidos para a obtenção do título de Doutor em ciências, na área de Fármacos, Medicamentos e Insumos para Saúde.

Thesis presented to the Institute of Biology of the University of Campinas in partial fulfillment of the requeriments for the degree of Doctor in Sciences.

Orientador: Dr. Andre Luis Berteli Ambrosio

Este trabalho corresponde a versão da tese defendida pelo aluno José Edwin Neciosup Quesnãy e orientado pelo Prof. Dr. Andre Luis Berteli Ambrosio.

CAMPINAS

2020

Agencia de fomento: FAPESP Processo: 2015/02734-7 2019/02261-2

Ficha catalográfica
Universidade Estadual de Campinas
Biblioteca do Instituto de Biologia
Mara Janaina de Oliveira - CRB 8/6972

N28h

Neciosup Quesñay, José Edwin, 1988-
Heterologous production, purification, functional characterization, and structural prediction of the human mitochondrial pyruvate carrier / José Edwin Neciosup Quesñay. – Campinas, SP : [s.n.], 2020.

Orientador: Andre Luis Berteli Ambrosio.
Tese (doutorado) – Universidade Estadual de Campinas, Instituto de Biologia.

1. Ácido pirúvico. 2. Lipossomas unilamelares. 3. Bioquímica. 4. Microscopia eletrônica de transmissão e varredura. 5. Proteínas de membrana. I. Ambrosio, Andre Luis Berteli. II. Universidade Estadual de Campinas. Instituto de Biologia. III. Título.

Informações para Biblioteca Digital

Título em outro idioma: Produção heteróloga, purificação, caracterização funcional e predição estrutural do carregador mitochondrial de piruvato humano
Palavras-chave em inglês:
Pyruvic acid
Unilamellar liposomes
Biochemistry
Scanning transmission electron microscopy
Membrane proteins
Área de concentração: Fármacos, Medicamentos e Insumos para Saúde
Titulação: Doutor em Ciências
Banca examinadora:
Andre Luis Berteli Ambrosio [Orientador]
Richard Charles Garratt
Maria Cristina Nonato Costa
Shaker Chuck Farah
German Gustavo Sgro
Data de defesa: 18-11-2020
Programa de Pós-Graduação: Biociências e Tecnologia de Produtos Bioativos

Identificação e informações acadêmicas do(a) aluno(a)

-ORCID do autor: https://orcid.org/0000-0002-9161-8871

-Curriculo Lattes do autor: http://lattes.cnpq.br/7487810695070066

Campinas 18 de Novembro de 2020

EXAMINATION COMMITEE

Dr. Andre Luis Berteli Ambrosio

Presidente da Comissão Examinadora

Dr. Richard Charles Garratt

Dra. Maria Cristina Nonato Costa

Dr. Shaker Chuck Farah

Dr. Germán Gustavo Sgro

Os membros da comissão examinadora acima assinaram a Ata de defesa, que se encontra no processo de vida acadêmica do aluno

A Ata da defesa com as respectivas assinaturas dos membros encontra-se no SIGA/Sistema de Fluxo de Dissertação/Tese e na Secretaria do Programa Biociencias e Tecnologia de Produtos Bioativos da Unidade do Instituto de Biologia.

DEDICATION

Dedicate to my parents and siblings

PERSONAL ACKNOWLEDGEMENTS

I am extremely grateful to Dr Andre Ambrosio for the guidance support and principally for the trust he gave me through these 5 years, all advices were fundamental to the evolution of this research and myself.

I would like to express my sincere gratitude to Dr. Richard Garratt, which I met in Peru, for give me the opportunity to meet researchers in Brazil.

To my friends and lab mates, From LNBio, LNNano, IFSC-USP and UoB; Raghavendra Krishna, Zeyaul Islam, Igor Monteze, Angela Fala, Marilia, Ana Carolina, Alliny, Angela Buitrago, Matheus, Camila Tanimoto,Vijay Balakrishnan, Douglas Adamoski, Antonio Borges, Sarah Lee, Naomi Pollock and Steph Nestorow. It has been great to know all of you during my time!!!

To Tim Dafforn from University of Birmingham, Isabel de Morais from Membrane Protein Laboratory (MPL-Diamond light source), Pietro Ciancaglini from USP-Ribeirao Preto, Sandra Dias from LNBio-CNPEM, Saskia Bekker from University of Warwick, Christos Savva from University of Leicester for all their scientific and technical support.

To my friends Edgar Llontop, Paola Zabarburu. Erick Suclupe, Juan Falla, Diego Leonardo for helping me survive all the stress and not let me give up.

Express my eternal appreciation towards Lidiani and her parents Elydia and Afonso for all unconditional support and patient during the writing of this thesis

Finally, I am fully Indebted to my parents José Reynaldo Neciosup Neciosup and Candelaria Quesñay Roque, they support and encouraged me to leave my home to pursuit a scientific life. To Arliz, Cinthya, Katherine and Junior who have always been there for me no matter where I am.

ACKNOWLEDGMENTS OF SCIENTIFIC, TECHNICAL AND FINANCIAL SUPPORT

To the financial support from the Sao Paulo State Research Foundation, FAPESP, via scholarships 2015/02734-7 (FAPESP.DD) and 2019/02261-2 (FAPESP.BEPE.DD).

This study was financed in part by Coordenação de Aperfeicionamento de Pessoal de Nivel Superior – Brasil (CAPES) – Finance Code 001.

To the Brazilian Biosciences National laboratory (LNBio) and Brazilian Nanotechnology National Laboratory (LNNano), Brazilian Center for research in Energy and Materials (CNPEM) for support and access to facilities.

To the graduate program in Biosciences and Technology of Bioactive Products of Institute of Biology, University of Campinas.

To São Carlos Physics Institute, University of São Paulo.

To Dr. Isabel de Moraes and the Membrane Protein Laboratory, at Diamond Light Source, Didcot, UK.

To Dr. Tim Dafforn group at School of Biosciences, University of Birmingham, UK, in special to Dr. Naomy Pollock, for continuous assistance.

To the Midlands Regional Cryo-EM Facility, University of Leicester, UK.

To the Advanced Bioimaging RTP Facility, University of Warwick, UK.

RESUMO

O piruvato é considerado o ponto central do metabolismo celular, chave para a geração de energia e blocos biossintéticos. Quando a oxidação do piruvato pelo ciclo do ácido cítrico é necessária, o piruvato citosólico deve ganhar acesso à matriz mitocondrial em um processo que se acredita envolver ativamente duas subunidades carreadoras de piruvato mitocondrial (MPC) organizadas em hetero-oligômeros. Desde 2012, quando as identidades moleculares de mamíferos MPC1 e MPC2 (e MPC3 em leveduras) foram finalmente apresentadas, vários estudos *in vitro* e *in vivo* revelaram uma interação inesperada entre duas ou mesmo três subunidades de proteínas que definem diferentes conjuntos funcionais, em um contexto metabólicos específicos; estes têm implicações claras na fisiologia da homeostase e em algumas doenças. No entanto, o mecanismo funcional baseado em estrutura de MPC permanece indefinido, apesar dos intensos esforços empregando ferramentas computacionais e técnicas experimentais de última geração. Nesta tese, a produção recombinante de MPC humano, através de uma estratégia de co-expressão, é incialmente descrita; no entanto, não foi observada formação substancial de complexos e, predominantemente, subunidades individuais foram purificadas. Em contraste com MPC1, que co-purifica com uma chaperona de levedura, demonstramos que os homo-oligômeros MPC2 promovem o transporte eficiente do piruvato em proteolipossomos. Os requisitos funcionais derivados e as características cinéticas do MPC2 assemelham-se aos demonstrados anteriormente para o MPC na literatura. De maneira distinta, a inibição química do transporte é observada apenas para um derivado de tiazolidinediona. O papel de transporte autônomo para MPC2 é validado em células, quando a expressão ectópica de MPC2 humano em levedura sem MPC endógeno estimulou o crescimento e aumentou o consumo de oxigênio celular. A detecção de várias espécies oligoméricas de MPC2 em isolados mitocondriais, proteínas purificadas e bicamadas lipídicas artificiais sugerem complexos funcionais de alta ordem (> 2 subunidades). Mudanças significativas no conteúdo da estrutura secundária de MPC2, conforme sondado por dicroísmo circular de radiação sincrotron, suportam ainda mais a interação entre a proteína e os ligantes. A cristalografia de raios X foi prejudicada pela incapacidade de se obter cristais adequados tanto, por difusão de vapor, quanto em fase cúbica lipídica, apesar da obtenção de condições iniciais promissoras. Por fim, a análise por crio-microscopia eletrônica de MPC2 reconstituído em nanodiscos de copolímeros sintéticos permitiu a proposição de uma montagem estequiométrica para o complexo. Coletivamente, nossos resultados fornecem bases para o papel independente do MPC2 na homeostase e doenças relacionadas ao metabolismo desregulado do piruvato e representam uma rota promissora para a determinação de um modelo atômico de alta resolução para MPC2 humano.

ABSTRACT

Pyruvate is considered the central hub in the cellular metabolism, key for the generation of both energy and biosynthetic blocks. When the oxidation of pyruvate by the citric acid cycle is required, cytosolic pyruvate must gain access to the mitochondrial matrix in a process thought to actively involve two mitochondrial pyruvate carrier (MPC) subunits assembled into heterotypic oligomers. Since 2012, when molecular identities of mammalian MPC1 and MPC2 (and MPC3 in yeast) were presented, range of *in vitro* and *in vivo* studies has since revealed an unexpected interplay between two or even three protein subunits that define different functional assemblies on a metabolic context-specific basis; these have clear implications on the physiology of homeostasis and diseases. However, the structure-based functional mechanism of MPC remains elusive, despite intensive efforts by different research groups that employ state-of-the-art computational tools and experimental techniques. In this thesis, the recombinant production of human MPC through a co-expression strategy is first described; nevertheless, substantial complex formation was not observed, and predominantly individual subunits were purified. In contrast to MPC1, which co-purifies with a host chaperone, we demonstrated that MPC2 homo-oligomers promote efficient pyruvate transport into proteoliposomes. The derived functional requirements and kinetic features of MPC2 resemble those previously demonstrated for MPC in the literature. Distinctly, chemical inhibition of transport is observed only for a thiazolidinedione derivative. The autonomous transport role for MPC2 is validated in cells when the ectopic expression of human MPC2 in yeast lacking endogenous MPC stimulated growth and increased oxygen consumption. Multiple oligomeric species of MPC2 across mitochondrial isolates, purified protein and artificial lipid bilayers suggest functional high-order complexes. Significant changes in the secondary structure content of MPC2, as probed by synchrotron radiation circular dichroism, further supports the interaction between the protein and ligands. X-ray crystallography was hampered by the inability to grow suitable crystals by vapor diffusion and in lipidic cubic phase, despite the successful obtention of promising hit conditions. Lastly, cryo-electron microscopy analysis of MPC2 reconstituted into synthetic copolymer nanodiscs allowed for the proposition of a stoichiometric assembly. Collectively, our results provide the initial framework for the independent role of MPC2 in homeostasis and diseases related to dysregulated pyruvate metabolism and may represent a promising route for the determination of a high-resolution atomic model for human MPC2

Summary

CHAPTER 1. INTRODUCTION

1.1 Mitochondrial transport of pyruvate and the MPC

A significant fraction of the metabolic reactions in a eukaryotic cell, especially those that connect sugar, fat, and protein catabolism to energy generation and biosynthesis, occurs in the mitochondria. These ubiquitous subcellular organelles have the production of ATP (adenosine triphosphate), through oxidative phosphorylation, regarded as their primary function. The aerobic (oxygen-dependent) generation of ATP requires the controlled exchange of metabolites from the cytosol to the so-called mitochondrial matrix, where a series of coordinated enzymatic reactions take place. For instance, one of the foremost steps is the decarboxylation of glycolytic pyruvate to generate acetyl coenzyme A, which is then oxidized to produce the reducing equivalents NADH and $FADH_2$; these deliver electrons to the electron transport chain, to build up a proton motive force that powers ATP production at the inner membrane cristae.

However, two distinct lipid bilayer membranes separate the mitochondrial matrix from the cytoplasm (Figure 1). Briefly, besides anchoring enzymes, the outer mitochondrial membrane, or OMM, is permeated by pore-forming integral transmembrane proteins that facilitate the trafficking of ions and small uncharged molecules (< 5000 Da) from the cytosol to the perimitochondrial space. The import of larger substrates, such as peptides or proteins, requires the active function of translocase complexes of the outer membrane (TOM).

Because of the intrinsically high porosity of the OMM to small molecules, the perimitochondrial or intermembrane space (IMS), is aqueous and chemically similar to the cytosol. The second lipid membrane that encloses the ISM is called the inner mitochondrial membrane, or IMM. With distinct protein-to-lipid ratio and lipid composition (including the unusual cardiolipin) compared to the OMM, the IMM is also heavily folded into invaginated structures called cristae (Figure 1). These features combined create a much less permeable membrane that acts as both an electrical insulator and chemical barrier at the matrix; also, with an extensive surface area, the IMM harbours over one hundred selective and specialized membrane transporters, among other proteins, such as the components of the electron transport chains the ATP synthase. Both the physical and chemical compartmentalization of matrix are necessary features for specialized mitochondrial metabolism.

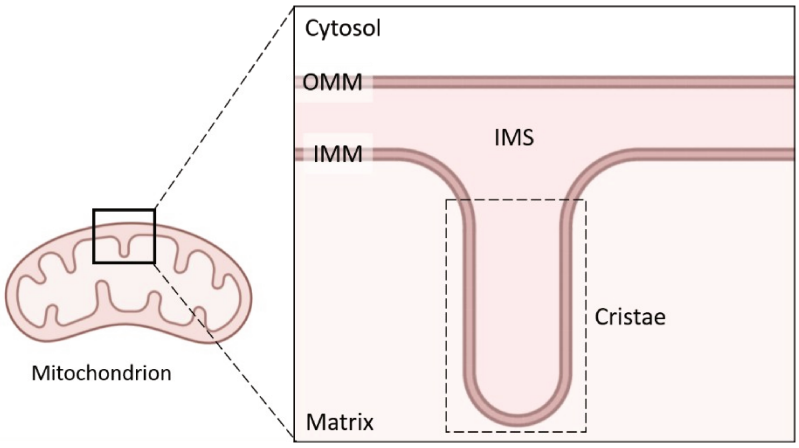

Figure 1. Schematic representation of the mitochondrial structure. Mitochondria are separated from the cytosol by an outer double layer phospholipid membrane (OMM), that covers and contains the organelle. The inner membrane (IMM), also a double layer of phospholipids, is located within and has many folds called cristae; the folding increases the surface area inside the organelle, thereby generating more space for more membrane-linked reactions to occur, and increases the mitochondria's output. The space between the outer and inner membranes is called the intermembrane space (IMS), and the high-viscosity space inside the inner membrane is called the matrix. Figure created by the author using Biorender.com.

Relevant to this thesis is the mitochondrial metabolic fate of pyruvate, which was first described by Hans Krebs, William Johnson, and others in the 1930´s (KREBS; JOHNSON, 1937), on the metabolism of ketonic acids in animal tissues. Pyruvate, which is a three-carbon keto-acid anion, is regarded as one of the most versatile nutrients in the cell, lying at the intersection between different catabolic and anabolic pathways. It is most often the end-product of glycolysis but can also be converted back to carbohydrates (such as glucose itself) via gluconeogenesis and can undergo decarboxylation by the Pyruvate Dehydrogenase Complex to produce acetyl-CoA. Notably, acetyl-CoA is required for the Citric Acid Cycle, and the synthesis of fatty acids, steroids, neurotransmitters, and others. In a series of reversible reactions by the same enzymes, pyruvate can be (i) carboxylated into oxaloacetate by Pyruvate Carboxylase, (ii) transaminated into alanine by Alanine Transaminase, and (iii) reduced to lactate by Lactate Dehydrogenase.

To enter mitochondria, cytosolic pyruvate crosses the OMM to reach the IMS, probably through the large, relatively non-specific, voltage-dependent anion channel (VDAC), and it is then transported together with a proton across the IMM by the mitochondrial pyruvate carrier (MPC) subunits 1 and 2 in mammalians and subunits 1 to 3 in yeast. More specifically, nearly

four decades after the demonstration of the protein-mediated transport of pyruvate across the IMM (HALESTRAP; DENTON, 1974), two concurrent studies identified the oligomeric complex formed by the MPC subunits in yeast as necessary and sufficient for this task (BRICKER et al., 2012; HERZIG et al., 2012) These original findings inspired many subsequent investigations that have further characterized MPC-dependent pyruvate transport in the cellular context (BENDER; PENA; MARTINOU, 2015; SCHELL et al., 2014; VACANTI et al., 2014), with multiple groups showing that either the loss of MPC1 or MPC2 in mitochondria is sufficient to confer similar loss of function phenotypes (BENDER; PENA; MARTINOU, 2015; COMPAN et al., 2015; LIANG et al., 2015; VANDERPERRE et al., 2015; VIGUEIRA et al., 2014). A recent review on the vast physiology of MPC was presented (ZANGARI et al., 2020).

Human MPC1 and MPC2 are small integral membrane proteins of, respectively, 12 kDa (UniProtKB Q9Y5U8) and 14 kDa (UniProtKB O95563). When the work reported in this thesis was first conceived, back in 2013, the only model for the functional organisation of MPC embedded in the IMM proposed that yeast MPC1 and MPC2 should function together via the formation of an oligomeric assembly of approximately 150 kDa (BRICKER et al., 2012).

With the primary sequences identified, it became crucial to classify MPC into a proper protein family to make further predictions. Since its discovery MPC has been in different families considering diverse criteria. Initially, as mitochondrial carrier MPC was included into mitochondrial carrier family (named MCF or SLC25), however proteins members of SCL25 family are small (35 – 40 kDa), acts as monomers and have a conserved amino acid sequence motif, PX(D/E)XX(K/R) known as carrier signature (CS) (PALMIERI, 2013; PEBAY-PEYROULA et al., 2003). MPC1 and MPC2 protein are 12kDa and 15kDa respectively (BRICKER et al., 2012) and acts as a heterodimer or homodimer. These characteristics diverge to other know mitochondrial carrier proteins.

Bioinformatical analysis suggests that MPC is related to the SWEET transporters (Sugars Will Eventually be Exported Transporters) or heptahelical PQLC2 protein family (JEŹÉGOU et al., 2012). Also, due to its homology to the bacterial homo-dimeric Semi-SWEET glucose transporters (XU et al., 2014), MPC has been proposed to be a possible two-fold pseudo-symmetrical dimer (VANDERPERRE et al., 2015). It is important to mention that a SWEET domain consists in the connection, via transmembrane helix, of two semi-SWEET domains which are composed of a single 1-3-2 triple transmembrane helix bundle (THB)(FENG;

FROMMER, 2015). Structural predictions reveals at least two and three transmembrane helices of MPC1 and MPC2 respectively (HALESTRAP, 2012; HERZIG et al., 2012). Recently, the hypothesis of a 4TM MPC precursor duplication might originated MPC1 and MPC2 make, to proposed that MPC belong to the transporter-opsin-G protein-coupled receptor (TOG) superfamily with heptahelical TMS arranged in a 3+1+3 membrane topology(MEDRANO-SOTO et al., 2020). Finally, according to Pfam (FINN et al., 2014), MPC proteins, SWEET transporters and PQ-loop protein family are members of the MtN3-like clan. These models are summarized in Figure 2.

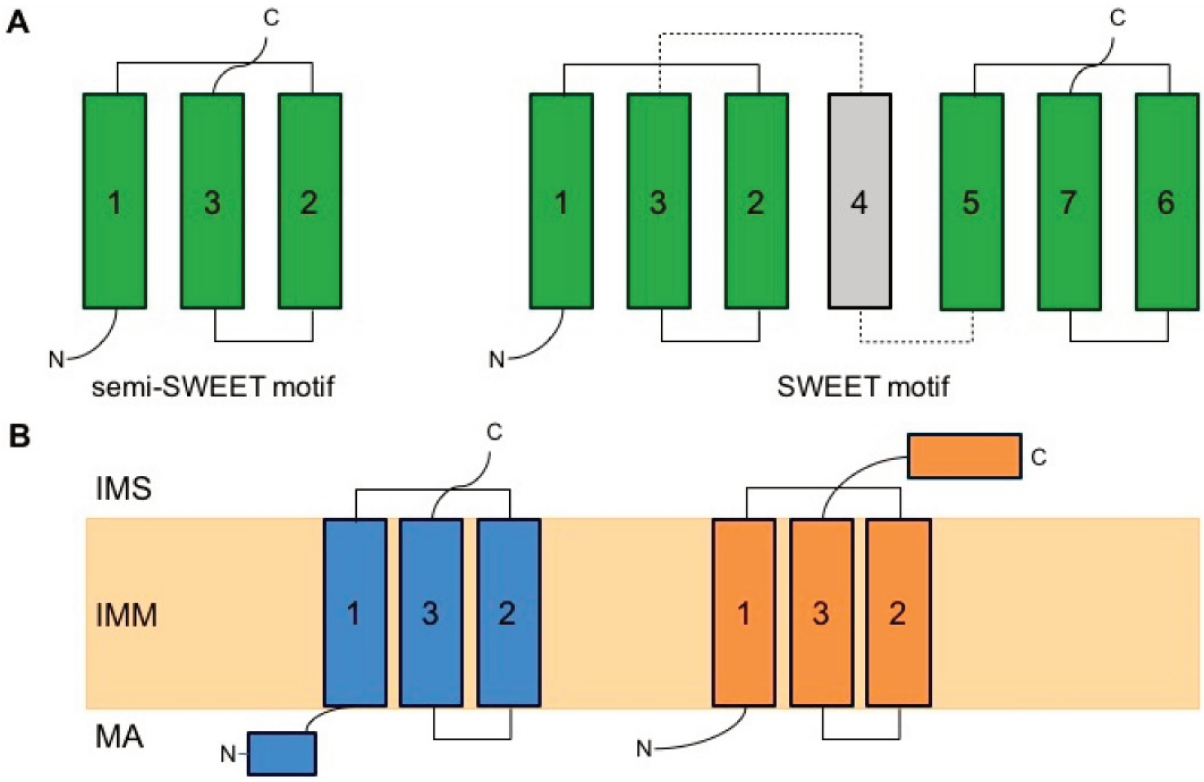

Figure 2. Proposed topology for mammalian MPC. (A) Bacterial semi-SWEET and SWEET motifs. Semi-SWEET is composed of a triple helix bundle in this specific order 1-3-2. SWEET contains two semi-SWEET motifs linked together by a helix. All the helices are crossing the membrane, as experimentally demonstrated. **(B)** Model for the topology of MPC1 and MPC2 in the inner mitochondrial membrane (IMM). Here, a semi-SWEET-like structure is proposed for both MPC1 and MPC2. MA: matrix; IMS: inner mitochondrial membrane. Extracted from (ZANGARI et al., 2020).

In terms of functional organisation while embedded in the IMM, it has been proposed that the three MPC subunits form two context-specific hetero-complexes, depending on the metabolic state of the cell: (i) MPC1:MPC2 complex exist during fermentative growth and (ii) MPC1:MPC3 is favoured during respiratory growth (BENDER; PENA; MARTINOU, 2015; TIMOŃ-GÓMEZ; PROFT; PASCUAL-AHUIR, 2013). The latter was recently demonstrated to mediate pyruvate transport when reconstituted in proteoliposomes (TAVOULARI et al., 2019). In contrast, mammalians, including humans, are proposed to present only MPC1:MPC2 hetero-complex (BRICKER et al., 2012) and MPC1-like:MPC2 (VANDERPERRE et al., 2016a) complexes, additionally it has been reported a functional characterisation of human MPC2 in complete absence of its "mandatory partner MPC1. However, the formation of a possible homodimer or high-order oligomer complexes of MPC2 remains is still elusive.

1.2. Objectives.

In accordance to the previous session, following the identification of MPC and the growing body of physiological studies related to this protein, the isolation and reconstitution of MPC1:MPC2 into proteoliposomes is still considered necessary to perform the ultimate proof-of-concept experiment to measure pyruvate transport (HALESTRAP, 2012; MCCOMMIS; FINCK, 2015; VANDERPERRE et al., 2015); additionally, this demonstration will set the framework to seek the structure-based mechanism of active pyruvate transport mediated by MPC. Within this context, we propose the following main objective for this work: **To demonstrate, through recombinant production of MPC, its ability to promote pyruvate transport in an artificial lipid system, associated with the description of the structure-based functioning mechanism.**

To achieve this major goal, the following specific objectives are outlined:

- to establish a eukaryotic system for the heterologous expression of human MPC;

- to perform chromatographic purification of recombinant MPC by exploiting its physicochemical properties;

- to develop a quantifiable transport assay based on small unilamellar vesicles;

- to perform structure-based studies of MPC by X-ray crystallography and cryo-electron microscopy using protein samples purified to homogeneity.

CHAPTER 2. MATERIALS AND METHODS

2.1. Construct design and cloning.

The pBEVY-GU (MILLER; MARTINAT; HYMAN, 1998) (bi-directional expression vector for yeast, galactose inducible, URA3 selection) was a generous gift from Dr. Graham D. Pavitt (University of Manchester, UK). We are also grateful to Dr. Pascal Egea (University of California, Los Angeles) for the kind gift of alternative vectors from the pBEVY series. Standard molecular biology techniques were used to modify the original pBEVY-GU plasmid to add (i) the coding sequence for an 8xHis tag (with a four-amino acid spacer, VDGS) to the 3′ end of multiple cloning site 1 and (ii) a PreScission Protease recognition sequence, followed by EGFP at the 3′ end of multiple cloning site 2. Codon-optimized, synthetic genes encoding human MPC1 (NCBI Reference Sequence: NP_057182.1) and MPC2 (NCBI Reference Sequence: NP_001137146.1) were acquired from GenScript, USA. The restriction sites SalI/BamHI and XmaI/EcoRI were used for subcloning *MPC1* and *MPC2*, respectively. Standard techniques were also used to transfer the poly-histidine tag from the C-terminus of MPC1 to the C-terminus of EGFP. The additional constructs MPC1-mTFP+MPC2-GFP-10xHis, MPC2 alone (plasmid construct devoid of the coding sequence for MPC1), and MPC2.C54S were generated using standard molecular biology techniques. The plasmids were propagated in TOP10 chemically competent bacteria (Thermo Fisher, USA). These experiments were performed in collaboration with the postdoctoral fellow Dr. Raghavendra SK Nagampalli and the undergraduate student Amanda CT Silva.

2. 2. Preparation of competent cells and transformation into yeast.

The expression plasmids were transformed into a triple deletion mutant yeast strain (JRY2242, W303 *mpc1Δmpc2Δmpc3Δ, his3 lys2 met15 trp1 ura3*) (BRICKER et al., 2012), kindly provided by Jared Rutter (University of Utah, USA). The procedure for transformation was adapted from a previously published protocol (DREW et al., 2009). Briefly, one yeast colony was inoculated into 5 mL of yeast peptone dextrose medium (YPD) and cultured overnight in an orbital shaker at 200 rpm, 30 °C. The following day, 0.8 mL of the overnight culture was diluted into 30 mL of YPD in a 250-ml flask and grown as above until reaching an OD_{600} of 0.8. The cells were centrifuged at 4,000 *g* for 10 min at 4 °C, and the pellet was resuspended in 25 mL of sterile water. The centrifugation process was repeated, and the competent cells were initially resuspended in 1 mL and then 0.4 mL of 100 mM lithium acetate. Subsequently, the transformation was performed on ice, unless otherwise mentioned. To the 50 µL of competent cells, 240 µL of 50 % (w/v) PEG 3350 was added for each transformation. A total of 25 µl of 2 $mg.mL^{-1}$ single-stranded carrier DNA was added to each tube and incubated for 5 s. Subsequently, 50 µL of DNA encoding human pyruvate carrier (100-150 ng) diluted in sterile water was added to each tube and incubated for 5 s, followed by heat shock for 45 min at 42 °C. The cells were centrifuged at 8,000 *g* for 1 min at RT, and the pellet was resuspended in 100 µL of sterile water. The cell suspension was plated onto SD-URA plates and incubated for 3 days at 30 °C. These experiments were performed in collaboration with the postdoctoral fellow Dr. Raghavendra SK Nagampalli.

2.3. Protein expression and purification.

Typically, for large-scale overexpression of recombinant MPC, colonies from the SD-URA plates with the highest fluorescence levels were selected and used as pre-inoculum, with large-scale cultures (typically 4 L) grown in shake flasks. Two hundred-milliliter cell cultures (in 500 mL flasks) transformed with MPC plasmids were grown overnight in YPD (2 % glucose) with shaking at 200 rpm at 30 °C. The following morning, 10 mL of the overnight culture was added to 500 mL of YPD (0.2 % glucose) in a 2 L flask and cultured as above until the OD_{600} reached 0.8. Then, 2 % galactose (from a 20 % stock) was added to the culture. After 22 h, the cells were harvested via centrifugation at 4,000 *g* for 10 min. The pellets were suspended in 400 mL of buffer containing 1X PBS, supplemented with 150 mM NaCl, 10 % glycerol, 2 mM β-

mercaptoethanol, and a protease inhibitor mix. Cell lysis was performed using a benchtop cell disruptor (Constant Systems) at increasing pressures (25, 28, 30, 32, 35, and 38 kpsi). After lysis, the cell suspension was centrifuged at 10,000 *g* for 10 min at 4 °C. The supernatant was retained and further ultra-centrifuged at 150,000 *g* for 2 h to pellet the membranes. Isolated membranes of MPC1-8xHis or MPC2-10xHis were resuspended in similar solubilization buffer (SB) containing 1X PBS, pH 8.0, and 150 mM NaCl; 0.5 mM TCEP: 1 % (w/v) C12E8 was used for MPC2-10xHis, and 1 % (w/v) DDM was used for MPC1-8xHis. Membrane-detergent mixtures at a 2:1 ratio were rotated for 1 h at 4 °C. The suspension was cleared via ultra-centrifugation at 100,000 *g* for 45 min, and 10 mM imidazole was added to the solubilized solution. The solubilized samples were incubated for 3 h at 4 °C with TALON beads (Clontech) pre-equilibrated with SB (supplemented with 0.1 % (w/v) C12E8 + 0.1 % (w/v) DDM for MPC2-GFP-10xHis and with 0.1 % (w/v) DDM for MPC1-8xHis). Following incubation, the sample was loaded onto a glass column (Bio-Rad) and washed with 20 column volumes (CVs) of SB containing 0.1 % (w/v) DDM and 15 mM imidazole. The column was subsequently washed with another 20 CVs of the same buffer containing 30 mM imidazole. Bound proteins were eluted with SB containing 0.1 % (w/v) DDM and 300 mM imidazole. A similar procedure of column washing and elution was followed for both MPC2-10xHis and MPC1-8xHis. The eluted protein from the MPC1-8xHis construct was collected, concentrated to 5 $mg.mL^{-1}$ and immediately loaded onto a Superdex 200 PG 16/30 column (GE Healthcare, Sweden) pre-equilibrated in 20 mM TRIS, pH 8.0, 150 mM NaCl, 0.5 mM TCEP and 0.03 % DDM. The protein eluted from MPC2-10xHis construct was dialyzed overnight against 20 mM TRIS, pH 8.0, 300 mM NaCl, 5 % glycerol, 0.05 mM TCEP and 0.03 % DDM in a 6,000-Da MWCO dialysis bag (Spectrum Laboratories, USA) in the presence of 10:1 (GFP fused pyruvate carrier: protease) GST-tagged PreScission Protease at 4 °C. After dialysis, the digest was passed through TALON (Clontech, USA) and GST (GE Healthcare, USA) beads equilibrated in dialysis buffer. The flow-through containing the membrane protein was collected and concentrated to 5 $mg.mL^{-1}$ and loaded directly onto a Superdex 200 PG 16/30 column previously equilibrated with 20 mM TRIS, pH 8.0, 300 mM NaCl, 5 % glycerol, 0.05 mM TCEP and 0.03 % DDM. MPC2-10xHis in the absence of TCEP, and additional constructs, such as MPC2 alone (plasmid construct devoid of the coding sequence for MPC1) and the MPC2.C54S mutant, were similarly purified as described above. For all MPC constructs used in the present study, a typical purification preparation starting with inducible expression from four liters of yeast culture resulted in approximately 1 mg of pure protein sample after full purification.

The electrophoretic analysis was performed using Tricine-SDS-PAGE. These experiments were performed in collaboration with the postdoctoral fellow Dr. Raghavendra SK Nagampalli and the laboratory of Dr. Isabel de Moraes, at the Membrane Protein Laboratory, Diamond Light Source, Didcot, UK.

2.4. Confocal Microscopy.

The Mito-mCherry plasmid for yeast expression used for mitochondrial labeling was kindly provided by Jean-Claude Martinou (Université de Genève, Switzerland). Yeast co-transformed with either of the MPC-expression plasmids or Mito-mCherry were cultured under the same conditions described above to facilitate the expression of GFP-labeled MPC. Subsequently, 10 mL of 22-h induced cells (at OD_{600} of 1) was centrifuged at 250 rpm for 5 min. The pellet was resuspended in 1 mL of YPD. From this, 7 µL of cells were added to a slide and sealed with a cover slip. Samples were examined in the Biological Imaging Facility (LIB) at LNBio, using a Leica TCS SP8 confocal on a Leica DMI 6000 equipped with an HCX PL APO 63x/1.40 CS2 objective. These experiments were performed in collaboration with the postdoctoral fellow Dr. Raghavendra SK Nagampalli.

2.5. Quantitative PCR.

Total RNA was extracted using the TRIzol reagent (Invitrogen Corporation), and 5 µg of total RNA was used for retrotranscription using GoScript™ Reverse Transcription System (Promega). Real-time quantitative PCR for *MPC1* and *MPC2* was performed using the SYBR Green PCR Master Mix (Applied Biosystems). The threshold cycle (CT) values of the target genes were normalized to the actin gene, and relative expression ratios were calculated using the 2-ΔΔCT Ct method ((LIVAK; SCHMITTGEN, 2001). Next, the readings were normalized to the URA3 transcripts to calculate the levels of transformed plasmids. The primer sequences were as follows: (1) Actin: ACT1.qPCR.For: 5′ – ATTCTGAGGTTGCTGCTTTGG – 3′ and ACT1.qPCR.Rev: 5′ – TGTCTTGGTCTACCGACGATAG – 3′; (2) URA3: URA3.qPCR.For: 5′ – TGGCAGCAACAGGACTAGGATG – 3′ and URA3.qPCR.Rev: 5′ – CGAACAGAAGGAAGAACGAAGGAAG – 3′; (3) Human MPC1: hMPC1.qPCR.For: 5′ – TGACCTTTGCTTTGTGTTGC – 3′ and hMPC1.qPCR.Rev: 5′ –

CACCTTGGATCAATTGTGCT – 3′; (4) Human MPC2: hMPC2.qPCR.For: 5′ – CGATATGGCTAGACCAGCAG – 3′ and hMPC2.qPCR.Rev: 5 ′– ACAGCGAACAAAGACCAATTT – 3′.). These experiments were performed in collaboration with the graduate student Carolline Ascençao.

2.6. Fluorescence size-exclusion chromatography (FSEC).

The appropriate detergent for protein extraction from membrane pellets was determined by FSEC analysis (DREW et al., 2009). A total of 250 µL of solubilized membranes containing the overexpressed EGFP-fused pyruvate carrier in DDM (Anatrace, OH, USA) for MPC1 and C12E8 (Anatrace, OH, USA) for MPC2 was loaded onto a Superdex 200 PG 16/30 column. The column was pre-equilibrated with 20 mM TRIS, pH 8.0, 150 mM NaCl, 0.5 mM TCEP and 0.03 % DDM for MPC1-8xHis and 20 mM TRIS, pH 8.0, 300 mM NaCl, 5 % glycerol, 0.5 mM TCEP and 0.03 % DDM for MPC2- and connected to an AKTA start FPLC system at 4 °C. The flow rate was set at 1 $mL.min^{-1}$. Fractions of 200 µL were drawn from the elution into 96-well optical plate. GFP emission was measured at 512 nm on bottom read mode, with an excitation wavelength of 488 nm, using an EnSpire microplate reader (Perkin Elmer, Massachusetts, USA). These experiments were performed in collaboration with the postdoctoral fellow Dr. Raghavendra SK Nagampalli.

2.7. Calibration of gel filtration columns.

Standard proteins from the low and high molecular weight Gel Filtration calibration kits (GE Healthcare, USA) were used. Protein resuspension buffer and running buffer were 20 mM TRIS, pH 8.0, 300 mM NaCl, 5 % Glycerol, 0.5 mM TCEP and 0.03 % DDM. These experiments were performed in collaboration with the postdoctoral fellow Dr. Raghavendra SK Nagampalli.

2.8. Mass spectrometry.

The protein bands from gel-filtration-purified samples were extracted from tricine-SDS-PAGE gels. The gels were first stained with Coomassie dye for band identification and excision. Bands were then isolated and destained in methanol (50 %)/acetic acid (2.5 %) solution, and the

samples were reduced, alkylated, and digested with trypsin (SHEVCHENKO et al., 1996). Peptides (4.5 µL) were separated by a C18 (75 µm x 100 mm, 1.7 µm particle size) nanoUPLC (nanoAcquity, Waters) coupled with a Q-Tof Premier mass spectrometer (Waters) with a nanoelectrospray source at a flow rate of 0.6 $\mu L.min^{-1}$. The gradient was 2-35 % acetonitrile in 0.1 % formic acid over 31.6 min for the digested proteins. The nanoelectrospray voltage was set to 3.5 kV, with a cone voltage of 30 V, and the source temperature was 80 °C. The instrument was operated in the 'top three' mode, in which one MS spectrum is acquired, followed by MS/MS of the top three most-intense peaks detected. After MS/MS fragmentation, the ion was placed on an exclusion list for 60 s. The spectra were acquired using MassLynx v.4.1 software, and the raw data files were converted to a peak list format (mgf) using Mascot Distiller v.2.4.0.0 software 2011 (Matrix Science Ltd.) and were searched against the Human UniProt-SwissProt database (92,180 sequences; 36,693,332 residues; release date March 2016) and the Yeast UniProt-SwissProt database (550,299 sequences; 196,347,838 residues; release date March 2016), with *Saccharomyces cerevisiae* taxonomy (7,743 sequences) using Mascot engine v.2.3.2 (Matrix Science Ltd.) with carbamidomethylation as a fixed modification, oxidation of methionine as a variable modification, one trypsin missed cleavage and a tolerance of 0.1 Da for both precursor and fragment ions. These experiments were performed in collaboration with the postdoctoral fellow Dr. Raghavendra SK Nagampalli and the laboratory of Dr. Adriana F Paes Lemes, at LNBio/CNPEM, Campinas.

2.9. Preparation of liposomes and proteoliposomes.

The purified MPC protein samples were reconstituted into liposomes using previously described procedures (XU et al., 2014; YONEDA et al., 2014) with minor modifications. Briefly, asolectin from soybean extract (Sigma Aldrich) was dissolved in chloroform and dried into a thin film by blowing gaseous N_2. This film was then resuspended to a final concentration of 4 $mg.mL^{-1}$ in buffer containing 20 mM TRIS, pH 8.0, 300 mM NaCl, 5 % glycerol, 0.5 mM TCEP and 0.03 % (w/v) DDM and heated at 70 °C for 1 h with vortexing every 10 min. This suspension was sonicated in a water-bath sonicator at 40 kHz for 1 min to obtain the homogenized lipid-detergent solution. The purified proteins were added to the solution at a lipid-to-protein ratio of 10:1 (w/w), along with 0.05 % (w/v) DDM to avoid protein denaturation. The ternary protein-lipid-detergent mixture was freeze-thawed three times for full reconstitution and then sonicated for 1 min under

the aforementioned conditions. In order to remove the detergent and allow proteoliposome formation, Bio-Beads SM-2 resin (Bio-Rad) was added at a ratio of 1:0.2 (w/w) and incubated at 4 °C with exchange after 5, 10 and 40 min, followed by ultra-centrifugation of the suspension at 100,000 *g* for 45 min, and the final proteoliposome pellet was resuspended in 20 mM TRIS, pH 8.0, 300 mM NaCl, 5 % glycerol, and 0.5 mM TCEP. Protein-free liposomes (small unilamellar vesicles, or SUVs) were prepared following a similar procedure, except that the protein solution was replaced with the gel filtration buffer. Purified MPC2-10xHis in the absence of TCEP, as well as the purified proteins from the additional constructs, such as MPC2 alone (plasmid construct devoid of the coding sequence for MPC1) and the MPC2.C54S mutant, were reconstituted into liposomes following the above protocol. The size and homogeneity of the liposomes and proteoliposomes were assessed via dynamic light scattering and Nanoparticle Tracking Analysis (Fig. 5A), as described below. Dynamic light scattering analysis was performed to check for unwanted bursting or swelling of the liposomes and proteoliposomes upon incubation with the pyruvate solution (Fig. 5B). These experiments were performed in collaboration with the postdoctoral fellow Dr. Raghavendra SK Nagampalli and the laboratory of Dr. Pietro Ciancaglini, at the Departamento de Química, Faculdade de Filosofia, Ciências e Letras de Ribeirão Preto, Universidade de São Paulo.

2.10. Nanoparticle Tracking Analysis.

The size, homogeneity, and concentration of the liposomes and proteoliposomes were assessed via NTA, as available on the NanoSight instrument (Malvern) Dynamic light scattering measurements were performed on a NanoSight NS300 (Malvern Instruments Ltd., United Kingdom). Fifty microliters of total proteoliposomes was diluted in 1 mL of filtered buffer (20 mM TRIS, pH 8.0, 300 mM NaCl, 5 % glycerol, 0.5 mM TCEP); 500 µL of this suspension was injected into the sample chamber using a sterile syringe. All measurements were performed at 18 °C, and the average of quintuple readings was determined. These experiments were performed in collaboration with the postdoctoral fellow Dr. Raghavendra SK Nagampalli.

2.11. *In vitro* pyruvate transport: radiolabelled substrate.

Radiolabelled pyruvate transport experiments were performed as described previously (BENDER; PENA; MARTINOU, 2015; BRICKER et al., 2012; HERZIG et al., 2012) with minor

modifications. The transport assay was initiated by the addition of 50 µL liposome/proteoliposomes samples with 50 µL of radiolabelled ^{14}C-pyruvate at 0.1 µCi dissolved in transport buffer containing 120 mM KCl, 100 mM MES pH 6.5. Upon incubation at desired time points (1, 5, 10 and 30 minutes), at room temperature, the transport assay was stopped by adding 900 µL of 50 mM cold pyruvate in PBS pH 7.4. The vesicles were centrifuged at 15,000 g for 30 minutes followed by PBS wash two times. To the resulting pellet, 1 ml of scintillation buffer was added, and the imported ^{14}C-pyruvate was quantified by scintillation counter. To demonstrate the pH dependence on the transport, 50 µL of the liposome/proteoliposomes were added with radiolabelled pyruvate in buffer containing 120 mM KCl, 100 mM TRIS pH 8.0 and incubated for 30 minutes at room temperature. The reaction was stopped, and the measurement of imported ^{14}C-pyruvate was carried out as described above. Further, to validate the inhibition of pyruvate transport 50 µL of the liposome/proteoliposomes samples were pre-incubated for 30 minutes with UK5099 and rosiglitazone dissolved in 0.1 % DMSO at a final concentration of 50 µM respectively. To these samples, radiolabelled pyruvate in transport buffer containing 120 mM KCl, 100 mM MES pH 6.5 was added and incubated for 30 minutes at room temperature. By following the procedure described the above reaction was stopped, and the imported ^{14}C-pyruvate was quantified by the scintillation counter. Background values in each experiment were measured by the simultaneous addition of ^{14}C pyruvate and its corresponding stop solution. These experiments were performed in collaboration with the postdoctoral fellow Dr. Raghavendra SK Nagampalli and the laboratory of Dr. Ariel M Silber, at the Laboratório de Bioquímica de Tripanossomatídeos, Departamento de Parasitologia, Instituto de Ciências Biomédicas, Universidade de São Paulo.

2.12. *In vitro* pyruvate transport: enzymatic assay.

Transport analysis was performed at room temperature and initiated by mixing 50 µL of the liposome/proteoliposome samples with 100 µL of 50 µM sodium pyruvate in a 96-well flat-bottom Greiner plate. To induce a pH gradient of 1.5 units between the inner and outer vesicle environments, sodium pyruvate (Sigma, USA) was resuspended at the desired concentration in transport buffer containing 120 mM KCl and 100 mM MES, pH 6.5. Upon incubation for the desired times (1, 3, 5, 15 and 30 min) at room temperature, 50 µL of stop buffer (2 nM LDHA, 0.5 mM NADH, 50 mM TRIS, pH 8.0) was added. The mixture was immediately subjected to

quantification of absorbance at 340 nm on an EnSpire plate reader (Perkin Elmer, USA) to track the oxidation of NADH. In addition, the necessity of a collapsed proton electrochemical gradient was measured as described above with minor modifications. Briefly, sodium pyruvate was also dissolved in transport buffers containing 120 mM KCl, 100 mM TRIS, pH 8.0 (for ΔpH = 0). Raw absorption readings were converted to amounts of NADH using an extinction coefficient of 6,220 $M^{-1}.cm^{-1}$. Initial velocities for LDHA under all conditions were obtained using linear regression, keeping unrestrained intercepts. When appropriate, analysis of covariance (ANCOVA) was performed to determine whether the difference between two similar slopes was statistically non-significant (indicated as n.s. in the figures and respective legends). Velocities were rounded up to the first significant digit. The obtained enzyme velocities for each transport condition were compared with an LDHA standard curve (Fig. 8D) generated under the same chemical conditions used in the assay but in the absence of liposomes or proteoliposomes, termed Ctrl (-L/PL). Spontaneous oxidation of NADH was shown not to occur during the experimental timeframe. The plasmid for bacterial expression of human LDHA was a kind gift from Anne Le (Johns Hopkins Medicine, USA). Experiments to demonstrate the MPC2 pyruvate transport inhibition were performed at room temperature. Fifty microliters of liposome/proteoliposome samples were pre-incubated for 30 min with UK5099 and rosiglitazone dissolved in 0.1 % DMSO at a final concentration of 50 µM. As a control, liposome/proteoliposome samples were also similarly incubated with 0.1 % DMSO. These experiments were performed in collaboration with the postdoctoral fellow Dr. Raghavendra SK Nagampalli.

2.13. Isolation of yeast mitochondria.

Mitochondrial isolation was carried out according to the procedure described (DIEKERT et al., 2001) with minor modifications. Briefly, 100 ml of 3Δ yeast with MPC2 was grown in YPD medium for 22 hours at 200 rpm, 30°C. Cells were recovered by centrifugation for (3,000g 5 minutes) at 4°C washed once in water and resuspended in 1ml of ice-cold 20 mM HEPES pH 7.4, 0.6 M sorbitol and 1 mM PMSF buffer at 0.5g cells/ml. Glass beads of approximately two-thirds the final volume was added, and the cells were broken by vortex for 15 s. This process is repeated for three times after chilling on ice for every 15 s. The resulting suspension was centrifuged at 600g for 5 min, and the obtained supernatant is carefully transferred to a fresh tube and further centrifuged at 10,000 g for 10 min. The resulting pellet containing mitochondria were

resuspended in 1 ml of 20 mM HEPES pH 7.4, 80 mM KCl, 5 mM $MgCl_2$, and 250 mM sucrose. The presence of MPC2 in the resulting pellet was further confirmed by tracking GFP emission measured at 512 nm using Enspire (Perkin Elmer, Massachusetts, USA). A similar protocol was followed to isolate the mitochondria of 3Δ yeast cells in the absence of MPC2. These experiments were performed in collaboration with the postdoctoral fellow Dr. Raghavendra SK Nagampalli.

2.14. Quantification of transport using 14C pyruvate in isolated mitochondria.

Two hundred and fifty micrograms of isolated mitochondria of 3Δ yeast in the absence and presence of MPC2 was added with radiolabelled pyruvate at a similar concentration as described above in transport buffer containing 120 mM KCl, 100 mM MES pH 6.5 and incubated for 30 minutes at room temperature. The uptake was stopped by adding 900 µL of 50 mM cold pyruvate in PBS pH 7.4. The mitochondria were centrifuged at 15,000 g for 5 minutes, followed by PBS wash two times. To the resulting pellet, 1 ml of scintillation buffer was added, and the imported ^{14}C-pyruvate was quantified by scintillation counter. To corroborate the inhibition of pyruvate transport, mitochondria were pre-incubated for 30 minutes with UK5099 and rosiglitazone in a related way as it was carried out for vesicles. The inhibitor bound mitochondria were supplemented with radiolabeled pyruvate in transport buffer containing 120 mM KCl, 100 mM MES pH 6.5, and incubated for 30 minutes at room temperature. The reaction was stopped and the measurement of imported ^{14}C-pyruvate was carried out as described above. These experiments were performed in collaboration with the postdoctoral fellow Dr. Raghavendra SK Nagampalli and the laboratory of Dr. Ariel M Silber, at the Laboratório de Bioquímica de Tripanossomatídeos, Departamento de Parasitologia, Instituto de Ciências Biomédicas, Universidade de São Paulo.

2.15. Substrate specificity assay.

Lactate was assessed using the L-lactate colorimetric assay kit from Abcam, Inc. (ab65331) according to the manufacturer's instructions, with minor modifications. Substrate specificity analysis was performed at room temperature and initiated by mixing 50 µL of the liposome/proteoliposome samples with 100 µL of 50 µM sodium lactate (Sigma, USA) in a 96-well flat-bottom Greiner plate. Sodium lactate (Sigma, USA) was suspended to the desired final

concentrations of 30, 60, and 120 µM in transport buffer containing 120 mM KCl, 100 mM MES, pH 6.5, which was also used to dissolve sodium pyruvate. Upon incubation for 30 min at room temperature, 50 µL of the lactate enzyme mix provided with the kit was added, and the plate was measured at 450 nm. Data processing and analysis were performed as described above for pyruvate transport. The obtained enzyme velocities for each transport condition were compared with a lactate standard curve obtained in a vesicle-free solution, termed Ctrl (-L/PL). The experiments were repeated four to six times, and the means ± standard deviations obtained were graphically represented. These experiments were performed in collaboration with the postdoctoral fellow Dr. Raghavendra SK Nagampalli.

2.16. Chemical crosslinking of MPC2.

Crosslinking of MPC2 in mitochondrial extracts was performed according to previously published (BENDER; PENA; MARTINOU, 2015), but using DSS instead. For crosslinking of purified protein and protein reconstituted in proteoliposomes, MPC2 was prepared as described above, except that HEPES was used instead of TRIS in the final gel filtration buffer (20 mM HEPES, pH 8.0, 300 mM NaCl, 5 % glycerol, 0.05 mM TCEP and 0.03 % DDM). Approximately 10 µg of protein was used in each reaction and incubated with DSS at 0.2, 0.4, 2 and 4 mM for 30 min at room temperature. The reactions were stopped using 50 mM TRIS, pH 8.0.

2.17. Cell Growth assays.

Yeast cells co-transformed with pBEVY and pYES2 plasmids were grown overnight and inoculated in 5 mL of SD-URA medium supplemented with 0.2 % glucose for 22 h at 30 °C, 200 rpm. Cells were recovered by centrifugation for 5 min at 3000 *g*, 4 °C, washed twice and then resuspended in 2.5 mL of SD-URA-LEU-VAL supplemented with 0.2 % glucose. OD_{600} was adjusted to 0.034 (approximately 0.23 at 10 mm path-length) for all conditions using an EnSpire Plate Reader (Perkin-Elmer). Then, 10 µL of each cell culture was added to a 96-well plate containing 200 µL of SD-URA (supplemented with 0.2 % glucose + 0.2 % galactose) in the presence and absence of leucine and valine, or a combination of both. Optical density was measured every 5 min, while cells were left to grow inside the EnSpire Plate Reader, with shaking

at 200 rpm, at 30 °C. The pYES2 plasmid was a kind gift from Dr. Celisa Caldana (LNBio). These experiments were performed in collaboration with the graduate student Douglas Adamoski.

2.18. Oxygen consumption measurements.

Yeast cells were grown overnight and inoculated on 10 mL of SD-URA medium supplemented with 0.2 % glucose for 22 h at 30 °C, 200 rpm. Cells were recovered via centrifugation for 5 min, 3.000 g at 4 °C and resuspended in 1 mL of 25 mM HEPES-Buffered DMEM, pH 7.1 (Sigma, D5030). OD_{600} was adjusted to 0.034 (approximately 0.23 at 10-mm path-length) for all conditions using an EnSpire Plate Reader (Perkin-Elmer), and cells were centrifuged and resuspended again in the same buffer to remove any residual glucose. Measurements were performed using an Oxytherm (Hansatech, Norfolk, UK). Briefly, 970 µL of buffered DMEM was pre-warmed to 30 °C with shaking at 100 rpm in a reaction chamber. Next, 30 µL of OD-standardized cells was added, and the chamber was equilibrated open for 1 min. The chamber was then closed and incubated for 8 min to measure the basal respiration, followed by another 8 min for glucose (0.08 % final concentration to induce mitochondrial oxidation of pyruvate and not fermentation to ethanol (TAKEDA et al., 2015), and the final 8 min for ethanol (2 % final concentration to inhibit any residual fermentation (BROWN et al., 1981; FERNANDES et al., 1997). The raw oxygen concentration in the chamber collected every second was used to calculate multiple linear regressions of 150 s in length and average the oxygen consumption rate using the R software package. These experiments were performed in collaboration with the graduate student Douglas Adamoski.

2.19. Determination of MPC2-GFP-10xHis orientation in lipid bilayer membrane.

Triplicate 400 µl aliquotes of proteoliposomes were prepared, with one control sample left untreated. PreScission protease at a ratio of 1:10 (protease: GFP fused pyruvate carrier) was added. All the samples were left gently shaking overnight at 4°C and ultracentrifuged at 100,000 g for 45 min the following day. The supernatant from the protease un-treated and treated along with the control proteoliposomes were loaded into 96 well plate to measure the GFP emission using Enspire (Perkin Elmer, Massachusetts, USA). Results were normalized to the intensity observed in the presence of PreScisison protease, and the percentage digested was calculated and

represented graphically. Further, the similar set of samples were resolved on a 15 % Tricine gel and imaged by using a CCD camera after exposure to blue light at 460 nm with a 515 nm filter cutoff, for 0.2 s. These experiments were performed in collaboration with the postdoctoral fellow Dr. Raghavendra SK Nagampalli and Dr. Zeyal Islam.

2.20. Recombinant expression and purification

Colonies transformed with the MPC2-10his plasmid were grown in YPD (2% glucose) shaken at 200 rpm in 125-ml flasks at 30°C overnight. The next day, 0.8 ml of overnight culture was added into 30 ml of YPD (0.2% glucose) in a 250 ml flask and allow it to grow in the above-mentioned conditions until OD 600 reaches 0.8. Ten- microliter of each overnight culture was streaked onto a fresh SD–URA plate and incubated at 30 °C for 3 days. At OD 0.8, 2 % of galactose (20 % stock) was added to culture and let it growth for 22h. For large-scale overexpression is used typically 10-20 L. Cells were transferred to a clear 96-well optical plate and GFP emission was measured at 512 nm on bottom read, with an excitation wavelength of 488 nm, using Enspire (Perkin Elmer, Massachusetts, USA).

2.21. Membrane pellet preparation.

After the 22-h expression, the cells either for MPC2-10his or MPC1-8his plasmids was harvested as described and resuspended in approximately 10 ml per liter of cell culture with Lysis buffer (LB). Cell lysis was carried out using the Constant Systems cell disrupter (Constant Systems) at increasing pressures; 25, 28, 30, 32, 35 and 38 kPsi. After lysis, the cell suspension was centrifuged at 10,000 g for 10 min at 4 °C. The supernatant was retained and further ultra-centrifuged at 150,000 g for 2h to pellet the membranes.

2.22. Purification of human mitochondrial pyruvate carrier 2.

Isolated membranes of MPC2-10his are resuspended in solublization buffer (SB) containing 1x PBS pH 8.0, 150 mM NaCl, 0.5 mM TCEP 1% (wt/vol) C12E8. Membrane-detergent mixture at 2:1 ratio was allowed to rotate for 1h at 4°C. The suspension was cleared by ultracentrifugation at 100,000 g for 45 min, and 10 mM imidazole was added to the solubilized

solution. TALON beads (Clontech) preequlibrated with SB- 0.1% (wt/vol) C12E8 + 0.1% (wt/vol) DDM and incubated the solubilized sample for 3 h at 4 °C. Upon incubation the sample was loaded onto a onto a glass column (Bio-Rad) and washed with SB containing 0.1% (wt/vol) DDM and 15 mM imidazole for 20 column volumes (CV). The column was subsequently washed with another 20 CVs in the same buffer containing 30 mM imidazole. Bound proteins were eluted with SB containing 0.1% (wt/vol) DDM and 300 mM imidazole. The eluted protein was dialyzed overnight in a 6,000-Da MWCO dialysis bag (Spectrum Laboratories, USA) in the presence of 10:1 (GFP fused pyruvate carrier: protease) precission protease against and 20 mM Tris pH 8.0, 300 mM NaCl, 5 % glycerol, 0.05 mM TCEP and 0.03% DDM at 4°C. After dialysis, the digest was passed through TALON (Clontech) equilibrated in dialysis buffer. The flowthrough containing the membrane protein was collected and concentrated to 5 mg/ml and loaded straight onto Superdex 200 PG 16/30 column (GE Healthcare, Uppsala, Sweden) preequilibrated in 20 mM Tris pH 8.0, 300 mM NaCl, 5 % glycerol, 0.05 mM TCEP and 0.03% DDM.

2.23. SEC-MALLS in detergent.

Protein complexes in DDM and UDM were analysed by SEC coupled to multiangle laser light scattering (MALLS) in-line detectors. Following 50-kDa MMCO concentration, IMAC and gel filtration purified PDCs were applied to a 24-ml Superdex 200 column operated by an Alliance high-pressure liquid chromatographer (HPLC; Waters Corporation) at 0.5 ml/min. OD280, refractive index, and laser light scattering were measured using the 2489 UV/Vis (Waters Corporation), OptiLab rEX (Wyatt Technology), and miniDAWN TREOS (Wyatt Technology) detectors, respectively. Data were processed using the “protein conjugate” analysis module of the Astra software package version 5.3.4.18 (Wyatt Technology). The protein and detergent dn/dc values used were 0.187 and 0.143 ml/g for DDM and 0.187 and 0.150 ml/g for UDM respectively. These experiments were performed in collaboration with the postdoctoral fellow Dr. Raghavendra SK Nagampalli and the laboratory of Dr. Isabel de Moraes, at the Membrane Protein Laboratory, Diamond Light Source, Didcot, UK.

2.24. Synchrotron Radiation Circular Dichroism (SRCD).

To analyse the secondary structure content of MPC2 alone and upon incubation with 25 µM pyruvate and 50 µM rosiglitazone, SRCD experiments were performed using a nitrogen-flushed Module X end-station spectrophotometer at B23 Synchrotron Radiation CD Beamline at the Diamond Light Source, Oxfordshire, UK19. In addition to this, to characterize MPC2 behaviour in different solvent environment high-throughput synchrotron radiation circular dichroism (HT-SRCD) experiments have been also been carried out20. 50 different buffer conditions have been designed and the secondary structure content of MPC2 in these conditions was investigated using this technique. Results obtained were processed using CDApps and OriginLab with Tm calculated using Boltzmann equation. Secondary structure estimation from CD spectra was carried out using CDApps using Continll algorithm. These experiments were performed in collaboration with the postdoctoral fellow Dr. Raghavendra SK Nagampalli and the laboratory of Dr. Isabel de Moraes, at the Membrane Protein Laboratory, Diamond Light Source, Didcot, with important assistance from the beamline crew.

2.25. Detergent screening for crystallization.

To identify the conditions those, promote crystal contact, MPC2 that was originally purified in DDM (12 carbons long) was screened for its stability in shorter detergents during gel filtration. Detergents like UDM (11 C), DM (10 C), NM (9 C), and OG (8 C) were used in this screening. These experiments were performed in collaboration with the postdoctoral fellow Dr. Raghavendra SK Nagampalli and the laboratory of Dr. Isabel de Moraes, at the Membrane Protein Laboratory, Diamond Light Source, Didcot, UK.

2.26. CMC (Critical micelle concentration) screening of UDM.

Following the identification of UDM as the suitable shorter detergent for purification of MPC2 we also screened the required CMC of UDM from 3 to 1.5 times to purify human MPC2. These experiments were performed in collaboration with the postdoctoral fellow Dr. Raghavendra SK Nagampalli and the laboratory of Dr. Isabel de Moraes, at the Membrane Protein Laboratory, Diamond Light Source, Didcot, UK.

2.27. Crystallization of MPC2 using vapour diffusion.

The purified MPC2 was concentrated to 11 mg/ml in buffer containing 20 mM Tris pH 8.0, 300 mM NaCl, 5 % glycerol, 0.05 mM TCEP and 0.058 % UDM and set for crystallization trials in the presence and absence of 2.5 mM pyruvate. Crystallization screens those are specific to the membrane proteins such as MemGold, MemGold2. These experiments were performed in collaboration with the postdoctoral fellow Dr. Raghavendra SK Nagampalli and the laboratory of Dr. Isabel de Moraes, at the Membrane Protein Laboratory, Diamond Light Source, Didcot, UK.

2.28. Crystallization of MPC2 using lipid cubic phase (LCP).

The purified MPC2 was concentrated to 18 mg/ml in buffer containing 20 mM Tris pH 8.0, 300 mM NaCl, 5 % glycerol, 0.05 mM TCEP and 0.058 % UDM and added to monoline (MO) at a ratio of 2:3 (w/v). The detailed protocol for setting up LCP 1. The frozen monoline was incubated at 38 °C 2. Two glass Hamilton syringes of different sizes (the bigger one normally is for the lipid), (the mosquito only takes 100 or 50 µl) 3. Make sure the spacers are clean by rubbing them on the glove (if no trace of grease is found they are clean) 4. Press the spacer tightly on the syringe to be sure of the weight of MO is correct tare the balance with the empty syringe and weigh it again with the MO in it 5. Once the weight of MO is established set the pipette for slightly more (2 to 5 µl). Press the tip full of MO hard against the syringe and slowly move the plunger down (no air can go inside) 6. Once the MO syringe is loaded you can load the other one with the protein, using the same method previously used 7. Connect the first syringe, loaded with protein, to the connector by holding the metal parts. Once it's connected push the plunger very slowly until you see a drop of protein forming at the end of the connector. This is to avoid air bubbles in the syringe system. Then connect the syringe with MO on the other side of the connector 8. Mix the two for about 5 minutes or until LCP is created (becoming totally transparent with no ripples). Push the LCP into the smaller of the syringes, put the needle and crew the cap and dispense with the mosquito. Crystallization screens those are specific to the membrane proteins such as MemGold, MemGold2, MemStart & MemSys and MemMeso were used and the sandwich LCP plates were incubated at 20°C. These experiments were performed in

collaboration with the postdoctoral fellow Dr. Raghavendra SK Nagampalli and the laboratory of Dr. Isabel de Moraes, at the Membrane Protein Laboratory, Diamond Light Source, Didcot, UK.

2.29. Expression and purification of recombinant Membrane Scaffold Protein (MSP).

MSPs Plasmids, pMSP1D1, pMSP2N2, pMSP1E3D1, were acquired from Addgene (plasmids #20061, # 29520, #20066 respectively). The expression and purification were carried out as described(BAYBURT; GRINKOVA; SLIGAR, 2002) with minor modifications. The purified plasmids were transformed into competent BL21 (DE3) *Escherichia coli*, Rosetta2 strain (EMD Biosciences, Darmstadt, Germany), and plated on LB-agar containing appropriate antibiotics. A single colony was grown overnight at 37◦C in 30 ml LB medium containing 30 mg/ml kanamycin with shaking at 180 rpm to generate a starter culture. The starter culture was added to 0.5–1 litre of LB medium and incubated at 37°C with shaking at 180 rpm until an OD 585 of 0.6–0.7 was reached. MSP production was induced by adding isopropyl b-D-1-thiogalactopyranoside (IPTG) to a final concentration of 1 mM. The cells were harvested 3–4 h after induction by centrifugation (3000 g, 30 min). The cell pellet was stored at 80 °C or used directly for purification. MSPs were purified following the methodology described by Inagaki et al. (INAGAKI; GHIRLANDO; GRISSHAMMER, 2013) . Briefly, the stored cell pellet (20 g) were resuspended in 50 ml of buffer A (50 mM Tris, pH 7.4, 200 mM NaCl), and then passed twice through a Cell disruptor. Cell debris was removed by centrifugation at 55,000 rpm for 45 min and 4 °C in a Type 70 Ti rotor on a Beckman Coulter Optima L-90K Ultracentrifuge, and then imidazole was added to the supernatant to a final concentration of 25 mM. The sample was passed through a 0.2 µm filter (Stericup, Millipore, CA, USA) and loaded onto a Ni-NTA column (8 ml bed volume, Qiagen, CA, USA), equilibrated with buffer B (buffer A containing 25 mM imidazole). The resin was washed with buffer B and MSPs were eluted with buffer C (buffer A containing 280 mM imidazole). 3 Fractions containing MSP were identified by SDS-PAGE. Pooled fractions were concentrated, and the imidazole was removed by passage over Superdex 200 10 300 column (GE Healthcare) equilibrated with buffer A. Sample was stored at -80 °C or used directly for reconstitution. These experiments were performed in collaboration with the postdoctoral fellow Dr. Raghavendra SK Nagampalli and Dr. Zeyaul Islam.

2.30. hMPC2-GFP assembling into MSP.

1 mg soybean azolectin (Sigma) was dissolved in chloroform and dried in N2, protected from light. Dried phospholipids were solubilized in 1ml buffer containing, 20 mM Tris pH 8.0, 150 mM NaCl, 5 % glycerol, 0.05 mM TCEP and 0.058% DDM-CHS, vortex/heat (60 °C) every 10 minutes for 1 hour, then bath sonicated for 1 min at RT and then stored on ice. The phospholipid solution was freshly prepared for each reconstitution experiment. For incorporation of the hMPC2 in lipid nanodiscs, the MPC solubilized in DDM were mixed with soybean azolectin solution and the MSP to a final MPC/MSP/Lipids molar ratio of 1:4:40, The mixture was incubated for 20 min at RT. A control sample was prepared with no MPC added at this step. Detergent extraction, leading to the assembly of MPC-MSP lipid nanodiscs or proteo-liposomes in the control sample, was accomplished by bio-beads to a final mg ratio of 200:1 bio-beads/lipids. The samples were incubated for 5, 5 and 45 minutes and finally subjected to centrifugation (80,000 g, 45 min, 4◦C) to separate the nanodiscs from any large aggregates and liposomal material. The collected supernatant was injected into a superdex 200 10 300 column previously equilibrated with 20 mM Tris pH 8.0, 150 mM NaCl and collected only the fluorescence fraction (since GFP attached to hMPC). These experiments were performed in collaboration with the postdoctoral fellow Dr. Raghavendra SK Nagampalli and Dr. Zeyaul Islam.

2.31. Purification of SMA-encapsulated MPC2.

hMPC2-GFP Membrane pellet was resuspended to 50mg/ml in buffer A (50 mM Tris-HCl pH 8, 0.25 M NaCl, 10% Glycerol) then the SMA solution XIRAN® SL 30010 P20 (Polyscope Polymers B. V.), was directly added to a final concentration of 2.5%. After incubation for 3 hours continuous stirring at room temperature, the solution was centrifuged at 185,500g for 45 to remove un-solubilized particles. The supernatant was then incubated overnight at 4°C with Cobalt or Nickel beads resin (5ml resin per gram of membrane pellet) previously equilibrated with buffer B (50 mM Tris-HCl pH 8, 0.15 M NaCl,3% glycerol). Affinity chromatography was made by gravity washing resin with 20 CV of buffer B followed by 5 CV of buffer B containing 20 mM Imidazole and then eluted with 2 CV of Buffer B containing 200mM Imidazole. The dropwise collected fractions were pooled and concentrated injected to a Superdex 200 10 300 column previously equilibrated with 50 mM Tris pH 8.0, 150 mM NaCl and collected only the fluorescence fraction (since MPC contains GFP attached). Same protocol was executed to test

other SMA products such as DIBMA, SMA2000, and other XIRAN polymers. The experiment was conducted under the supervision of Naomi Pollock at University of Birmingham - UK.

2.32. Negative staining sample preparation.

5µL of protein solution (0.1mg/mL) was placed onto a carbon-coated copper previously glow discharged carbon coated grid and incubated for 1 min. In parallel 4 drops of 2% Uranyl Acetate (UA) stain was pipetted onto a piece of parafilm. After incubation, sample was removed using filter paper followed by 4 cycles of incubation/blotting (Pick up 1drop of UA with the grid, leave 1 min and remove with filter paper), finally air dry. Grids were imaged using a Talos microscope fitted with a Tungsten filament operating at 120 kV. The experiment was conducted under the supervision of Saskia at University of Warwick - UK.

2.33. Cryo-EM grids preparation and sample conditions.

GO solution 10X (Sigma) was diluted to 0.2mg/mL with distillated water, and centrifugated at approximately 300 RCF to remove aggregates. 3ul of diluted GO solution was placed incubated for 1 minute onto carbon side of Au 300 R1.2/1.3, 300 mesh grids (Quantifoil Micro Tools GmbH, Jena, Germany), previously glow discharged for 40sec at 0.2mBar and 40mA and. In parallel we prepared 3 drops of 20ul ddH2O in a clean area (e.g. with parafilm). After incubation, GO solution was removed with filter paper followed by two times wash (take up first drop of ddH2O with the carbon side and remove with the filter paper, same for the second drop) and finally a third wash (take up third drop of ddH2O with the back side of the grid, remove with filter paper and dry for 5 minutes). 3ul of 0.1mg/ml protein sample was place onto the previously prepared grid, the grid was blotted (30sec wait, 4 sec Blotting, 10 Blot force and 100% Humidity) and flash-frozen in liquid ethane with a FEI Vitrobot Mark IV. CryoEM grids were loaded into a FEI Titan Krios G3 electron microscope operated at 300 kV. These experiments were performed in collaboration with Dr. Christos Savva at Cryo-EM Facility of University of Leicester.

2.34. Data Acquisition and Image Processing.

Best grids were used for data collection in Titan Krios transmission microscope with a Volta phase plate that enables near-atomic resolution single-particle reconstruction. Image data are ideally recorded in super-resolution mode as multi-frame exposures of each region of interest. Multi-frame exposures were recorded using a Falcon 3 direct electron detector cameras (DED), after searching for straight ice-embedded proteins spanning holes in the carbon support film. Spherical aberration coefficient (cs) was 2.7mm, and the nominal magnification 75K, the calibrated physical pixel size was 1.08 Å. The values for second condenser aperture and the illumination area was 50µm and 1.8 µm respectively. Defocus range was stablished at -0.7 µm, and the dose rate on specimen 0.7 e-/pix/sec, fractionated from 75 frames, finally the specimen was exposed for 60 seconds. These experiments were performed in collaboration with Dr. Christos Savva at Cryo-EM Facility of University of Leicester.

Since the total dose given to an area of interest is fractionated, images were aligned by post-processing to eliminate specimen movement originating from the physical drift of the specimen stage To correct specimen motion, we used MotionCor2 software(ZHENG et al., 2017), Local contrast-transfer functions were estimated from aligned non-dose-weighted micrographs using GCTF ().All subsequent image-processing steps were performed on the dose-weighted micrographs using the single-particle method reconstruction as implemented in RELION(SCHERES, 2012) or CryoSPARC(PUNJANI et al., 2017), Best micrographs were selected by inspection of Fourier Transforms (FT) of the images. Reference-free two-dimensional classification applied to the extracted particles until obtain best quality classes. The experiment was conducted under the supervision of Sarah Lee at University of Birmingham - UK.

2.35. Lipid extraction and Thin Layer Chromatography (TLC) analysis.

To MPC2-GFP membrane extract diluted at 0.5mg/ml were added add 2ml methanol and 1ml chloroform, the mixture was vortexed for 10 minutes then heated for 30 minutes at 50 C, and vortex again for 10 minutes. Sample was centrifugated at 16,000 × g for 10 minutes (15 – 20 C), the organic layer was collected and dried at 40C. 1 – 5ul of the lipid extracts were spotted onto a TLC silica gel plate and *E. coli* lipids (PE, PG, and CL) were used as a reference. Lipid separation was performed having the mobile phase composed of methanol, acetic acid and chloroform in the

ratio of 12.5:4:32.5 and were visualized by heating TLC plates treated previously with Phosphomolybdic Acid (PMA) solution in order to activate the stain.

CHAPTER 3. RESULTS

3.1. Purification of recombinant MPC.

Human MPC1 and MPC2 proteins were co-expressed from codon-optimized genes in a heterologous yeast system (*Saccharomyces cerevisiae* JRY472) that was modified to lack endogenous MPC (Δ*mpc1/2/3*). This mutant strain is hereafter referred to as 3Δ (BRICKER et al., 2012). All restriction maps used in this thesis are listed in Figure 3. A bi-directional expression plasmid was initially engineered to contain MPC1 fused to an 8xHis tag and MPC2 linked to a cleavable monomeric GFP (Fig. 3 and 4A). This system enabled the detection of inducible expression levels and cellular compartmentalization as well as subsequent purification via cobalt-based immobilized metal affinity chromatography (Co-IMAC) of the target complex. Controlled expression (Fig.4B) and proper mitochondrial localization of MPC were confirmed (Fig.4C), using an alternative plasmid (Fig.3D). n-Dodecyl-β-D-maltoside (DDM, at 1 %) was identified as a suitable detergent for the extraction of proteins from membrane pellets. The target proteins were purified via Co-IMAC, followed by gel-filtration chromatography (GF), both of which were carried out in the presence of 0.03 % DDM (Fig. 4A, center panel). A sharp monodisperse peak was obtained after GF, which corresponded to a molecular weight of 64 kDa for the protein-detergent complex (Fig.4A, right panel). Surprisingly, the peak sample derived from human MPC1 was strongly associated with the yeast 60S ribosomal protein L28, both bands were identified using mass spectrometry (Table 1). In addition, traces of co-purified, GFP-fused MPC2 were confirmed via silver staining and in-gel fluorescence (Fig. 4A, inset).

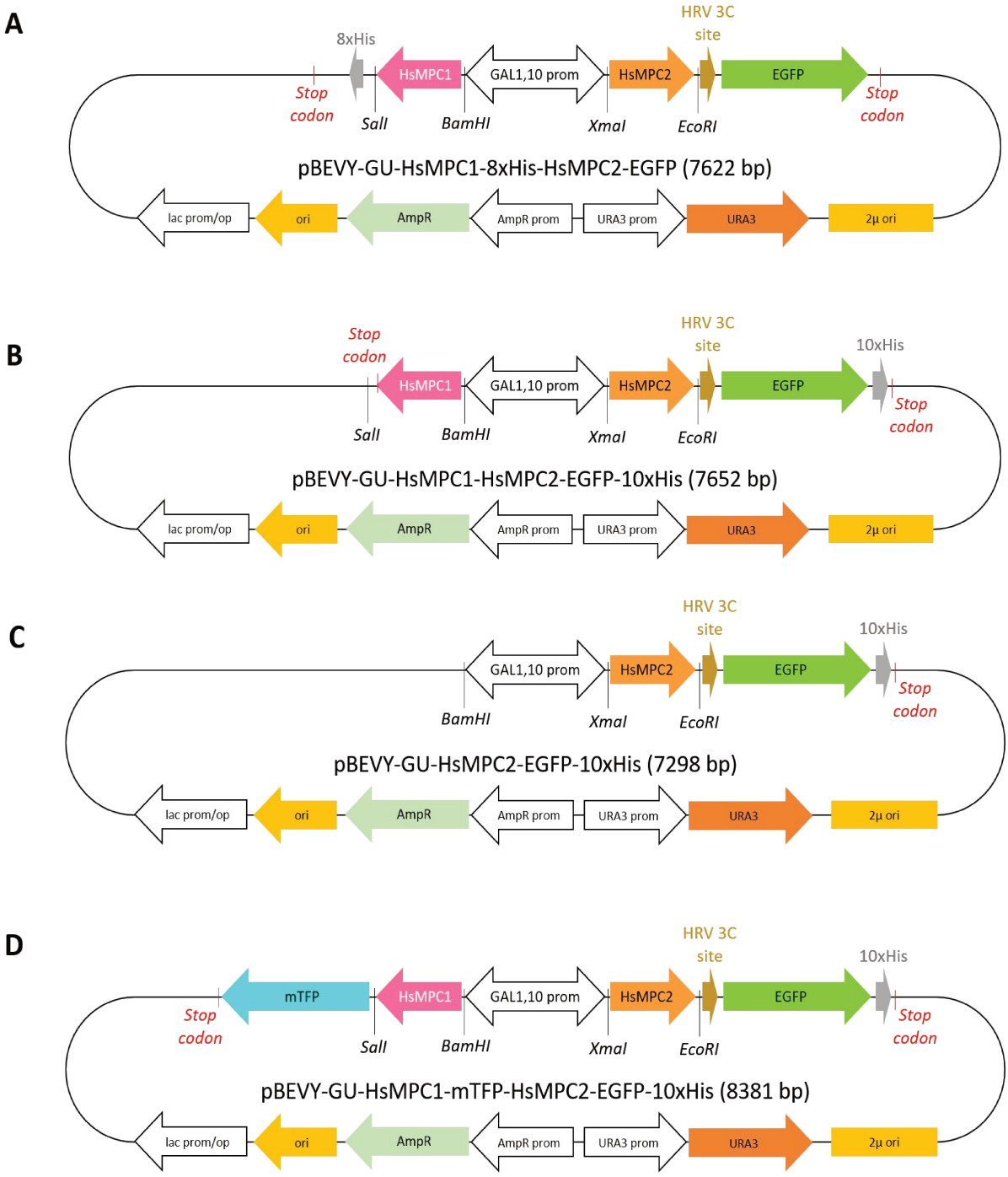

Figure 3. Restriction maps and modifications used in this thesis. **A**. pBEVY-GU plasmid containing Human MPC1 and six histidine tag fused to its C-terminal and MPC2 fused to EGFP. **B**. The six Histidine tag of MPC1 was removed and ten histidine tag was added after

EGFP in MPC2. **C**. Human MPC1 was completely removed from pBEVY-GU plasmid. **D**. An alternative plasmid was generated containing only a fluorescent protein mTFP after MPC1.

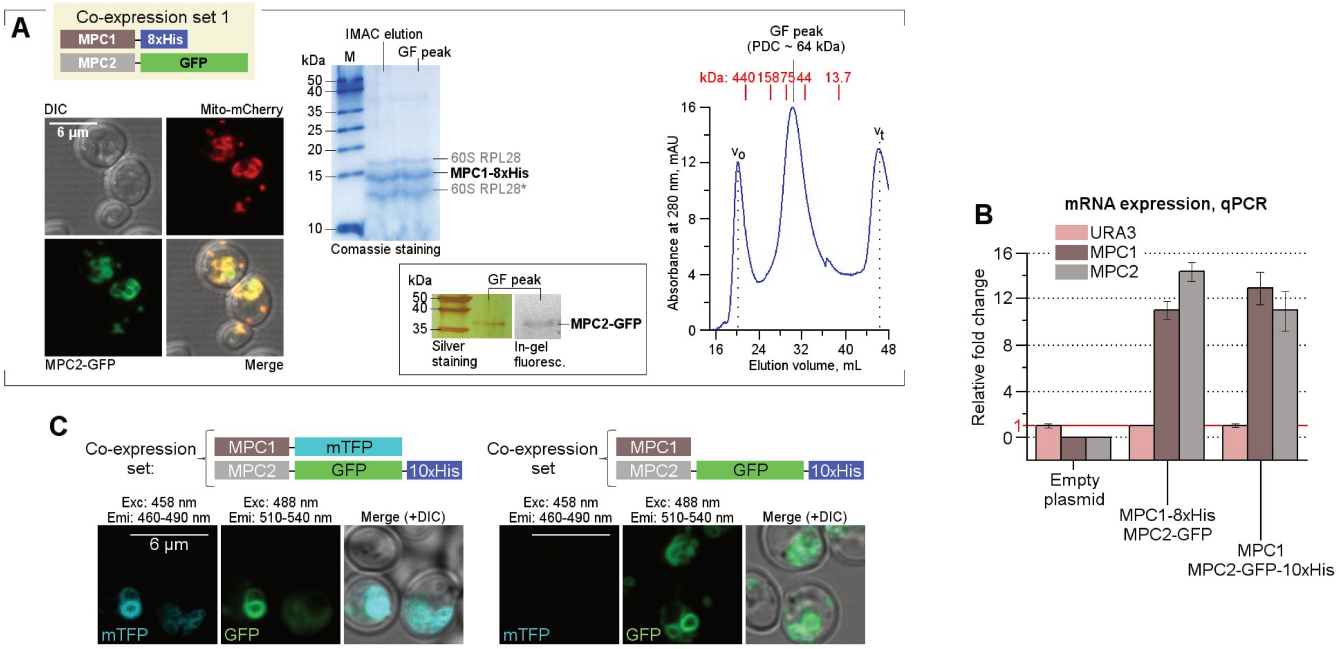

Figure 4. Recombinant expression and purification of human MPC. (A) A schematic of the initial human MPC protein constructs expressed in yeast (co-expression set 1). Left panel: Proper localization to the mitochondria was confirmed via confocal microscopy. DIC: Differential interference contrast. Middle panel: Electrophoretic analysis of MPC1-8xHis samples purified using Co-IMAC and GF. *N-terminally truncated portion of 60S RPL28. The inset displays the silver staining and in-gel fluorescence detection of trace amounts of MPC2-GFP, which co-purified with MPC1. Right panel: The corresponding GF trace showed a predominant protein-detergent monodisperse peak at approximately 64 kDa. **(B)** In order to confirm the proper expression of the recombinant MPC subunits at the transcriptional level, and under control of galactose-inducible promoters GAL1 (for MPC1) and GAL10 (for MPC2), quantitative polymerase chain reaction (qPCR) was performed, upon mRNA extraction. Expression of actin was used a housekeeping marker and subsequent normalization by URA3 levels was performed. Values are given as expression fold change, relative to URA3 expression (red solid line). Values are mean ± s.d. (for quadruplicates). **(C)** Mitochondrial localization of MPC1 is confirmed, by the specific detection of a C-terminally fused mTFP (left panel), compared to unlabelled MPC1 (right panel). Respective excitation wavelengths and the emission detection windows for emission are described. Figure adapted from (NAGAMPALLI et al., 2018).

Intrigued by the trace amounts of human MPC2 isolated during the complete purification of MPC1, as well as the lower-than-expected molecular weight, we generated an alternative plasmid construct. In this new construct, the poly-histidine tag from MPC1 was transferred to the C-terminus of the MPC2-GFP fusion (Fig. 3B and 5), similar to a previously successful approach employed for other eukaryotic membrane proteins expressed in yeast (NEWSTEAD et al., 2007). Upon confirmation of proper mitochondrial localization of the new construct (Fig. 5B, left panel), the recombinant proteins were successfully extracted with 1 % C12E8 (octaethylene glycol monododecyl ether) and purified in the presence of 0.03 % DDM via Co-IMAC, followed by GFP-10xHis removal and GF (Fig. 5, middle panel). Again, a single monodisperse protein-detergent peak was obtained, which corresponded to a molecular weight of 70 kDa (Fig. 5, right panel). This sample was shown to exclusively contain MPC2, which was then purified to homogeneity (Table 2).

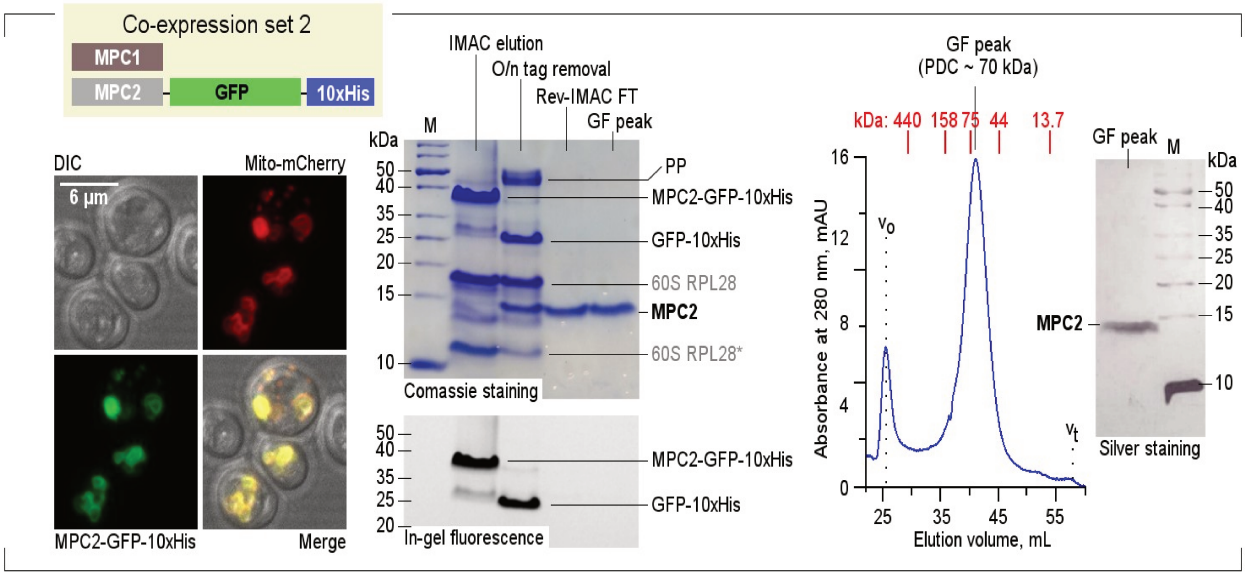

Figure 5. Alternative strategy for the recombinant expression and purification of human MPC. Diagram of the alternative MPC constructs (co-expression set 2) and corresponding confocal microscopy (left panel). Middle panel: Electrophoretic (Tricine-SDS-PAGE) analysis of representative chromatography steps. PP: PreScission Protease. Right panel: GF peak and silver staining analysis revealed that pure monodisperse MPC2 (associated with DDM) was obtained at an equivalent molecular weight of 70 kDa. In all GF profiles above, vo indicates void volume, and vt indicates the total liquid volume of the GF column. The corresponding elution volumes for calibration standards are shown in red. Figure adapted from (NAGAMPALLI et al., 2018)

Table 1. Identification of the purified protein bands by liquid chromatography coupled to tandem mass spectrometry (LC-MS/MS). Table adapted from (NAGAMPALLI et al., 2018)

Co-expression strategy and the respective bands identified	
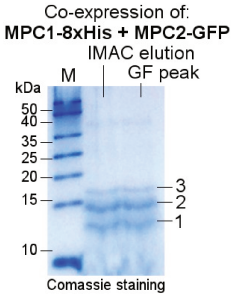	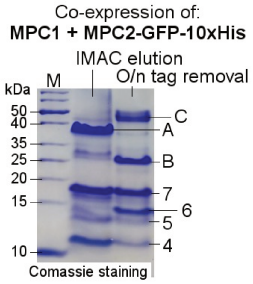

Bands identified by LC-MS/MS					
Band	**Protein**	**Database (accession number)**	**Sequence coverage, %**	**# of matches**	**Top-three highest score peptide sequences**
1	60S RPL28	Yeast (P02406)	49	42	ETAPVIDTLAAGYGK SASKETAPVIDTLAAGYGK IPNVPVIVK
2	MPC1	Human (Q9Y5U8)	70	43	NWLLFACHATNEVAQLIQGGR DYLMSTHFWGPVANWGLPIAAINDMK SPEIISGR
3	60S RPL28	Yeast (P02406)	53	79	ETAPVIDTLAAGYGK SASKETAPVIDTLAAGYGK INMDKYHPGYFGK
4	60S RPL28	Yeast (P02406)	46	38	ETAPVIDTLAAGYGK GRIPNVPVIVK IPNVPVIVK
5	60S RPL28	Yeast (P02406)	49	51	ETAPVIDTLAAGYGK SASKETAPVIDTLAAGYGK GRIPNVPVIVK
6	MPC2	Human (O95563)	73	107	LSTAQSAVLMATGFIWSR LLDKVELMLPEK TVFFWAPIMK
7	60S RPL28	Yeast (P02406)	53	79	ETAPVIDTLAAGYGK SASKETAPVIDTLAAGYGK INMDKYHPGYFGK

Other relevant bands (not by LC-MS/MS)		
Band	**Protein**	**Means of detection**
A	MPC2-GFP-10xHis	Inducible expression, Detected by In-gel fluorescence
B	GFP-10xHis	Cleavage product, Detected by In-gel fluorescence
C	PreScission Protease	Artificially added for tag cleavage

Table 2. Mass spectrometry identification of yeast proteins co-purified with human MPC2 (as in main text Figure 4). Table adapted from (NAGAMPALLI et al., 2018).

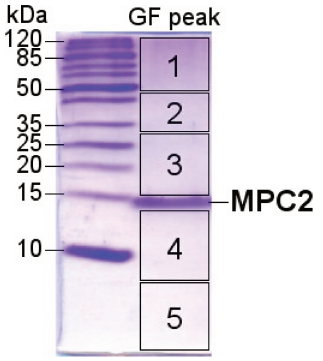

Region	Matches	Expected MW	Uniprot ID	Sequence coverage, %	Number of matches
1	Peptide matches not assigned to protein hits				
2	Zuotin	49	P32527	3	2
3	RANBP1	23	P41920	3	1
4	Peptide matches not assigned to protein hits				
5	60 RPL28	17	P02406	24	5

3.2. Functional reconstitution of MPC in lipid vesicles.

To evaluate the pyruvate transport activity of recombinant purified MPC *in vitro*, we reconstituted both purified protein products, individually and in combination, into asolectin liposomes (Fig. 6A-B). The choice for asolectin was based on previous literature (NAŁECZ et al., 1986).

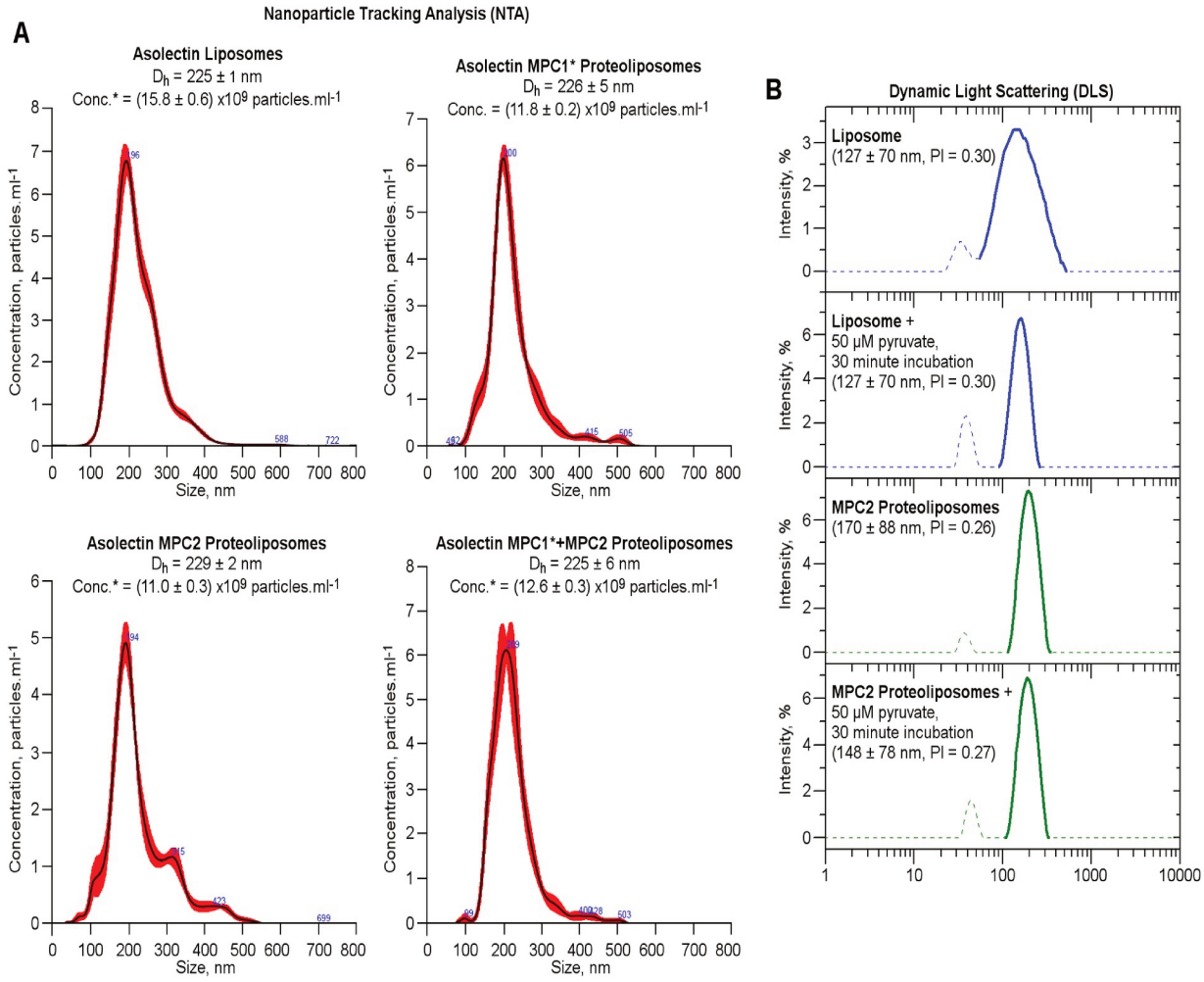

Figure 6. Qualitative analysis of lipo- and proteoliposomes. (A) Size and concentration analysis of asolectin liposomes, MPC1*, MPC2 and MPC1*+MPC2 proteolipsomes using Nanoparticle tracking analysis (NTA). An asterisk (*) indicates that MPC1 was co-purified with yeast RPL28. **(B)** To check for undesired swelling or bursting during the transport assays, protein-free liposomes and MPC2 proteoliposomes size distributions were assessed by dynamic light scattering (DLS) for before and after 30min incubation with 50 µM pyruvate. Figure adapted from (NAGAMPALLI et al., 2018).

Two independent approaches were adopted to demonstrate the protein-mediated substrate transport: (i) the canonical quantification of the increase in intravesicular ^{14}C-labelled pyruvate (BENDER; PENA; MARTINOU, 2015; BRICKER et al., 2012; HALESTRAP; P, 1975; HERZIG et al., 2012) and (ii) the quantification of the decrease in extravesicular pyruvate, as indicated by the enzymatic activity of lactate dehydrogenase A (LDHA). A pH gradient-dependent assay (ΔpH = 1.5) was derived in accordance with the chemical conditions recently established for mouse MPC (GRAY; RAUCKHORST;

TAYLOR, 2016). Notably, successful pyruvate transport activity was not observed for proteoliposomes reconstituted with MPC1 co-purified with RPL28 and traces of MPC2 (termed MPC1*). By contrast, compared to protein-free liposomes, which were used as a control, proteoliposomes containing MPC2 alone showed significant pyruvate transport activity. Similarly, vesicles co-reconstituted with comparable levels of MPC1* and MPC2 also induced the transport of pyruvate; however, the corresponding transport levels were similar to those obtained with MPC2 alone (Fig. 7).

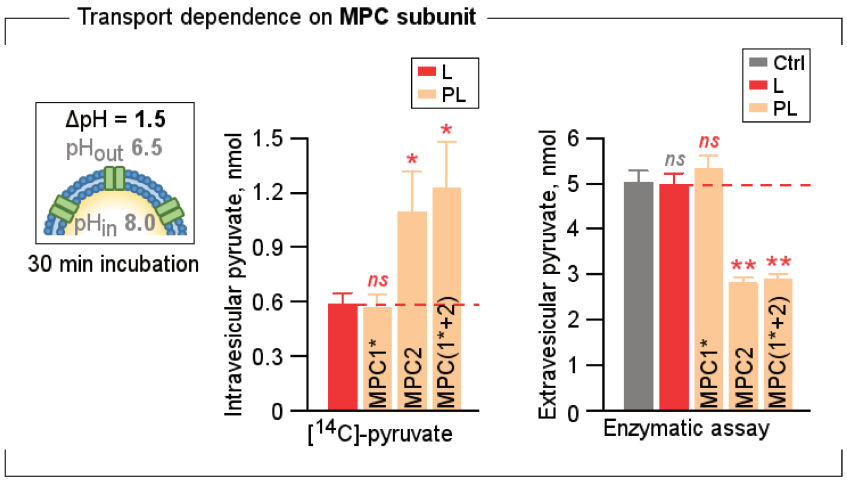

Figure 7. *In vitro* activity of MPC reconstituted into proteoliposomes. Quantification of intravesicular and extravesicular pyruvate, as detected based on ^{14}C radiolabeled assay (left panel) and enzymatic assay (right panel), respectively, in liposomes (L) and proteoliposomes (PL) reconstituted with MPC1 and MPC2 and a control condition free of lipid vesicles (Ctrl (-L/PL)). The inset indicates the pH gradient across the outer and inner vesicle environments. An asterisk (*) indicates that MPC1 co-purified with yeast RPL28. Figure adapted from (NAGAMPALLI et al., 2018).

Most importantly, the self-sufficient role of human MPC2 in pyruvate transport was further supported when this protein was overexpressed and purified from a plasmid construct lacking the MPC1 coding sequence (Fig 3C and 8A). As such, when reconstituted into proteoliposomes, this new construct (termed MPC2**) induced pyruvate transport across the bilayer at levels statistically similar to those mentioned above (Fig. 8B).

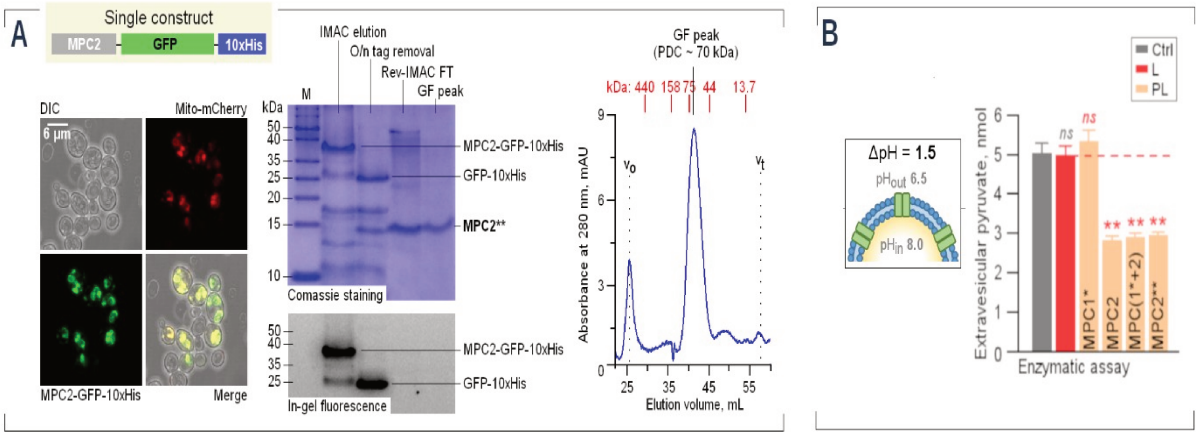

Figure 8. *in vitro* activity of alternative single construct MPC. (A). Diagram of the single expressed MPC2 construct and corresponding confocal microscopy (left panel). Middle panel: Electrophoretic (Tricine-SDS-PAGE) analysis of representative chromatography steps. PP: PreScission Protease. Right panel: GF peak analysis revealed that pure monodisperse MPC2 (associated with DDM) was obtained at an equivalent molecular weight of 70 kDa. In the gel-filtration profile above, v_o indicates void volume, and v_t indicates the total liquid volume of the GF column. The corresponding elution volumes for calibration standards are shown in red**. (B)** Quantification of extraliposomal pyruvate, as detected based on LDHA activity, in liposomes and proteoliposomes reconstituted with MPC1 and MPC2, individually and in combination. The inset indicates the pH gradient across the outer and inner vesicle environments. The control initial velocity for LDHA, at pH 6.5, in a liposome/proteoliposome-free condition is depicted as Ctrl (-L/PL), in black. An asterisk (*) indicates that MPC1 was co-purified with yeast RPL28. Two asterisks (**) indicate the activity of the MPC2 that was expressed and purified in the total absence of MPC1. Figure adapted from (NAGAMPALLI et al., 2018).

3.3. *In vitro* pyruvate transport is dependent on time and electrochemical gradient.

Within a pH gradient of 1.5 units, MPC2 proteoliposomes induced rapid pyruvate transport. Pyruvate intake, which exhibited saturation kinetics, was proficient during the first 5 to 10 min of incubation, presenting half-maximum efficiency between 2 to 4 min (Fig. 9A). The substrate concentration-dependence of uptake was also studied using radiolabeled substrate. The K_m value for pyruvate of MPC2 in artificial vesicles is 1.1 ± 0.4 mM (Fig. 9B). Similarly, the necessity of MPC2 activity on a *proton* electrochemical gradient was further confirmed; when the pH gradient was collapsed (ΔpH = 0), a decrease in pyruvate transport activity of about 70 to 80% was observed (Fig. 9C). The residual transport activity at ΔpH = 0 likely reflects the chemical potential of pyruvate moving down its own concentration gradient.

To quantify the decrease in extravesicular pyruvate as a function of pH, proper enzymatic activity calibration was carried out (Fig. 9D).

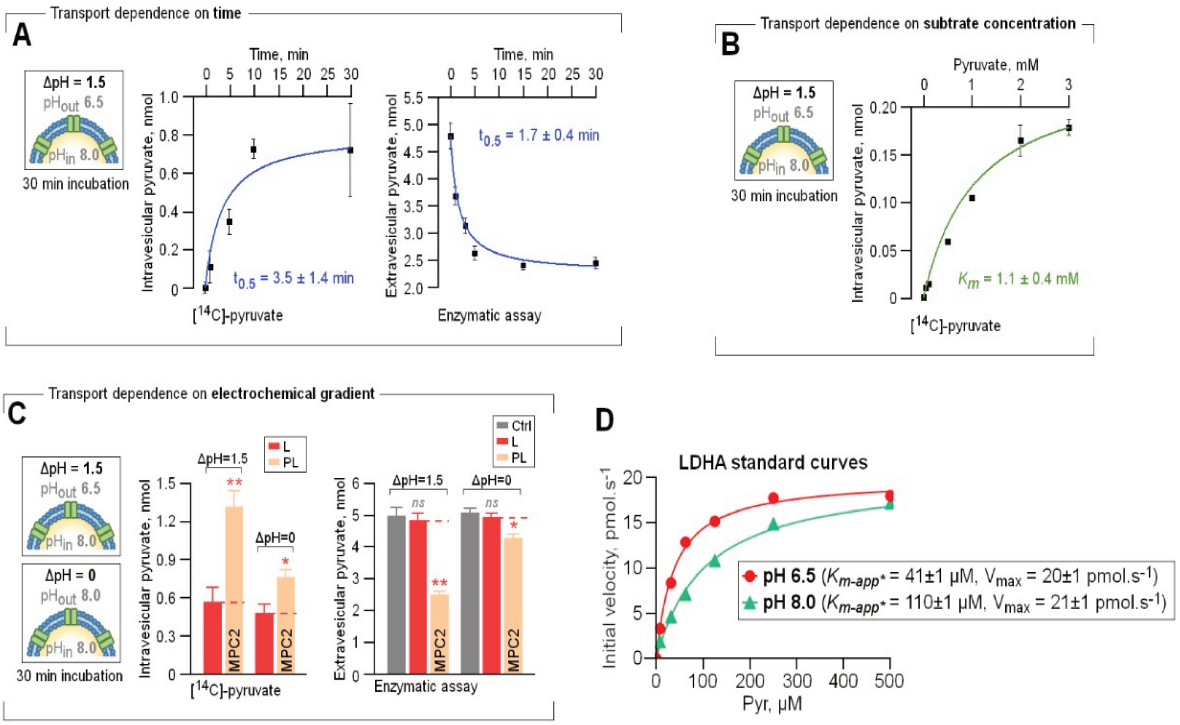

Figure 9. *in vitro* pyruvate transport is dependent on time, substrate concentration and electrochemical gradient. (A) Quantification of intravesicular and extravesicular pyruvate, as detected based on ^{14}C radiolabeled assay (left panel) and enzymatic assay (right panel), respectively in the MPC2-proteoliposome as a function of different incubation times with a ΔpH of 1.5 units. The inset indicates the pH gradient across the outer and inner vesicle environments. Half-maximum times were obtained by the fitting of hyperbolic saturation curves (solid blue lines, R^2 = 0.99 in both graphs. **(B).** Quantification of intravesicular pyruvate as detected based on ^{14}C radiolabeled assay in the MPC2-proteoliposome as a function of different pyruvate concentrations (0.125 mM - 3 mM) with a ΔpH of 1.5 units. The inset indicates the pH gradient across the outer and inner vesicle environments. The Km was obtained by fitting a hyperbolic saturation curve (solid green line, R^2 = 0.97). **(C)** Quantification of intravesicular and extravesicular pyruvate, as detected based on ^{14}C radiolabeled assay (left panel) and enzymatic assay (right panel), respectively in liposomes (L) and MPC2-proteoliposome (PL) after 30 min of incubation for ΔpH = 1.5 and ΔpH = 0. The inset indicates the pH gradient across the outer and inner vesicle environments. **(D)** Standard kinetic curves for LDHA, from which Michaelian parameters were extracted from different conditions and respective hyperbolic fitting: pH 6.5 (red circles) and pH 8.0 (green triangles). The respective apparent Km (Km-app, in respect to the final NADH concentration of 125 µM) and maximum velocities (Vmax) are indicated. Figure adapted from (NAGAMPALLI et al., 2018).

3.4. *In vitro* pyruvate transport is sensitive to chemical inhibition, redox modification, and substrate type.

The previous landmark demonstration of the carrier-dependent transport of pyruvate across the IMM involved the identification of monocarboxylate mimetic cinnamates as effective and specific MPC inhibitors (HALESTRAP; DENTON, 1974). In the present study, compared to the vehicle control (DMSO), UK-5099, a potent cyanocinnamate ($K_i \approx 10$ nM in mitochondrial extracts (HILDYARD et al., 2005), did not exert any significant inhibitory effect on *in vitro* MPC2-dependent pyruvate transport when used at a final concentration of 50 µM, as shown in (Fig. 10). On the other hand, when compared to the vehicle control, rosiglitazone (Rgz), at 50 µM, significantly decreased the MPC2-dependent internalization of pyruvate, by over 60 %, as shown in (Fig. 10). The finding that a thiazolidinedione (TZD) derivative, such as rosiglitazone, can directly and specifically decrease MPC2 activity has been substantiated by previous studies (COLCA et al., 2013; DIVAKARUNI et al., 2013); thus, further confirming the protein-mediated component of *in vitro* pyruvate transport.

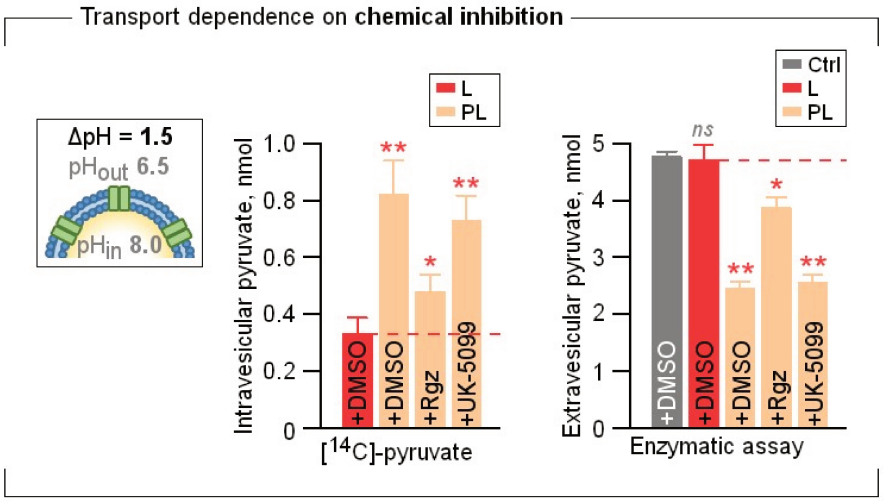

Figure 10. Pyruvate transport is dependent on chemical inhibition. Quantification of intravesicular and extravesicular pyruvate, as detected based on ^{14}C radiolabeled assay (left panel) and enzymatic assay (right panel), respectively in liposomes (L) and MPC2-proteoliposome (PL) in the presence of DMSO (vehicle control) and the well-established MPC inhibitors UK-5099 and rosiglitazone (Rgz). The inset indicates the pH gradient across the outer and inner vesicle environments. For all experiments, results are reported as mean ± standard deviations from triplicates to sextuplicates. Statistical significances were assessed by Welch's unpaired *t* test, where *ns* = non-significant, * = $p < 0.05$ and ** = $p < 0.001$. Figure adapted from (NAGAMPALLI et al., 2018).

The inhibitory mechanism of cinnamates was originally shown to rely on a reversible Michael addition to a cysteine thiol group in MPC; loss of conjugation was achieved by the addition of reducing agents such as β-mercaptoethanol (HALESTRAP, 1976; HALESTRAP; P, 1975). Here, although the complete elimination of TCEP (TRIS(2-carboxyethyl)phosphine) from the early steps of membrane preparation up to proteoliposome reconstitution still permitted the standard purification of MPC2 (left and midel panel. Fig. 11), complete functional inactivation was observed (right panel. Fig. 11). Re-incubating MPC2 with TCEP at the stage of proteoliposome reconstitution resulted in the recovery of approximately three quarters of the original activity (right panel. Fig. 11).

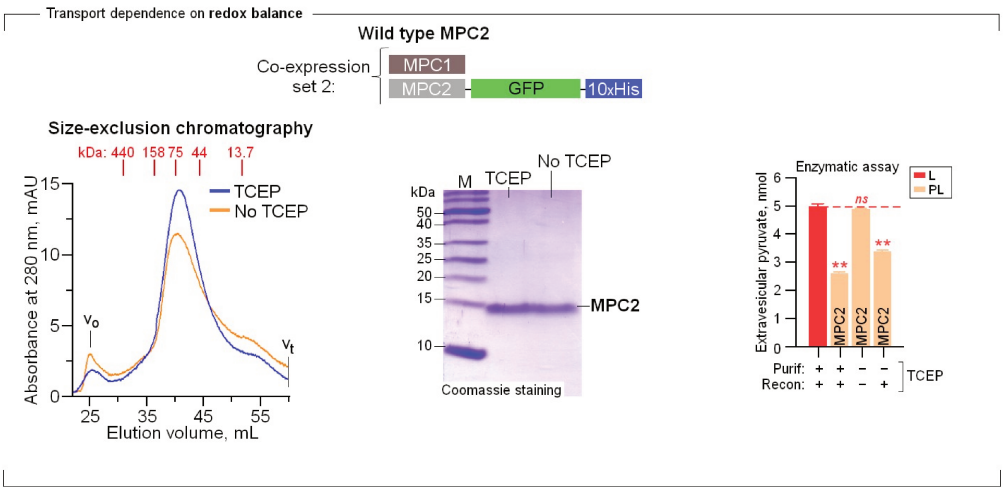

Figure 11. Purification of wild-type MPC2 in the absence of TCEP and its influence on pyruvate transport. A schematic depiction of human wild type MPC2-10xHis protein constructs co-expressed in yeast. Gel-filtration profile of wild type MPC2-10xHis in the presence (Blue) and absence TCEP (Orange). Peaks were obtained at an equivalent molecular weight of 70 kDa. v_o indicates void volume and v_t indicates the total liquid volume of the GF column. The corresponding elution volumes for calibration standards are shown in red. Inset represents the electrophoretic (tricine-SDS-PAGE) analysis of wild type MPC2-10xHis in the presence and absence of TCEP. The results enclosed in the right box depict the cinnamte independent transport activity of wildtype MPC2. Quantification of extraliposomal pyruvate in liposomes (L, red) and proteoliposomes reconstituted with wild-type MPC2 (PL, orange) in the presence and absence of TCEP, as well as supplemented TCEP. Figure adapted from (NAGAMPALLI et al., 2018).

To further explore the importance of redox modification on human MPC2 function, we generated a point mutant by replacing the single cysteine residue at position 54 with serine (left and center panel. Fig.12). Although the overall activity of the isosteric mutant (termed MPC2.C54S) was compromised, it was distinctly insensitive to TCEP (right panel. Fig.12). Together, however, these findings suggest that competent pyruvate transport also relies on a sulfhydryl-sensitive site on MPC2.

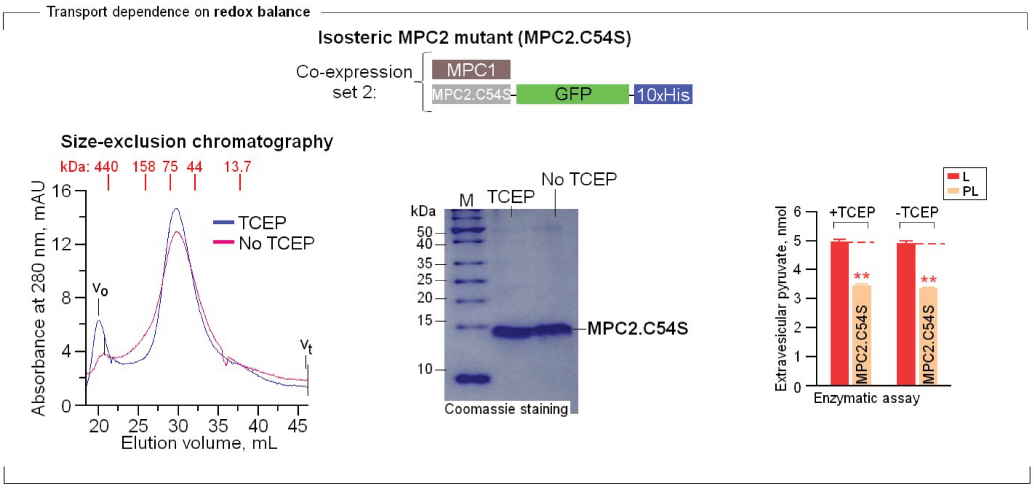

Figure 12. Purification of the isosteric MPC2 mutant (MPC2.C54S) TCEP and its influence on pyruvate transport. A schematic depiction of isosteric MPC2 mutant (MPC2.C54S) protein constructs co-expressed in yeast. Gel-filtration profile of isosteric MPC2 mutant (MPC2.C54S) in the presence (Blue) and absence TCEP (Pink). Peaks were obtained at an equivalent molecular weight of 70 kDa. v_o indicates void volume and v_t indicates the total liquid volume of the GF column. The corresponding elution volumes for calibration standards are shown in red. Inset represents the electrophoretic (tricine-SDS-PAGE) analysis of isosteric MPC2 mutant (MPC2.C54S) in the presence and absence of TCP. Quantification of extraliposomal pyruvate in liposomes (L, red) and proteoliposomes reconstituted with the isosteric MPC2 mutant (MPC2.C54S) in the presence and absence of TCEP. Figure adapted from (NAGAMPALLI et al., 2018).

Finally, among all of the many monocarboxylates metabolized in the cell, lactate and pyruvate are directly linked and structurally similar. However, MPC2 appears to be selective for pyruvate over lactate, as no detectable transport of the latter was observed over the range

of concentrations tested and under the chemical conditions shown to be successful for pyruvate (Figure 13).

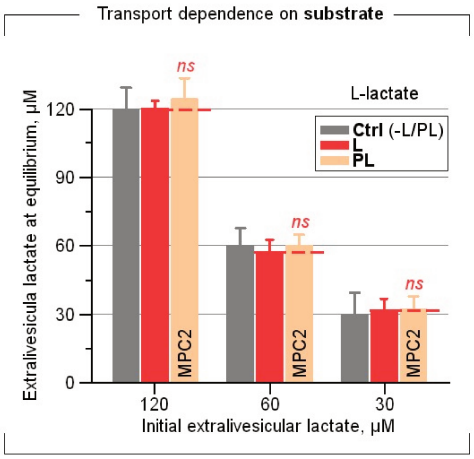

Figure 13. Substrate transport dependence of MPC. Quantification of extraliposomal lactate in liposomes (L, red) and proteoliposomes reconstituted with wild type MPC2-10xHis (PL, orange). Figure adapted from (NAGAMPALLI et al., 2018).

3.5. Ectopic expression of human MPC2 stimulated growth and induced glucose-dependent respiration in yeast.

The yeast strain JRY472 (3Δ), used in the present study to produce recombinant human MPC, carries a mutation in the *leu2* gene and is therefore dependent on external leucine to grow. In order to study the metabolic dependences on leucine and valine, as a function of MPC2 activity, cells were co-transformed with the plasmid pYES2 (LEU2). When cultured on synthetic dropout medium lacking both leucine and valine (-Leu -Val), this mutant strain grew with a doubling time of 123 ± 3 min (Fig. 14A, empty green circles). The sole ectopic expression of human MPC2 in this strain, however, decreased the doubling time by 57% (down to 53 ± 2 min; Fig. 14A, empty blue squares). Accordingly, expression of the MPC2 isosteric mutant (C54S), with expected intermediary transport activity compared with wild-type MPC2, showed a 42 % decrease in the doubling time of the same strain (71 ± 3 min; empty red triangles in Fig. 14A). Further supplementation of with only leucine (+Leu -Val) or only valine (-Leu +Val), or both amino acids (+Leu +Val), did not alter the doubling time of cells expressing MPC2 or MPC2.C54S (Fig. 14A; light colored shapes for individual nutrients and filled shapes for both nutrients at the same time). However, the individual or

combined addition of such amino acids significantly improved the doubling rates of 3Δ cells (bearing empty pBEVY plasmid) to about 85 minutes, or about 31% faster rates. Therefore, the improved growth of 3Δ cells expressing human MPC2 (as well as the isosteric mutant) reflect the mitochondrial use of glycolytic pyruvate for biosynthetic purposes, particularly for the production of branched chain amino acids.

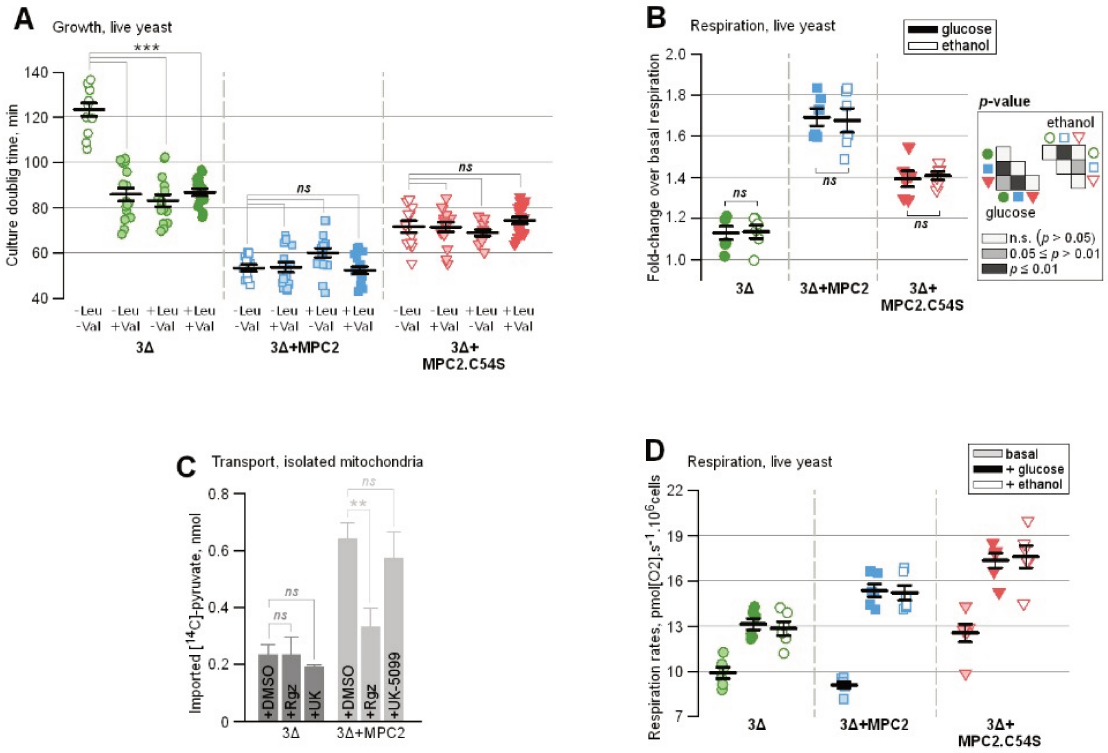

Fig. 14. Autonomous transport function of MPC2 *in vivo*. **(A)** Differential growth rates of 3Δ cells or JRY472 bearing an empty plasmid (green circles) or expressing either wild-type MPC2 (blues squares) or MPC2.C54S (red triangles) in the absence and presence of external leucine and valine. Lines indicate the mean ± standard error for three independent experiments. **(B)** Differential respiration rates of 3Δ cells or JRY472 (green circles) expressing either wild-type MPC2 (blues squares) or MPC2.C54S when exposed to glucose (filled geometric shapes) and ethanol (empty geometric shapes). Lines indicate the mean ± standard error for two independent experiments. **(C)** Quantification of imported pyruvate, as detected based on ^{14}C radiolabeled assay in isolated mitochondria from 3Δ yeast cells and 3Δ+MPC2 yeast cells in the presence of DMSO (control) and the inhibitors rosiglitazone (Rgz) and UK-5099. Results are reported as mean ± standard deviations from triplicates. **(D)** Oxygen consumption rates for 3Δ cells, displayed as basal rates (i.e., total absence of glucose, light colored shapes), after glucose addition (filled shapes) and after ethanol addition (empty shapes). Data for the control 3Δ cells transformed with empty pBEVY plasmid are shown as circles, and for 3Δ cells expressing either wild-type human MPC2 or the isosteric mutant (C54S) are shown as squares and triangles, respectively. In all cases, statistical significances

were assessed by Welch's unpaired *t* test, where *ns* = non-significant, * = $p < 0.05$, ** = $p < 0.001$ and *** = $p < 0.001$. Figure adapted from (NAGAMPALLI et al., 2018).

The ability of human MPC2 to stimulate pyruvate-dependent respiration in yeast cells was also evaluated by quantifying oxygen consumption in response to the addition of 0.08 % glucose to basal media. Whereas the mutant strain 3Δ responded to glucose addition with a slight, 10 % increase in oxygen consumption over basal respiration (1.1 ± 0.1-fold; filled green circles in Fig. 14B), the same cells expressing human MPC2 responded to glucose addition with a 70 % increase in oxygen consumption over basal respiration (1.7 ± 0.1-fold; filled blue squares in Fig. 14B). Again, as expected, the ectopic expression of MPC2.C54S led to a reduced increase in oxygen consumption over basal levels (1.4 ± 0.1-fold) in response to glucose addition (filled red triangles in Fig. 14B). To provide further evidence that all the added glucose was being oxidized via respiration, ethanol addition – which blocks residual fermentation – produced nearly the same response under all three test conditions (Fig. 14B, open shapes). Actual respiration rates are depicted in Fig. 14D.

Due to issues related to yeast cell wall permeability of both rosiglitazone and UK-5099, the inhibition sensitivity of MPC2 transport in a native environment was most properly addressed when mitochondria were extracted. First and most importantly, by comparing the incorporation of ^{14}C-pyruvate into mitochondria isolated from the both 3Δ and 3Δ+MPC2 yeast cells, we confirm that this subunit can play an autonomous role in promoting the active transport of this substrate (Fig. 14C). In addition, the same MPC2 response profile (or lack thereof) to rosiglitazone and UK-5099 as in the artificial vesicle system is herein established (Fig. 14C).

3.6. Oligomeric nature and secondary structure composition of human MPC2.

The lower-than-expected molecular weight of the purified protein-detergent complex that was obtained above (Fig. 3-5), led us to further investigate the oligomeric assembly of the functional MPC2. First, by isolating the mitochondrial extracts (DIEKERT et al., 2001), followed by short-range chemical crosslinking using disuccinimidyl suberate (DSS, 11.4 Å

linker), we observed the formation of MPC2 oligomers in its native lipid environment, starting from dimers up to higher-order molecular species, according to electrophoretic separation (Fig. 15A, left panel). When such an experiment was performed with purified protein, only the presence of dimeric species was resolved, probably due to the well-known association between the protein and the detergent (Fig. 15A, middle panel) (SEDDON; CURNOW; BOOTH, 2004). However, the subsequent reconstitution of purified MPC2 into proteoliposomes displayed a similar high-order, multi-species pattern that was observed in the mitochondrial extracts (Fig. 15A, right panel). This suggests that recombinant MPC2 in an artificial lipid bilayer, which was proven functional for pyruvate transport, shares oligomeric similarities to the native mitochondrial membrane environment.

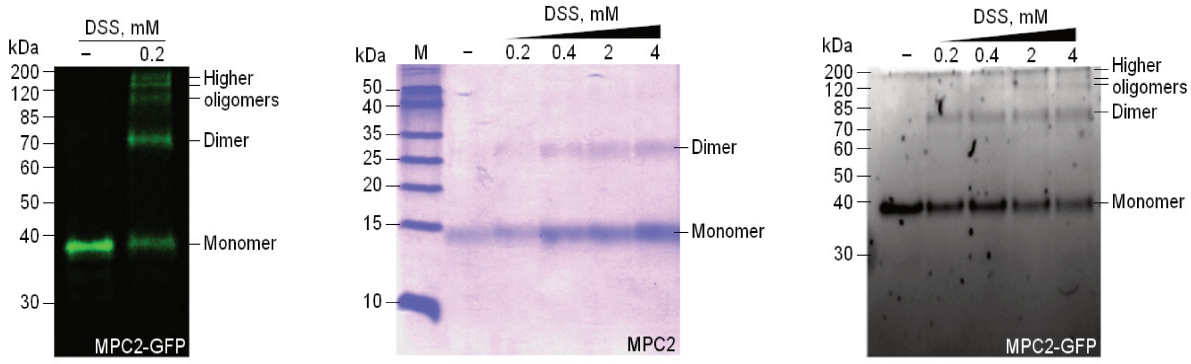

Figure 15. Oligomerization of human MPC2 by chemical cross-linking Chemical cross-linking suggested that MPC2 assembled into higher oligomers in a lipid environment. Left panel: Cross-linking of human MPC2 from isolated yeast mitochondrial extracts by 0.2 mM DSS. Middle panel: Cross-linking, using increasing DSS concentrations (0.2 – 4 mM), of purified MPC2-detergent (DDM) complex. Right panel: Cross-linking, using increasing DSS concentrations (0.2 – 4 mM), of purified MPC2 reconstituted in asolectin-derived lipid vesicles. Figure adapted from (NAGAMPALLI et al., 2018).

To investigate the secondary structure composition of human MPC2, and to gauge the conformational changes due to the binding of substrate and inhibitor, we performed synchrotron radiation circular dichroism (SRCD) analysis. SRCD indicated that this protein,

in the absence of any ligands, is predominantly helical in nature (Fig. 16, top left panel). The binding of pyruvate leads to improved structural stability since the helical content is increased from 44 % in the ligand-free control sample up to 56 % when the substrate is present (Fig. 16, top right panel); this might occur due to the fact that pyruvate needs to be transported across the channel of MPC2, by means of opening up or rearranging the structure. Conversely, the absence of TCEP lead to an overall increased disorder (Fig. 16, bottom left panel), which is in agreement with the lack of *in vitro* transport activity under a similar condition (Fig. 11-12). Notably, the addition of rosiglitazone had a minor impact on the secondary structure composition of MPC2 (45 % versus 44 % helices, respectively; Fig. 16, bottom right panel), which could probably be associated with weak binding and thereby explaining its limited inhibitory effects on *in vitro* transport (Fig. 10).

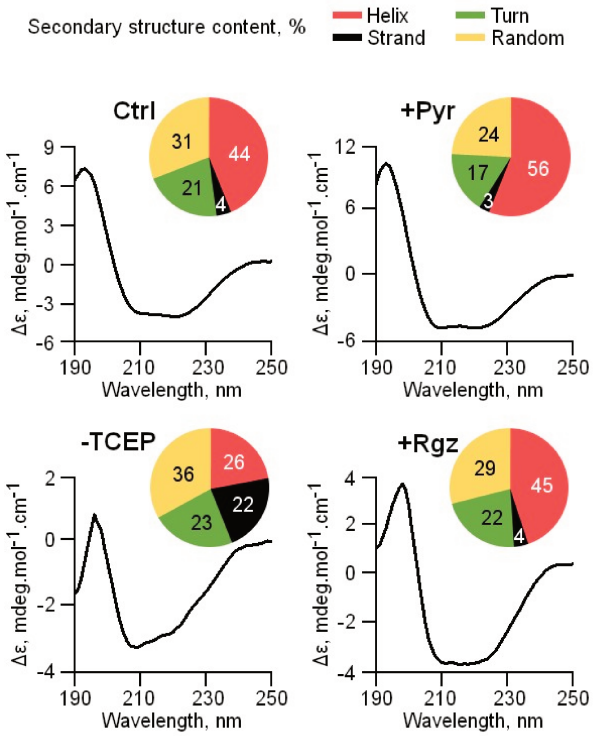

Figure 16. Secondary structure composition of human MPC2. Secondary structure analysis of MPC2 in presence and absence of ligands, as probed by Circular Dichroism. Far-UV CD spectra, as well as calculated percentage of secondary structure content in the form of pie-chart, for MPC2 alone (Ctrl; top left), in the presence of 25 µM pyruvate (+Pyr; top right), in the absence of TCEP (-TCEP; bottom left), and in the presence of 50 µM rosiglitazone (+Rgz; bottom right). Figure adapted from (NAGAMPALLI et al., 2018).

3.7. Orientation of MPC2 in proteoliposome membranes

Lastly, targeted digestion (ISLAM et al., 2013; WHITE; NIXON; BRADBURY, 2015) of intact MPC2-GFP-10xHis proteoliposomes, followed by fluorescence detection of cleaved GFP-10xHis, revealed that 22 ± 3 % of the fused particles were protected from proteolytic processing (Fig. 17). This indicates that the human MPC2 homotypic complex preferably oriented with the C-terminal end exposed to the outer surface of the artificial bilayer (78 ± 3 %); curiously, the dominant orientation is in consensus with the membrane topology proposed for the yeast homolog at the IMM (BENDER; PENA; MARTINOU, 2015). The current lack of a three-dimensional molecular structure of MPC2 limited our ability to provide a detailed, autonomous mechanism for pyruvate transport. Therefore, experiments are currently in progress to investigate the crystal structure of MPC2.

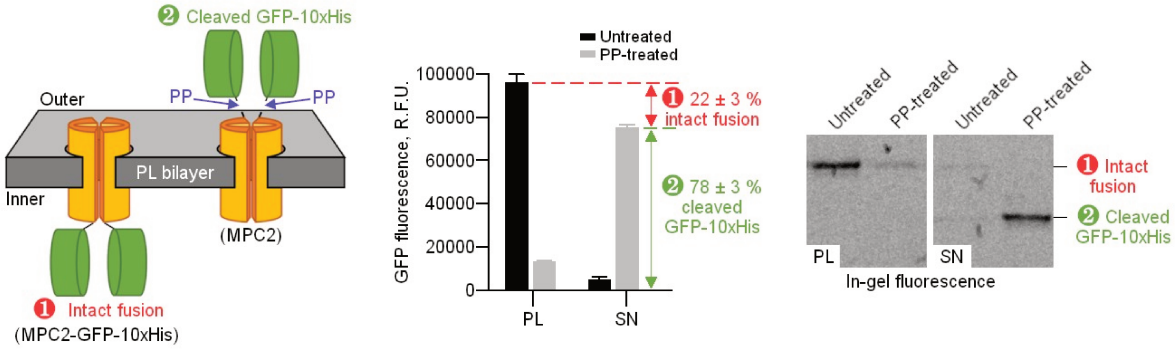

Figure 17. Experimental assay for MPC orientation. Right panel: A schematic representation indicating the possible MPC2-GFP-10xHis orientations in the artificial lipid bilayer of the proteoliposomes, as well as the two possible outcomes upon treatment with PreScission protease (PP): ❶ particles with the C-terminal fusion facing the interior of vesicles are protected from digestion by PP and ❷ cleavage of GFP-10xHis tag when the C-terminal fusion is oriented towards the outside of the lipid membrane. Middle panel: The corresponding samples were quantified in a plate reader for GFP fluorescence, and the relative populations are indicated as percentages. Left panel: Qualitative electrophoretic analysis of the proteoliposomes (PL) and supernatant (SN) samples, before and after treatment with PP. Figure adapted from (NAGAMPALLI et al., 2018).

3.8. Detergent screening for crystallization by FSEC

Following the similar protocol that has been optimized earlier (previous chapter), a single monodisperse protein-detergent peak was obtained. MPC2 purified in DDM was pure, monodisperse, homogenous and biologically active *in vitro.* However, protein purified following such methodology did not yield any crystals when screened by vapor diffusion. Disruption of the protein´s native oligomeric state by the detergent or the presence of excess micelles could possibly prevent the crystallization (CARPENTER et al., 2008). To identify the other detergents those that can promote crystal contact, MPC2, that was originally purified in DDM (12 carbons long) was screened for its stability in shorter detergents, regarding length of the aliphatic tail, during gel filtration. As such, detergents like UDM (Undecylmaltoside, 11 carbons), DM (Decylmaltoside 10 carbons), NM (Nonylmaltoside, 9 carbons), and OG (Octylmaltoside, 8 carbons) were used in a screening (Fig. 18). From the figure, it is evident that a sharp monodisperse peak derived of MPC2 is obtained when purified in the shorter detergents such as UDM and NM.

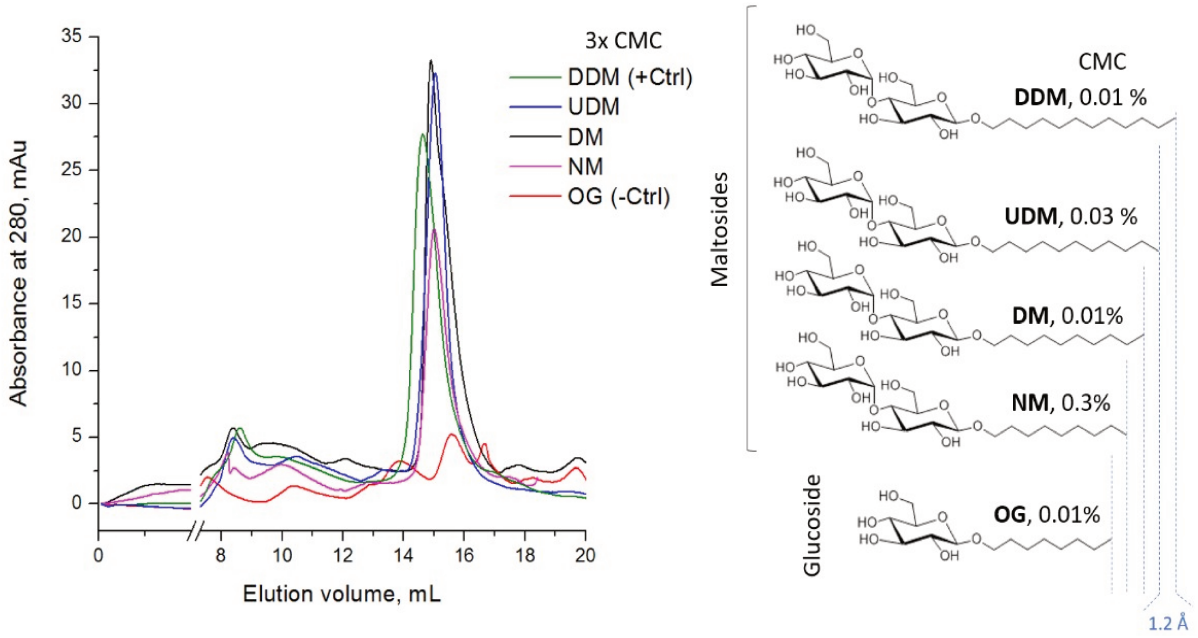

Figure 18: Screening of shorter detergents to promote crystal contact. A short tail detergent screening for MPC2 crystal formation via size exclusion chromatography. Schematic representation of all detergent tested with its respective critical micelle concentration.

3.9. Buffer and detergent screening by circular dichroism

The stability of MPC2 under 50 different buffer and detergents conditions were assessed by measuring the variation in the secondary structure content. From the graph presented below, A1-A9, B3, B4 and C3 illustrates significant helical components while others have the tendency to form more disordered structures possibly inducing aggregation. Among all the conditions that were tested, C3 drives the protein into more helical content (Figure. 19). This condition would be possibly explored during purification and future crystallization trials of human MPC2.

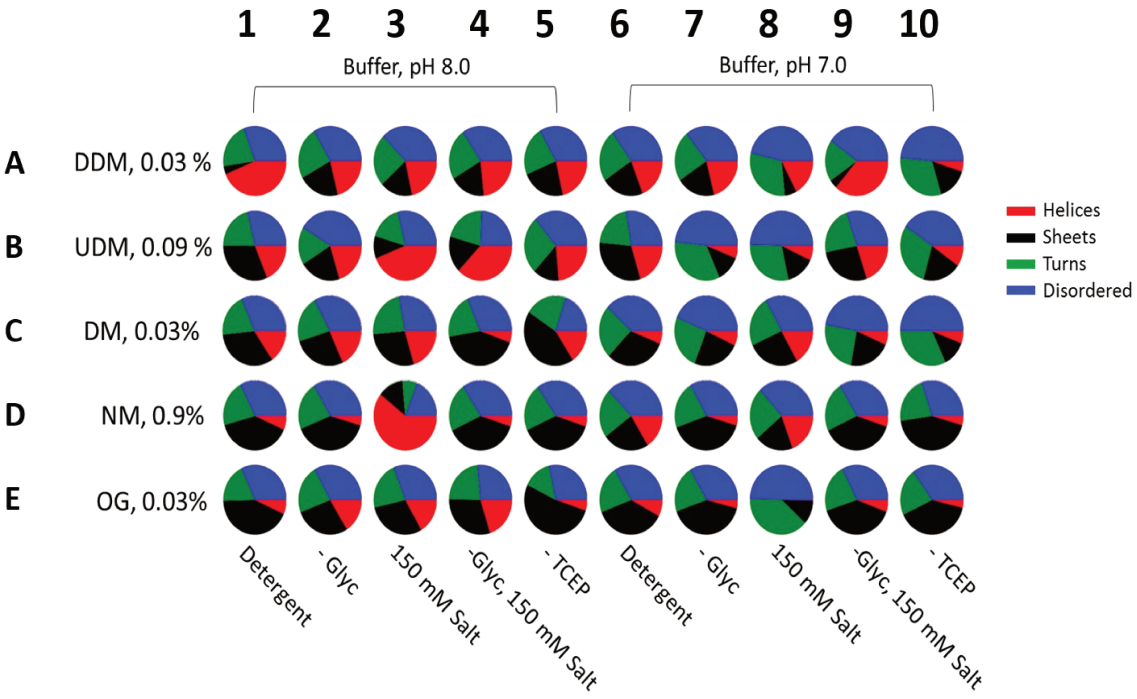

Figure 19: Variation in the secondary structure content of MPC2. The helices (red), sheets (black), turns (green) and disordered (blue) structures were evaluated at different conditions such detergents (DDM, UDM, DM, NM and OG), pH (7 and 8) and buffer composition. As can be noted the condition UDM, 150mM NaCl and pH 8 drives the protein predominantly into helical nature.

3.10. SEC-MALLS

Simultaneous measurements of light scattering, absorbance, and refractive index (three-detector method) during elution from gel filtration allowed calculation of the absolute molecular mass of MPC2 and detergent contribution to a PDC (protein-detergent complex). The absolute molecular mass of the PDC is ~57 kDa when purified in the detergents DDM or UDM, respectively. The molecular weight of the MPC2 when calculated using weight of PDC and co-monomer fraction A is ~13.5 kDA. This value agrees with that observed via SDS-PAGE (Fig. 4) and with theoretical estimates of the molecular weight. In addition, the data from the SEC-MALLS also suggests that MPC2 is homogenous when purified in either of the detergents DDM or UDM. However, a careful examination at the data signifies that MPC2 is slightly less poly disperse in the detergent UDM with a value of 1.001 while compared to 1.004 when purified in the detergent DDM (Fig. 20 top and bottom panel respectively). The NM detergent, which was also previously identified as a promising alternative to improve MPC2 purification was not tested further due to very low availability and higher cost.

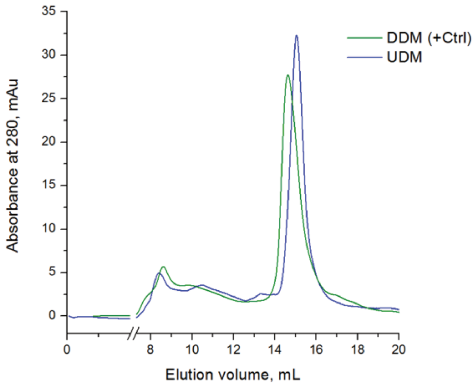

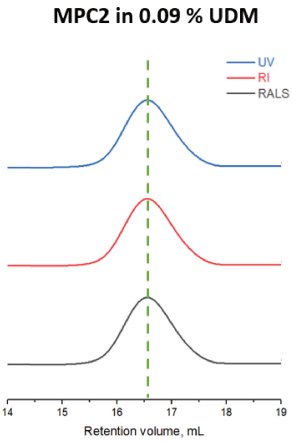

Calculation input parameters:

Protein Concentration ~ 1mg/mL
dn/dc = 0.1875
dA/dc =2.343

Detergent (UDM):
dn/dc = 0.1506
dA/dc = 0.02

Peak	1
MW Weight Average (Da)	54.033
Polidispersity	1.001
Weight Fraction of the Peak	1.000
Weight Fraction of Co-monomer A	0.247
RI Area (mVmL)	935.41
UV Area (mVmL)	50.46
RALS Area (mVmL)	99.29
Peak Retention Volume (mL)	16.506
Peak Concentration (mg/mL)	6.5857

Molecular weight of the protein fraction:
MW*WF(A)= 54, 033 * 0.247 =**13.4 kDa**
(14.5 kDa expected)

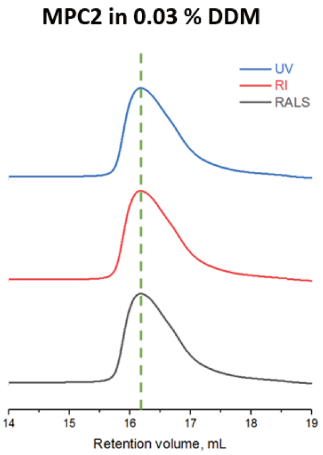

Peak	1
MW Weight Average (Da)	56.918
Polidispersity	1.004
Weight Fraction of the Peak	1.000
Weight Fraction of Co-monomer A	0.236
RI Area (mVmL)	640.42
UV Area (mVmL)	46.48
RALS Area (mVmL)	77.99
Peak Retention Volume (mL)	16.232
Peak Concentration (mg/mL)	6.5857

Molecular weight of the protein fraction:
MW*WF(A)= 56.918*0.236 = **13.4 kDa**
(14.5 kDa expected)

Figure 20: MPC2 characterisation by SEC-MALLS. Size exclusion chromatography chromatogram of Purified MPC2 in DDM and UDM at 0.09 and 0.03 % CMC**.** Protein and detergent contribution of UDM (top) and DDM (bottom) in purified MPC2 measured through SEC-MALS using the three-detector system**.**

3.11. CMC (Critical micelle concentration) screening of UDM

The lowest possible CMC of UDM at which MPC2 would be stable was further investigated after the identification of UDM and NM as the best shorter detergents to promote efficient crystallization of MPC2. It was observed that a sharp monodisperse peak derived of MPC2 is obtained when protein purified from 3X times to 1.5X times CMC of UDM (Fig. 21A). This suggests that MPC2 is relatively well stable at lowest possible CMC of the detergent UDM. However, to ensure that there would enough detergent micelles to stabilize MPC2 during purification a large-scale injection had been done with 2X CMC of UDM in the running buffer during gel filtration (Fig. 21B).

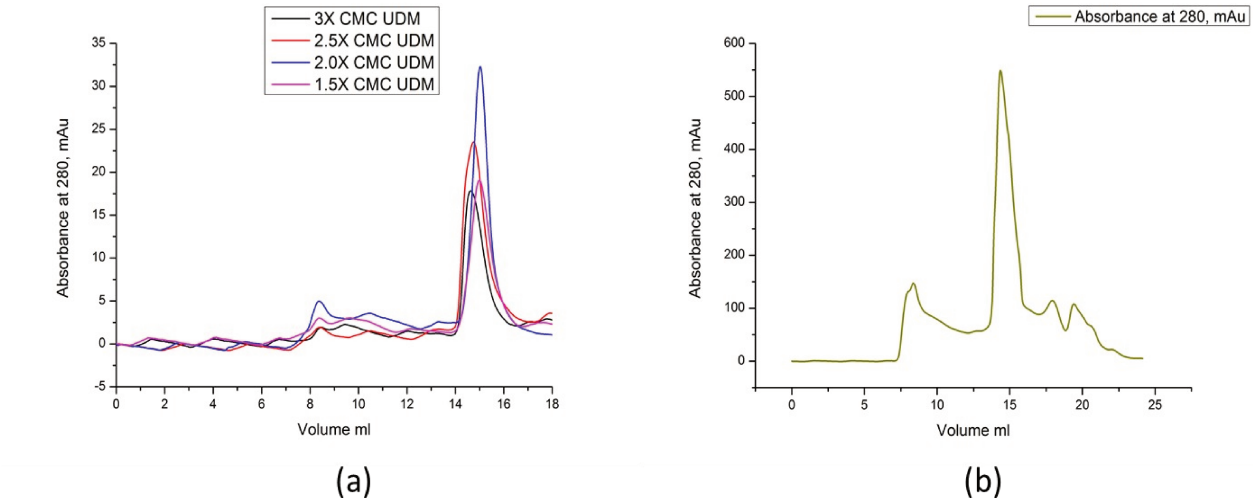

Figure 21: UDM CMC-screening for MPC2 purification. (A) Screening of lowest possible CMC of UDM to purify MPC2. (B) Large scale purification of MPC2 in 2X CMC UDM.

3.12. Crystallization of MPC2 using vapor diffusion

The purified MPC2 was concentrated to 11 mg/ml in buffer containing 20 mM Tris pH 8.0, 300 mM NaCl, 5 % glycerol, 0.05 mM TCEP and 0.058 % UDM and set for crystallization trials in the presence and absence of 2.5 mM pyruvate. Crystals that appeared after incubation for three days in the screen MemGold were tested on the microfocus beam I-23 at Diamond light source (Fig. 22).

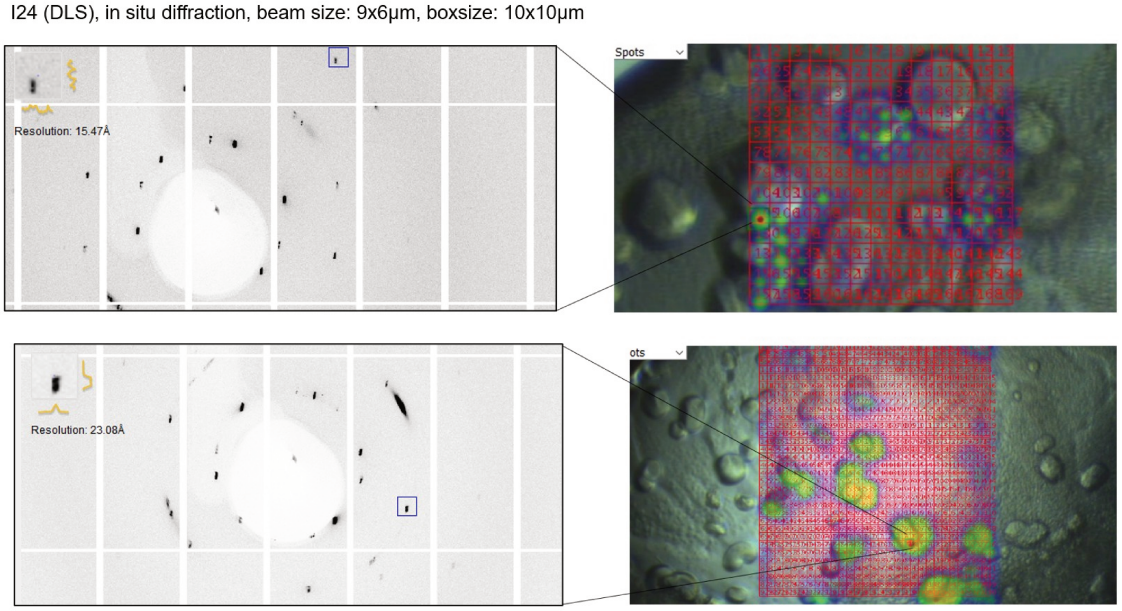

Figure 22: Vapor diffusion crystal formation of MPC2 (a) Crystals obtained and X-ray diffraction pattern in the presence of 2.5 mM pyruvate in 0.05 M sodium chloride, 0.02 M glycine pH 10.0 and 33% PEG 1000. (b) X-ray diffraction pattern and crystals obtained in 0.05 M sodium chloride, 0.02 M glycine pH 10.0 and 33% PEG 1000. Currently experiments are underway to optimize the conditions that yields better diffracting protein crystals.

3.13. Crystallization of MPC2 using lipid cubic phase (LCP)

In parallel, we set crystallisation trials using Lipidic cubic phase (Fig. 23). The purified MPC2 was concentrated to 18 mg/ml in buffer containing 20 mM Tris pH 8.0, 300 mM NaCl, 5 % glycerol, 0.05 mM TCEP and 0.058 % UDM and added to monooline (MO) at a ratio of 2:3 (w/v). Crystals that appeared after three weeks in the screen MemGold as below (Fig. 24). Currently experiments are underway to optimize the conditions that yields better diffracting protein crystals.

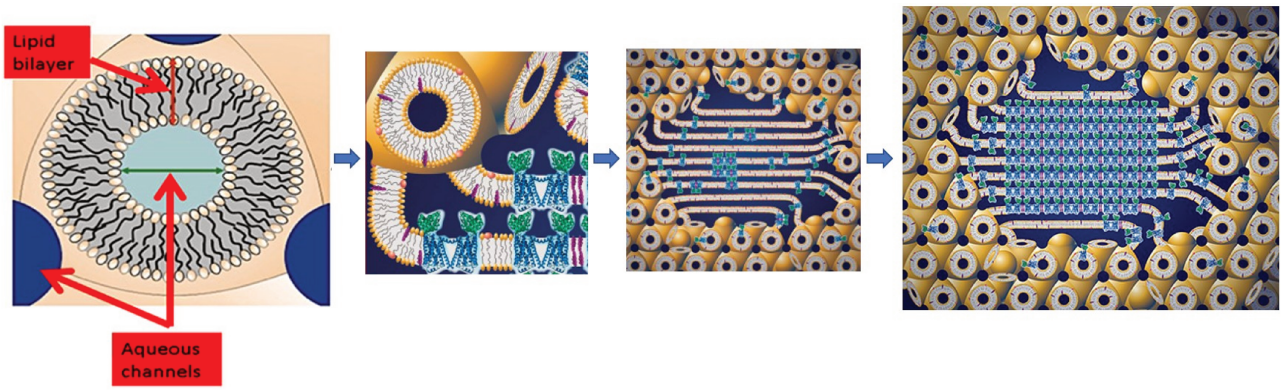

Figure 23: Lipidic cubic phase crystallisation. Graphical abstract of Lipidic cubic phase (LCP) crystallisation of membrane protein. Adapted from (CAFFREY, 2015).

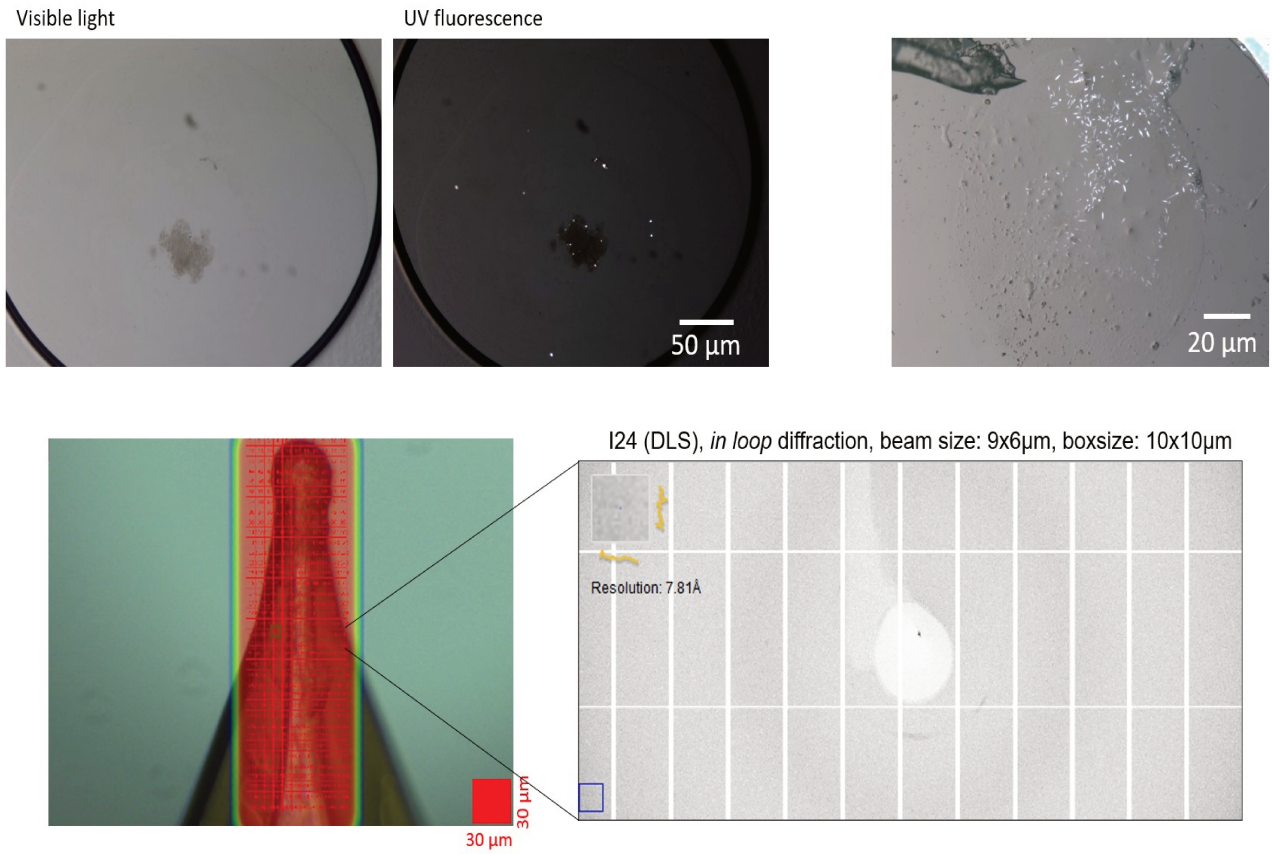

Figure 24: Crystals of MPC2 obtained by lipidic cubic phase. (Top row) MPC2 **c**rystals obtained by monoolein LCP, as observed through visible light and UV fluorescence. (Bottom row) *In loop* analysis of selected crystals showed no indication of X-ray diffraction.

3.14. Human MPC2 can be assembled into lipid nanodiscs.

Looking for alternative lipid-based methods to addressing MPC2 structure, new strategies were also tested here. The production of nanoscale discs with embedded MPC2 using membrane scaffold protein (MSP) (Fig. 25) and Styrene maleic acid (SMA) co-polymers (Fig. 27). Recombinant human MPC2-GFP was expressed and purified as previously reported (NAGAMPALLI et al., 2018), the attached GFP was cleaved from MPC2 protein. Three different membrane scaffold proteins (MSPs) were expressed and purified in the laboratory, they are MSP1D1, MSP2N2 and MSP1E3D1 with 24kD,45kD and 32kD size respectively (Fig. 26B.inset). These proteins were individually blended along with *E. coli* lipid extract, cardiolipin or asolectin phospholipids to produce MPC2 lipid nanodiscs.

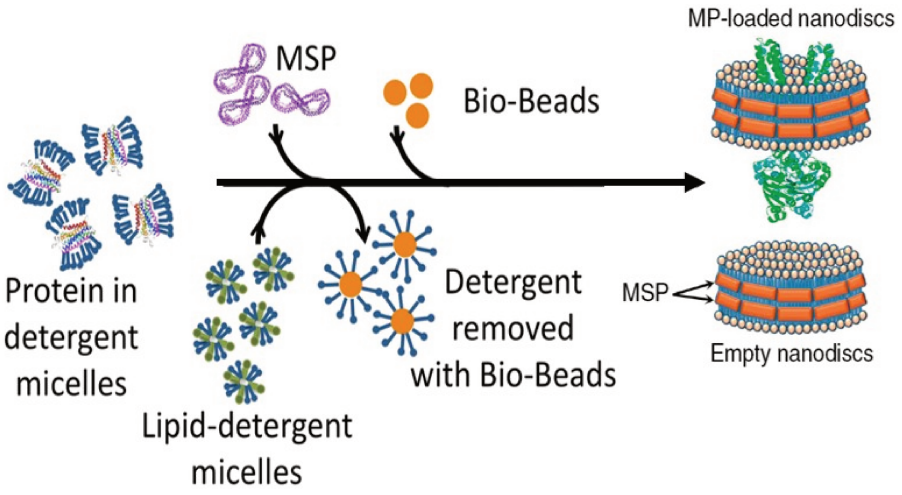

Figure 25: Graphical representation of membrane protein reconstitution into membrane scaffold protein (MSP) nanodiscs. Purified membrane protein target in detergent micelles is mixed with both membrane scaffold proteins and selected detergent-phospholipids micelles, resulted solution is incubated and then detergent removed by Bio-Beads to generate either empty nanodiscs or reconstituted membrane protein target into nanodiscs. Extracted from (MITRA, 2013).

Out of the three, only MSP1D1 was found to assemble MPC2 into lipid nanodiscs, in asolectin phospholipid presence. Curiously, asolectin has been also reported for functional reconstitution of human MPC2 into artificial lipid bilayer (NAGAMPALLI et al., 2018). Size exclusion chromatography analysis from nanodiscs solution shows populations made up of MSPD1 protein, asolectine nanodisc (empty discs), MPC2-GFP and MPC2 asolectin nanodiscs (Fig. 26A). Resulted elution peaks reveal that while an important fraction of protein is incorporated into nanodiscs after detergent removal, a considerable fraction of MSP1D1 free protein and empty nanodiscs were present. The MPC2 Nanodiscs peak indicates an approximately 107 kDa of molecular size, moreover empty nanodisc shows a 73kDa, and a difference of 34kDa can suggest a possible homo dimer conformation of MPC2 subunit in nanodiscs (MPC2 monomer= ~15kDa), however it is unclear if this dimeric configuration corresponds to the active arrangement of MPC.

The eluted fraction of MPC2 Nanodiscs peak was analysed by negative staining electron microscopy. Micrographs reveal a reduced number of particles and some of them forming, aggregates; furthermore, due to presence of heterogeneous particles on the carbon grids, it was difficult to identify any top or side view of assembled nanodiscs (Fig.26B)

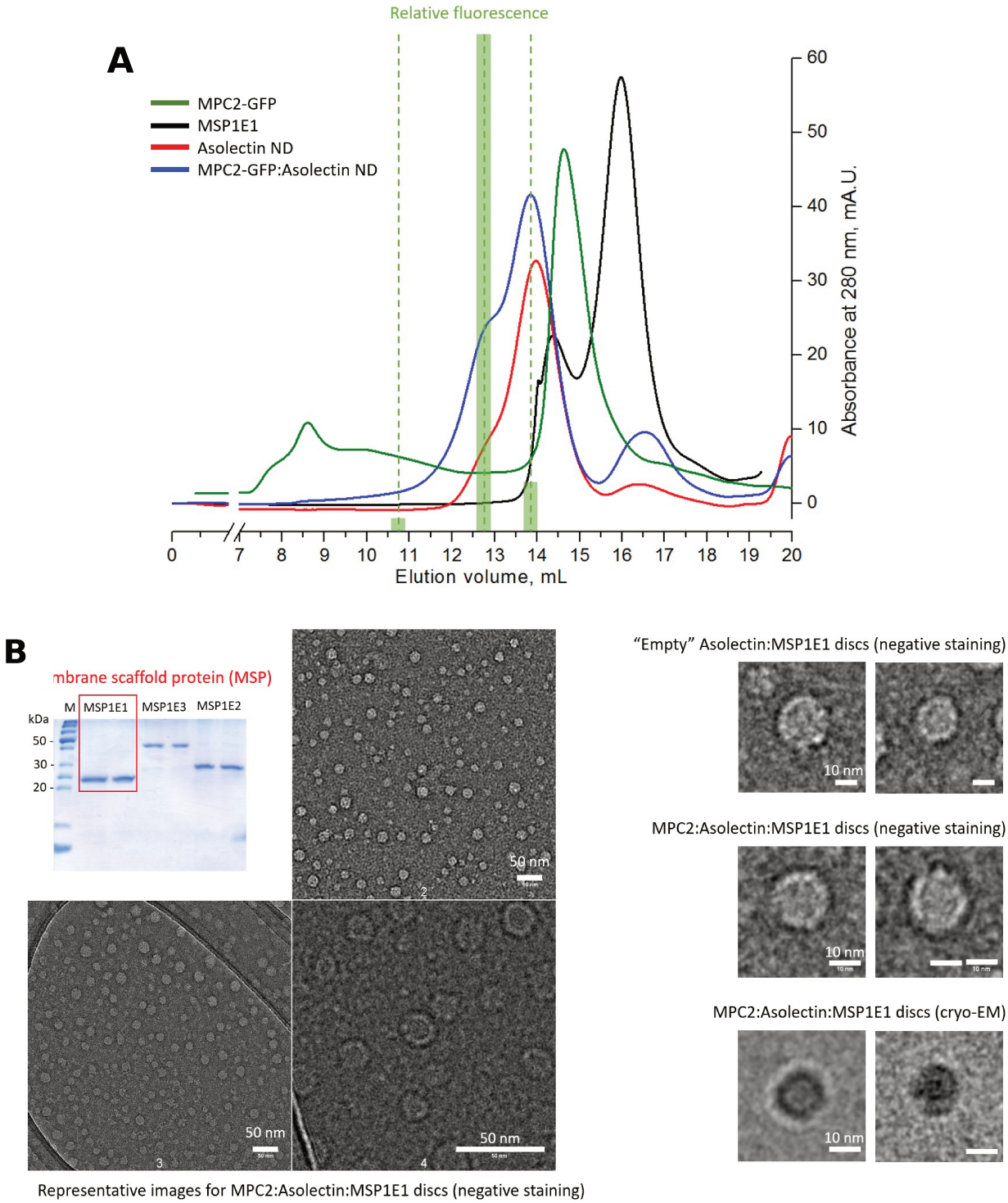

Figure 26. Assembling Human MPC2 into lipid nanodiscs. (A) Populations yielded from reconstitution step were separated by Size exclusion chromatograph, these populations are, Human MPC2-GFP reconstituted into MSP1D1, MSP1D1 protein, MSP1D1 nanodiscs (empty nanodiscs). Sample were applied into Superdex 200 10 300 column. Eluted fraction was selected by relative fluorescence **(B)** Purification of membrane scaffold protein (MSP1D1, MSP2N2, MSP1E3D1), these proteins were resolved in SDS PAGE 12%, samples were applied by duplicate**.** Negative stained electron microscopy Micrograph from Human

MPC2 reconstituted into lipid nanodiscs, the diameter of extracted particles was also measured indicating nanodiscs from 10 nm. Scale bar (50nm).

Negative stain micrographs also reveal that MSP limits the particle size of nanodiscs of ~10-13 nm (Fig. 26B. right panel). The small size of MPC2 complex probably facilitate its incorporation in MSP1D1, since MSP1D1 forms ~13nm size nanodiscs(DENISOV et al., 2004), as observed in our experiment. The controlled size of nanodiscs was observed despite non conclusive results obtained, and this synthetic membrane model can be used for developing structural experiments and be applied to other projects involving membrane proteins; The drawbacks of this approach includes, the presence of an extra protein like MSP that can interfere in the biophysical studies, the existence of empty discs during purification and, the fact that protein target still must be first detergent-solubilized.

3.15. Application of synthetic scaffold co-polymers on Human MPC2 purification.

Expression and pellet preparation of recombinant human MPC2-GFP were followed as described previously. GFP was maintained during all purification process. Membrane pellet was incubated in presence of three commercial Styrene Maleic Acid (SMA) co-polymers, all these SMA are composed of different proportion of Styrene (S) and Maleic Acid (MA), XIRAN®25010P (S:MA ratio 3:1), XIRAN®30010P (S:MA ratio 2.3:1), XIRAN®40005P (S:MA ratio 1.2:1). After three hours of incubation at room temperature, the sample incubated with XIRAN®25010P and XIRAN®30010P showed less turbidity than the sample incubated with XIRAN®40005P. Moreover, while XIRAN®30010P and XIRAN®25010P samples displayed highest fluorescence in supernatant after ultracentrifugation, a limited fluorescence was observed in supernatant from XIRAN®40005P sample. This contrast can be easily visible (Fig. 28. Left panel). All supernatants were analysed by fluorescence through size exclusion chromatography (FSEC), the resulted peaks confirm that XIRAN®30010P and XIRAN®25010P can turn human MPC2 soluble in absence of any detergent, however the intensity of the fluorescence can be progressively lost as the purification steps are executed (Fig. 28 right panel).

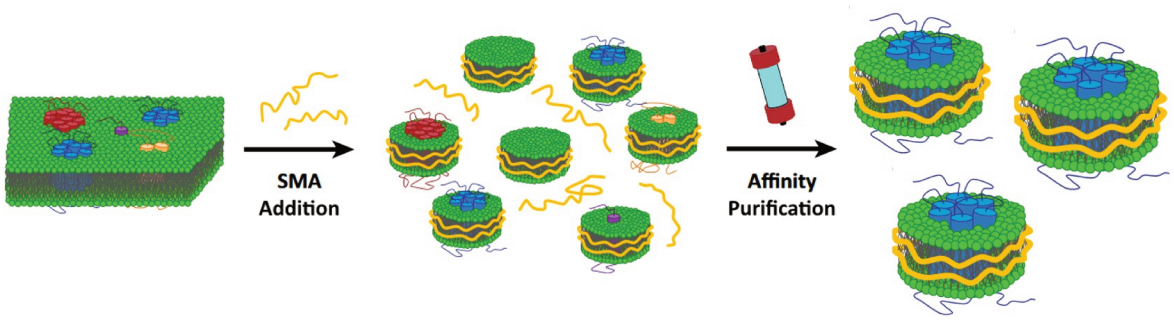

Figure 27: Cartoon representation of membrane protein purification using SMA . SMA addition to membrane allow the formation of nanodiscs containing different membrane proteins or only lipid material. Subsequent affinity purification allows for the isolation of nanodiscs with membrane of interest. (DÖRR et al., 2016)

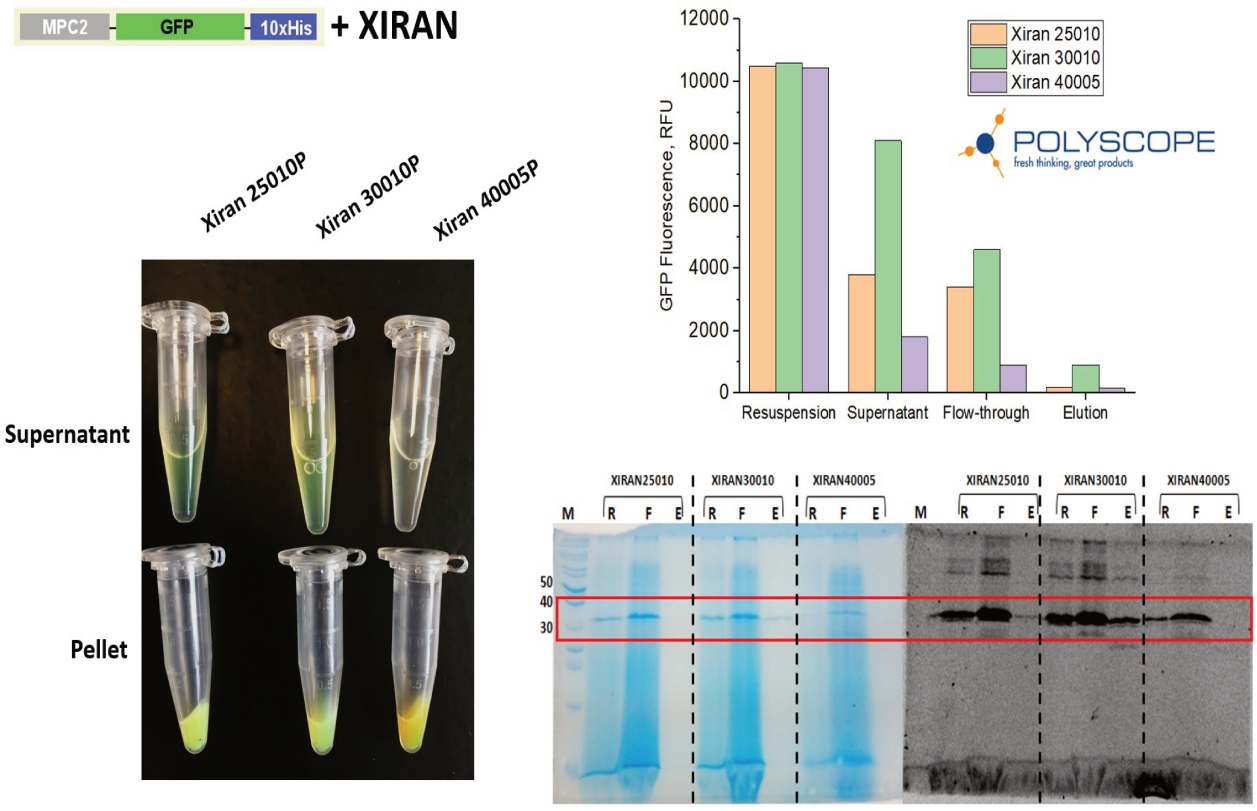

Figure 28. SMA co-polymers screening for MPC2 solubilisation. Commercial SMA co-polymers, XIRAN®25010P, XIRAN®30010P and XIRAN®40005P (Polyscope) employed for small scale solubilisation of MPC2-GFP. GFP Fluorescence can be observed the during incubation as well as post-ultracentrifugation in supernatant and final pellet, this fluorescence intensity decreases over the purification steps; this is from resuspension to elution. This

outcome is constant for all co-polymers investigated as shown in bars (middle). Samples from resuspension, flow-through and elution where loaded into SDS-PAGE which display a band of approximately 32kDa (Red rectangle) corresponding to MPC2-GFP in Coomassie stained SDS-PAGE or in-gel fluorescence.

Due its great protein extraction property and the fact that it does not absorbed at GFP wavelength (480nm) , XIRAN®30010P was used for large scale purification of Human MPC2-GFP(Fig. 29A), which resulted in around 70% of the total crude membrane pellet solubilised and a green fluorescence observed in soluble fraction, as previously reported in small-scale solubilisation (Fig. 28). The flow-through from IMAC was concentrate and then analysed by FSEC obtaining at least two peaks. Additionally, according to SDS PAGE the peaks are composed of two bands of 32 and 25 kDa.

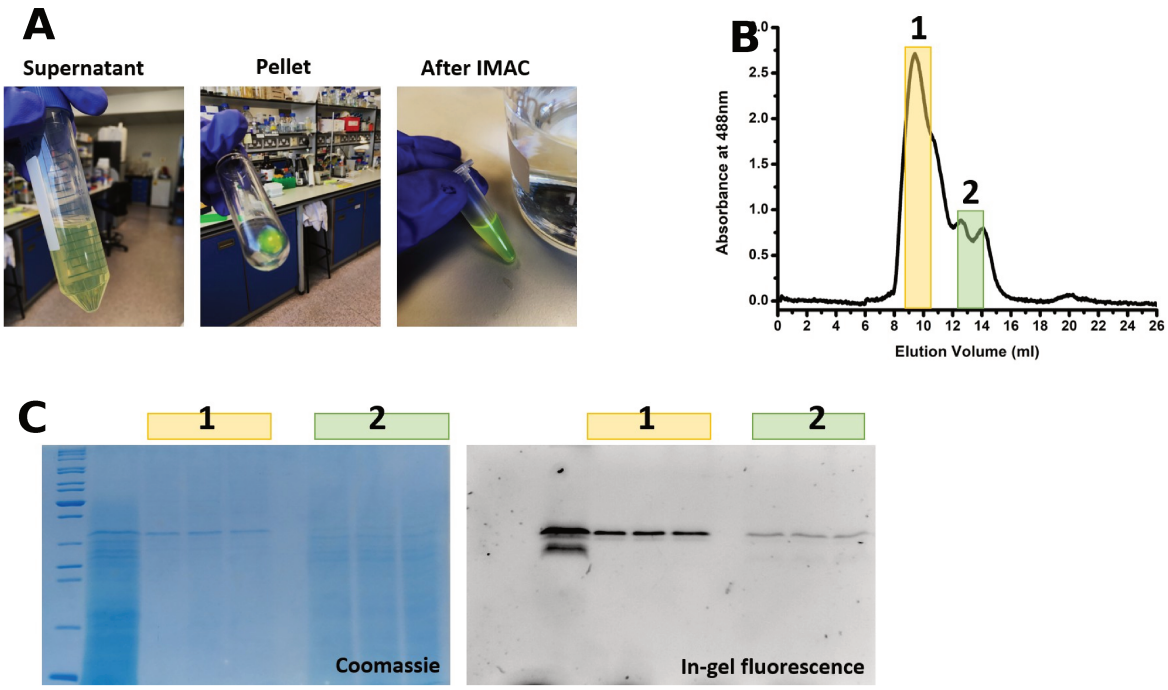

Figure 29. Large scale purification of recombinant human MPC2-GFP using SMA. (A) Commercial co-polymer XIRAN®30010P Images of large-scale purification steps (supernatant, pellet, and elution) showing green fluorescence. (B) Final FSEC from IMAC sample shows four populations which were resolved in Coomassie stained SDS-PAGE (C).

3.16. Electron Microscopy studies of SMA-encapsulated Human MPC2-GFP.

Before the specimen preparation for EM analysis, the size distribution profile of purified MPC2-SMALP sample was analysed by DLS, showing a single monodisperse peak

of particles with approximately 12nm diameter (Data not shown). Sample at 0.2 mg/ml concentration was examined by negative staining electron microscopy approach, the results displays micrographs containing well dispersed SMALPs particles of 10 -13 nm diameter size (Fig. 30A. left panel). Same purified sample at 0.1mg/ml of final concentration was placed onto graphene oxide grids and visualised at Cryo-EM conditions (Fig. 30A. right panel). 427 micrographs were collected using Phase plate in Titan Krios Microscope and Motion corrected using MotionCor2 software. Data was processed using Relion or cryoSPARC; this software identified blurred classes through particle classification (Fig. 30B), the "best classes" contain from 700 to 2700 particles. At least 4 or 5 blurred points are observed in all classes. A suggested model with MPC2 complex showing 4 GFP is presented based on particle classification results (Fig. 30B).

A

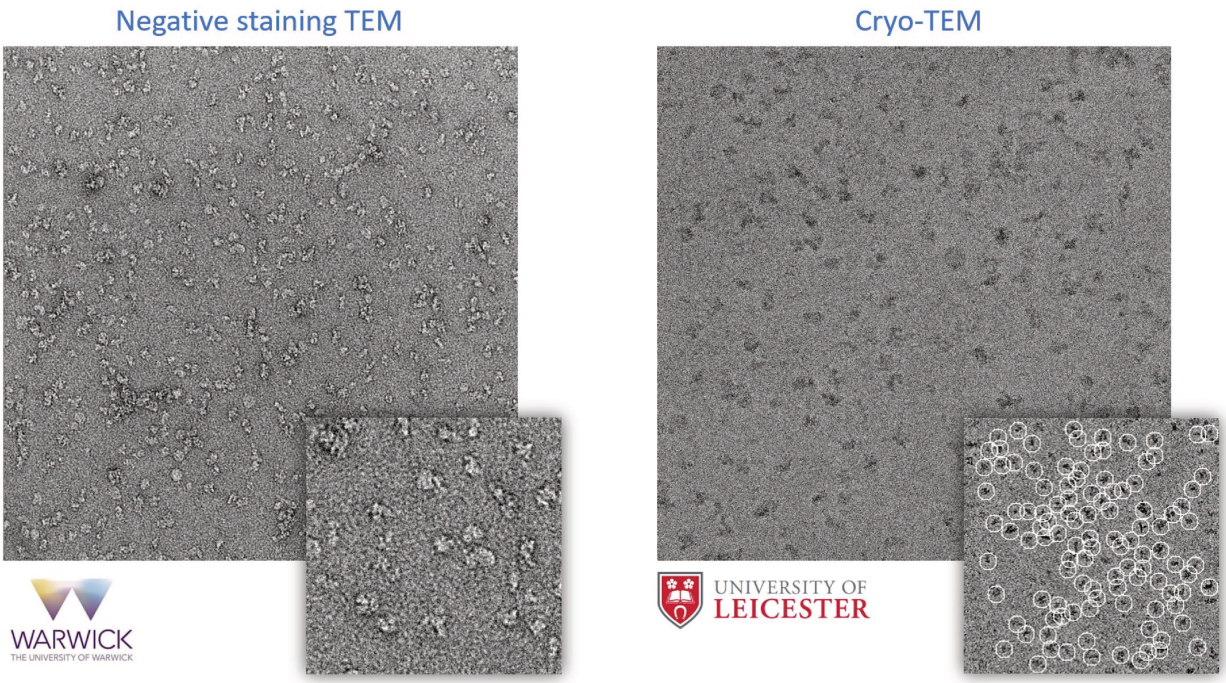

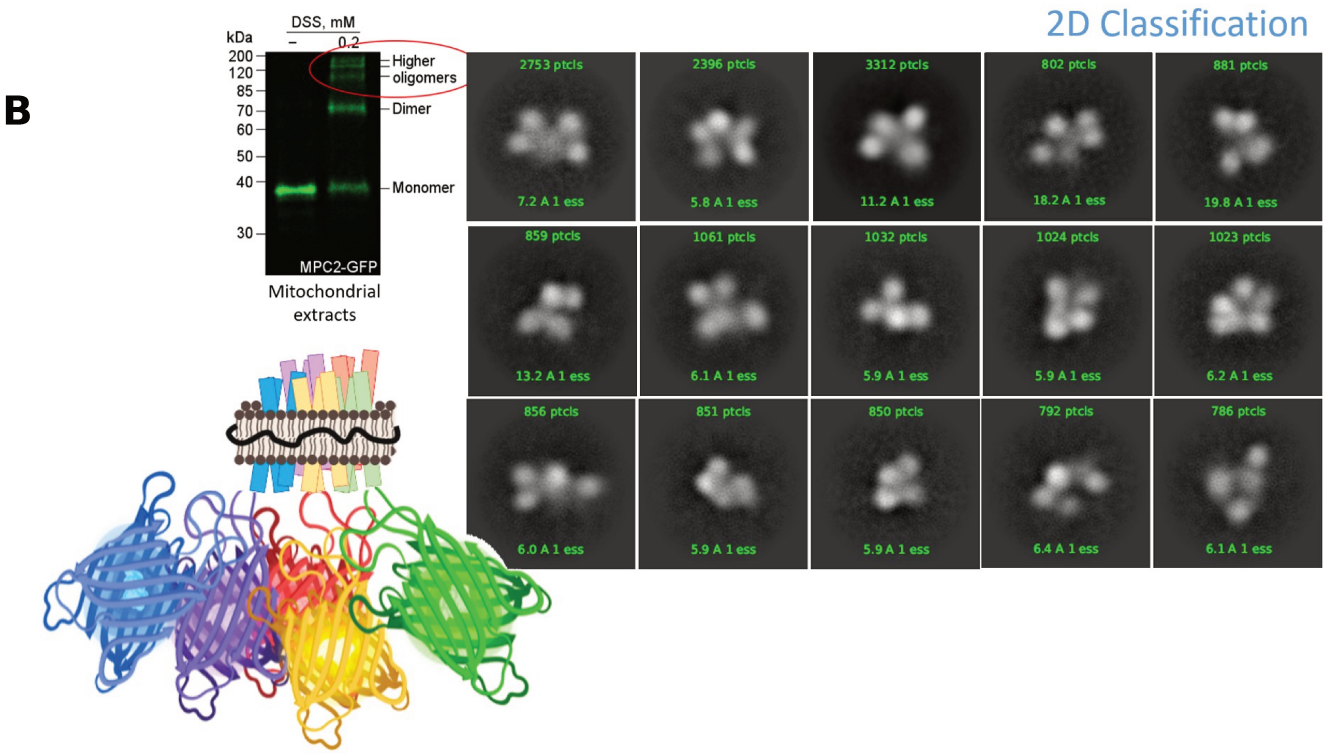

Figure 30. Preliminary electron microscopy analysis of SMA-encapsulated Human MPC2-GFP. (A). Negative stained and Cryo-EM micrograph showing particles of SMA-encapsulated Human MPC2-GFP of approximately 10nm size. (B) Particles were picked grouped by similarity and used to generate a possible model (bottom left, between four to five MPC2/GFP subunits), based on the number of GFP subunits . Micrographs scale bars (50nm). Particles from Negative stained and cryo-EM were analysed by CryoSparc software.

CHAPTER 4. DISCUSSION

4.1. Human MPC2 as a potential autonomous transporter.

A rich body of evidence has established MPC1 and MPC2 as mandatory components for the mitochondrial uptake of pyruvate in both intact cells and mitochondrial isolates (BENDER; PENA; MARTINOU, 2015; BRICKER et al., 2012; COMPAN et al., 2015; DIVAKARUNI et al., 2013; HERZIG et al., 2012; VACANTI et al., 2014; VANDERPERRE et al., 2015). Co-immunoprecipitation from purified mitochondria, followed by electrophoretic separation, suggested that MPC1 and MPC2 form an oligomeric complex of approximately 150 kDa (BRICKER et al., 2012). Here, we developed an experimental setup aimed at the co-expression and purification of recombinant human MPC as a heterocomplex. To this end, we used a bi-directional expression plasmid with inducible promoters that respond to galactose, such that both isoforms could be expressed simultaneously at high and similar levels. Moreover, we used a mutant yeast strain lacking the endogenous *mpc1*, *mpc2* and *mpc3* genes (BRICKER et al., 2012) to avoid cross-contamination with yeast MPC.

Regardless, only the human MPC2 subunit was purified to homogeneity and shown to function in both *in vitro* and *in vivo* pyruvate transport. This finding was further confirmed when MPC2 was expressed without MPC1 and shown to be similarly functional. MPC1 co-purified with the yeast 60S RPL28 protein and only traces of MPC2. In contrast to MPC2, MPC1 associated with 60S RPL28 was not active. While these results indeed confirm the existence of a MPC1:MPC2 interaction, they suggest that yeast may lack some critical and yet unidentified protein component for stable complex formation of human MPC1:MPC2, as previously proposed (HALESTRAP, 2012). The existence of novel and direct interacting partners for MPC has been experimentally postulated (FLOYD et al., 2016; HUTTLIN et al., 2015); moreover, a host non-membrane protein contaminant (60S RPL28) may act as a chaperone for human MPC1, potentially preventing detectable *in vitro* transport activity. Overall, our findings do not exclude the possibility that, in cells, MPC1 is a co-transporter working with MPC2; however, our data demonstrate that MPC2 can function as an autonomous pyruvate transporter and may work by itself in some specific conditions.

Collectively, the functional observations described above are consistent with previous and recent reports from many laboratories, suggesting that mitochondrial pyruvate transport by MPC is a rapid and specific process that depends on co-proton import and redox balance (GRAY; RAUCKHORST; TAYLOR, 2016; HALESTRAP; P, 1975; HALESTRAP, 1978). Our studies on the dependence of time for the transport activity of MPC2 in artificial vesicles (Fig. 8A) agree with those performed early on in mitochondria extracts containing MPC1 and MPC2 (HALESTRAP; P, 1975); half-maximum transport for MPC is achieved around 2 minutes. However, the K_m of MPC2 for pyruvate in vesicles is about 7 times higher than previously reported (1.1 mM in this study versus 0.15 mM quantified by Halestrap, 1975 (HALESTRAP; P, 1975). This could suggest that the MPC2 homo-oligomer is a relatively less efficient transporter than the proposed MPC1:MPC2 heterocomplex.

Here, the finding that the MPC2 autonomous activity can be inhibited by a TZD derivative, albeit partially, is also substantiated by previous literature (COLCA et al., 2013; DIVAKARUNI et al., 2013). Of note, these functional parameters, which were proven essential for the demonstration of the protein-dependent pyruvate transport, are further reinforced by the circular dichroism studies using synchrotron radiation. A challenging point, however, is that MPC2 alone is insensitive to UK-5099. Although MPC1, but not MPC2, was recently confirmed to be the real target of cinnamates (BRICKER et al., 2012; COLCA et al., 2013), the description of such a UK5099-insensitive MPC transport in cells remains elusive.

The dynamic stoichiometry of MPC subunits was recently shown to shift between hetero- and homo-oligomers in cells due to variations in both metabolic and tissue-related conditions (BENDER; PENA; MARTINOU, 2015; TIMOŃ-GÓMEZ; PROFT; PASCUAL-AHUIR, 2013; VANDERPERRE et al., 2015). Here, the study of the oligomeric composition of recombinant MPC2 by chemical crosslinking in native (mitochondrial extracts) and native-like (asolectin vesicles) environments, further support the formation of large homotypic assemblies as the functional components, ranging hundreds of kilodaltons, as previously proposed for the heterotypic MPC1:MPC2 complex (BRICKER et al., 2012). The true size of the MPC2 oligomers, however, is yet to be determined.

Given all the potential scenarios described above, a significant question arises: which physiological conditions promote MPC2-mediated pyruvate transport? Recently, MPC2 was shown to be strictly regulated by acetylation, which can critically determine the active or

inactive states of this protein (HORNBECK et al., 2015; LIANG et al., 2015; LUNDBY et al., 2012; VADVALKAR et al., 2017); indeed, acetylation has been directly linked to decreased cellular oxygen consumption rates and deficient pyruvate transport activity (VADVALKAR et al., 2017). Lethality in embryonic mice was caused by either the deletion of MPC2 (VIGUEIRA et al., 2014) or the knockout of MPC1, which in turn also lead to the instability of MPC2 at a post-translational level (VANDERPERRE et al., 2016b). We showed that human MPC2 alone could increase oxygen consumption in yeast cells driven by glucose addition and can rescue cell growth when valine is absent, suggesting that, in cells, human MPC2 facilitates mitochondrial pyruvate intake. This finding was further confirmed using the isosteric mutant. Curiously, MPC2 significantly increased oxygen consumption in the 3Δ mutant strain by 60 %; yet, compared with the control, MPC2 stimulated cell growth rates (measured as doubling time) by 16 % in this strain. These results suggest that MPC2 may play a role in the distinct energetic and biosynthetic fates of pyruvate, which should be further investigated, perhaps in association to regulation by post-translational modifications.

Our research interest on the metabolic changes undergone by breast cancer led us to survey the MPC2:MPC1 balance in health and disease. In particular, we analyzed the MPC2/MPC1 expression ratio in normal and tumor tissues from the Breast Invasive Carcinoma (BRCA) dataset publicly available at The Cancer Genome Atlas project. We noticed that, while normal tissues have a MPC2/MPC1 median ratio near 1, meaning both genes being equally expressed at RNA level, in tumor tissues the ratio is significantly higher, demonstrating increased unbalanced expression of these genes, with MPC2 ever more abundant, shown in log-2 scale). According to a Metacore analysis (Clarivate Analytics) a positive correlation with increase MPC2/MPC1 is observed for 56 out of 80 genes belonging to the oxidative phosphorylation pathway. While several of glycolytic genes also positively correlated with higher MPC2/MPC1, there was a consistent negative correlation between MPC2/MPC1 ratio and the expression of five lactate dehydrogenase and gluconeogenesis genes). Altogether, a shifted MPC2/MPC1 ratio in breast tumors may have an impact on respiratory metabolism, which could lead to an increase in the mitochondrial pyruvate oxidative metabolism. This scenario points to the hypothesis that MPC2 may work autonomously for the intake of pyruvate in some specific physiological conditions.

This scenario points to the hypothesis that a higher MPC2/MPC1 expression ratio in breast tumors may impact a more respiratory metabolism with a potential increase in the destination of pyruvate to the mitochondrial oxidative metabolism and suggest that MPC2 may work autonomously for the intake of pyruvate in some specific scenarios. Further research is necessary to identify the biological circumstances under which MPC2 function by itself and in association with MPC1.

In conclusion, although the heterotypic MPC component was initially proposed based on co-immunoprecipitation and yeast-based functional complementation assays (BRICKER et al., 2012), shreds of evidence still lacking regarding the direct interaction between MPC1:MPC2 at the level of the isolated proteins. In this context, our work provides the first demonstration of the heterologous expression and purification of human MPC1 and MPC2. MPC2, but not MPC1, was purified to homogeneity and found to be active and sufficient for pyruvate transport in artificial liposomes and in cells.

4.2. A transport assay alternative to radiolabelled substrates.

The compelling demonstration of the active transport mechanism of pyruvate across the inner mitochondrial membrane, as well as the subsequent identification of proteins responsible for such, were done by using ^{14}C-labelled radioactive pyruvate (BENDER; PENA; MARTINOU, 2015; BRICKER et al., 2012; HALESTRAP; DENTON, 1974; HERZIG et al., 2012). This experimental approach effectively confirms substrate entrance into mitochondrial extracts (BENDER; PENA; MARTINOU, 2015; BRICKER et al., 2012; HALESTRAP; DENTON, 1974; HERZIG et al., 2012) and allows for direct quantification of the parameters involved for transport. In the present work, we introduce a simple, automatable, and non-radiometric assay sufficiently sensitive to measure substrate transport into lipid vesicles. As opposed to a more canonical assay that quantifies the intravesicular content of the radiolabelled substrate, we propose an alternative novel assay that relies on the observed decrease in the content of extraliposomal pyruvate, as quantified by an enzymatic reaction; in this case, LDHA.

The validity of the enzymatic assay reported here is confirmed when the functional and kinetic parameters of mitochondrial pyruvate transport – collectively reported over the

decades – are reproduced using purified MPC and compared side-by-side with the radiolabelled substrate. In addition to allowing for direct and reliable quantification of the key parameters involved in transport, it could be multiplexed and streamlined, therefore adapted to a high-throughput screening approach for modulators of MPC2 using small-molecule libraries.

Therefore, besides the novel functional insights that our paper brings to the field of pyruvate transport, we expect that the successful application of an alternative enzymatic approach to quantify in vitro transport will be of the major interest to the *in vitro* biochemistry of membrane carriers in general; this kind of assay can be a suitable replacement to the prevalent radioactive-based assays, provided that the kinetics parameters of the probing enzyme do not become rate-limiting in respect to the kinetics of the carrier.

4.3. Preliminary structural analysis of human MPC2

4.3.1. Crystallization of MPC2

Preliminary data suggests that MPC2 purifies as monomer and with lower polydispersity in the detergent UDM. The SRCD suggests that MPC2 exists typically in alpha helical nature with Tm of 44 °C. Furthermore, high throughput SRCD data suggests when MPC2 is in the detergent NM and chemical condition 20 mM TRIS pH 8.0, 150 mM NaCl, 5 % glycerol and 0.5 mM TCEP the increases the helical content, and the gain in secondary structure may represent higher structural stability. Screening of shorter detergents for crystallization suggested MPC2 is stable and purifies as monodisperse in the detergents UDM and NM. MPC2 was found to be stable and monodisperse when the CMC of the UDM was reduced up to 1.5 times CMC. Crystallization of MPC2 yielded initial hit conditions and currently experiments are underway to get the diffraction-quality protein crystals.

3.3.2. Exploring the self-assembling MSP-nanodiscs to study MPC2 oligomeric conformation.

The ever-growing interest in membrane protein research entails the need for appropriate model systems to study them. The extraction of the protein of interest from native lipid environment without perturbing its properties in aqueous solution is a critical step. One

traditional strategy to facilitate the extraction is the use of detergents. they solubilise the protein inside a detergent micelle, which keep it relatively stable for structural and functional studies. For the recombinant human MPC2, it was already reported the complete detergent solubilisation, purification and its functional reconstitution into liposomes (NAGAMPALLI et al., 2018). However, structural details about its active state remain intriguing, especially when the formation of MPC2 high-ordered structures has been observed in crosslinking assays from detergent micelles, proteo-liposomes, and intact mitochondria. MPC2 is a small protein of 15kD size, displaying a monomer conformation in detergent micelles, and shows active in lipid environment. This suggests that the possible oligomer conformation previously observed needs to be studied in a more stable system with controlled size such as the MSP nanodiscs, that use phospholipids instead of the un-natural detergent environment. This process particularly needs a previous screening to find suitable(s) phospholipid as well as the proper MSP protein to stabilise the protein of interest. Here, we reported the successful assembling of human MPC2 into asolectin-based membrane bilayer enclosed by MSP1D1 protein. The resulted nanodiscs have 10-13 nm diameter . These results are in agreement with the ~13 nm diameter size reported for nanodiscs generates by MSP1D1 which typically contain two MSPs and, 120–160 lipid molecules per nanodisc (DENISOV et al., 2004). The correct assembling of MPC2 into nanodiscs occurred when asolectin was used, in contrast to other phospholipids we investigated such as DPC or *E. coli* lipid extract (data not shown). Asolectin is a Soybean phospholipid, that comprises roughly equal proportions of lecithin, cephalin and phosphatidylinositol along with minor amounts of other phospholipids and polar lipids. Curiously, this phospholipid was found also suitable to reconstitute MPC2 into artificial vesicles(NAGAMPALLI et al., 2018). According to size exclusion chromatography, the assembled MPC2 nanodisc structure correspond to around 107.4kDa size, while the empty nanodisc has 72.7kDa, suggesting that the difference of 34.7kDa corresponds to the inserted MPC2. Thereby, only two MPC2 subunits could be part of the inserted protein, resulting in a homo-dimeric conformation. Recently, it has been demonstrated hetero-dimer state of the MPC (MPC1/MPC3) complex in yeast (TAVOULARI et al., 2019). At this point, it is impossible to ensure that the dimer conformation of MPC2 is the active form found in liposomes. The requirement of an initial MPC2 purification in detergent micelle prior to MSP-nanodiscs assembling and the limited amount of nanodisc particles observed in negative stained micrograph, makes this approach less viable for structural studies.

4.3.2. A detergent-free isolation of MPC2 in a native lipid environment.

During detergent purification results in the disruption of the membrane lipid components, an essential component required to maintain the protein folding and function. The reinsertion of protein into an artificial lipid environment can recover the functional properties partially lost during detergent based purification. The application of amphipathic Styrene -Maleic Acid (SMA) co-polymer in the purification of the recombinant human MPC2 can avoid these time-consuming steps in complete absence of detergents. SMA co-polymers, specifically its commercial versions were analysed to select an appropriate candidate to isolate MPC2, since MPC2 has been expressed with GFP protein attached, it has been called MPC2-GFP. By following the GFP-based fluorescence, the stability of MPC2 (DREW et al., 2005) and the efficacy of polymers to solubilise MPC2-GFP can be easily monitored. From all polymers only XIRAN®25010P and XIRAN®30010P, showed a reduction of turbidity during incubation, which is a recurrent highlight that prove a significant protein extraction(SWAINSBURY et al., 2014). The effectiveness of these polymers can varies according its SMA ratio and structure(MORRISON et al., [s.d.]), In that sense, the S:MA ratio of XIRAN®25010P , XIRAN®30010P and XIRAN®40005P are (3:1), (2.3:1) and (1.2:1) respectively. Notably, recent studies have demonstrated that SMA ratio (2:1), also present in the original "SMA2000" used in the first demonstration of SMA solubilisation activity (KNOWLES et al., 2009), is more efficient in membrane solubilisation than SMA (3:1), these data are compatible to our results observed in Figure 27. Only XIRAN®30010P SMA ratio (2.3:1) displayed efficacy on extract MPC2-GFP during small-scale purification and yielding more soluble protein in elution step, confirmed by SDS-PAGE. SMA2000 and DIBMA are potential polymers (OLUWOLE et al., 2017) that were also tested, showing same ability to extract MPC2-GFP not only from total membrane fraction but also isolated mitochondria. A large-scale purification using XIRAN®30010P, resulted in the solubilisation of approximately 70% of total membrane fraction (1 gram). Furthermore, a huge GFP-fluorescence is easily visible in all purification steps, the presence of fluorescence indicates that MPC2 protein maintains the stability after its extraction from membrane(DREW et al., 2005). This condition is probably due to SMA co-polymers can extract proteins from original membrane environment preserving its lipid-protein interaction, these interactions with particular components of membrane stabilise membrane proteins(LEE, 2003). Finally, compared to buffer and polymer, only GFP fluorescence is absorbed at 488nm, this attribute

is used for FSEC analysis of eluted MPC2-GFP sample, which displayed four populations of 539, 308, 134 and 69.5 kDa. In SDS-PAGE, these fractions show bands corresponding to MPC2-GFP and free GFP. Compared to other detergent-based MP extraction methods, SMALPs system offers significant advantages. They are easy to manipulate and reduce the costs by eliminating the use of detergents, ensuring that the local lipid environment around the TP is preserved.

4.3.3. Characterisation of SMALP-MPC2 by Electron microscopy: a probable oligomeric organization

Recent advancement in electron microscopes sensitivity coupled with sophisticated software for transforming the captured images has led to obtain very high-resolution structures of medically important molecules. EM can provide information about different structural states, conformations, or oligomers of MPC2 using a single sample, thanks to RELION(SCHERES, 2012) class average routines. Here, SMA-Purified MPC2-GFP obtained from the first elution peak was imaged in either negative stain or freezing in vitreous ice conditions. First, the analysis of 0.1mg/ml of purified protein under negative stain showed dispersed particles throughout the micrograph. Uranyl acetate stain confers an increased amplitude contrast to visualise nanodisc particles, allowing further image processing in EMAN2 software(TANG et al., 2007). Same protein concentration was used to prepare Cryo-EM grids in presence of Graphene Oxide (GO), which is suitable for grid preparation with lower specimen concentrations and offer partial protection from the air-water interface(PALOVCAK et al., 2018), these grids were used for one day data collection in titan Krios Microscope with volta phase plate that enable near-atomic resolution single particle reconstruction(DANEV; BAUMEISTER, 2016). The analysis of particle classification showed not well-defined classes, probably due to flexible portion corresponding to attached GFP. The purpose of GFP is monitoring expression (in yeast system) and stability (during purification) of MPC2, however due to the possible dimeric conformation of MPC2 (~50kDa), GFP can also contributes to increase particle size being possible its EM visualisation. These distinct classes can also be explained by the possible doublets formation observed in AcrB-SMALPS(POSTIS et al., 2015), doublets are probably responsible for the Analytical ultracentrifugation profile of purified SMA-MPC2, the FSEC profile of SMA-MPC2 solubilisation at high ionic strength and/or the unprecise molecular weight determination of

MPC2 nanodiscs (Data not shown). However, the possible oligomer conformation of MPC2 in native conditions cannot be discarded (Fig. 29B)

4.3.4. TLC a tool for lipid identification in SMALP nanodiscs.

TLC is frequently used to aid in the separation and visualisation of the individual components of a reaction mixture based on their polarity. Here we extracted lipid components from MPC2-SMALPs sample to achieve the lipid composition associated to MPC2. The identification of the lipid membrane composition offers information of membrane proteins stability and activity in "native" environment. Despite the human MPC2 was overexpressed on yeast mitochondrial membrane and, PMA does not distinguish between different functional groups, these results may offer similarity characteristics to the original human mitochondrial source.

CHAPTER 5. CONCLUSION AND PERSPECTIVES

Nearly four decades after the demonstration of the protein-mediated transport of pyruvate across the inner mitochondrial membrane (IMM) (HALESTRAP; DENTON, 1974), two concurrent studies identified the oligomeric complex formed by MPC1 and MPC2 as necessary and sufficient for this task (BRICKER et al., 2012; HERZIG et al., 2012); MPC1 and MPC2 were proposed to function together via the formation of an oligomeric structure of approximately 150 kDa (BRICKER et al., 2012). These original findings inspired many subsequent investigations that have further characterized MPC-dependent pyruvate transport in the cellular context (BENDER; PENA; MARTINOU, 2015; SCHELL et al., 2014; VACANTI et al., 2014), with multiple groups showing that either the loss of MPC1 or MPC2 in mitochondria is sufficient to confer similar loss of function phenotypes (BENDER; PENA; MARTINOU, 2015; COMPAN et al., 2015; LIANG et al., 2015; VANDERPERRE et al., 2015; VIGUEIRA et al., 2014). However, the isolation and reconstitution of MPC1:MPC2 into proteoliposomes is still considered necessary to perform the ultimate proof-of-concept experiment to measure pyruvate transport (HALESTRAP, 2012; MCCOMMIS; FINCK, 2015; VANDERPERRE et al., 2015).

In this context, we report the first successful, large-scale, recombinant production and functional reconstitution of this family of solute carriers in an artificial lipid bilayer. We provide an unprecedented *in vitro* demonstration that human MPC2 functions independently of MPC1 to induce pyruvate transport, possibly as high-order oligomers. Transport activity is independently demonstrated via both the canonical import of radiolabelled substrate and a novel enzymatic assay that quantifies the decrease of extravesicular pyruvate. In cells, the ectopic expression of human MPC2 improved oxygen consumption and stimulated growth under nutrient-depleted conditions compared to yeast cells lacking endogenous MPC. Most importantly, these observations are consistent with those of early and recent publications, suggesting that mitochondrial pyruvate transport by MPC is a rapid and specific process that depends on co-proton import and redox balance and is sensitive to inhibition by a small molecule (COLCA et al., 2013; GRAY; RAUCKHORST; TAYLOR, 2016; HALESTRAP, 1975, 1978). Our findings open a discussion concerning pyruvate import regulation by at least two different molecular entities in human mitochondria: heterotypic MPC1:MPC2 and homotypic MPC2:MPC2. Our work also has immediate implications for the development of small-molecule-oriented therapeutics that specifically target MPC2 in pyruvate-related diseases such as cancer, Alzheimer's disease, and diabetes (DIVAKARUNI et al., 2013; HALESTRAP, 2012; MCCOMMIS; FINCK, 2015; PATTERSON et al., 2014; RAMPELT; LAAN, 2015; VANDERPERRE et al., 2015).

On other hand, according with our results indicating that recombinant human MPC2 displays a variety of oligomerization states, from dimers to large oligomers by chemical crosslinking. More importantly, according SEC-MALLS, the possible disruption of these MPC2 conformation into monomers is due to the detergent micelle's purification by removing protein from their native lipid environment. Therefore, the development of new protocols that stabilise membrane protein in lipid bilayer have allows their study in a nearer "natural" environment. These approaches include Membrane Scaffold Protein (MSP) nanodiscs and styrene maleic acid lipid particles (SMALPs). Here we report preliminary results of MPC2 isolation into membrane mimicking nanodiscs such as MSP-nanodiscs or SMALPs. and their application in single particle electron microscopy (EM) for its structural analysis. The advantages of SMALPs system are well established and described, See (POLLOCK et al., 2018; STROUD; HALL; DAFFORN, 2018). MPC2 was purified in presence of detergent and

then reconstituted into protein scaffold lipid nanodiscs, resulting in an apparent dimer conformation when they were analysed in size exclusion chromatography. Furthermore, MPC2 resulted in soluble self-assembled nanodiscs upon the addition of synthetic co-polymers, SMA200, DIBMA, or the commercial version of SMA (XIRAN®25010P and XIRAN®30010P). Finally, nanodiscs production derived from XIRAN®30010P characterised and visualised under electron microscopy conditions indicate a possible complex formation consisting of four MPC2 copies.

Although GFP serves as an invaluable tool for initial characterization of membrane proteins, it should be removed at some point during purification, prior to new structures studies of MPC2 by crystallization or cryo-EM, for both its relative size to MPC2 and intrinsic flexibility as a fusion tag, may hinder the interpretation of subsequent results; efforts are ongoing in this regard. The isolation of encapsulated MPC2 by non-denaturing electrophoresis should also be considered (POLLOCK et al., 2019).

REFERENCES

BAYBURT, Timothy H.; GRINKOVA, Yelena V.; SLIGAR, Stephen G. Self-Assembly of Discoidal Phospholipid Bilayer Nanoparticles with Membrane Scaffold Proteins. **Nano Letters**, *[S. l.]*, v. 2, n. 8, p. 853–856, 2002. DOI: 10.1021/nl025623k.

BENDER, Tom; PENA, Gabrielle; MARTINOU, Jean-claude. Regulation of mitochondrial pyruvate uptake by alternative pyruvate carrier complexes. *[S. l.]*, p. 1–14, 2015.

BRICKER, Daniel K. et al. A mitochondrial pyruvate carrier required for pyruvate uptake in yeast, Drosophila, and humans. **Science**, *[S. l.]*, v. 337, n. 6090, p. 96–100, 2012. DOI: 10.1126/science.1218099. Disponível em: http://www.ncbi.nlm.nih.gov/pubmed/17741173%5Cnhttp://www.ncbi.nlm.nih.gov/pubmed/22628558%5Cnhttp://www.pubmedcentral.nih.gov/articlerender.fcgi?artid=PMC3690818. Acesso em: 11 jun. 2019.

BROWN, S. W.; OLIVER, S. G.; HARRISON, D. E. F. F.; RIGHELATO, R. C. Ethanol inhibition of yeast growth and fermentation: Differences in the magnitude and complexity of the effect. **European Journal of Applied Microbiology and Biotechnology**, *[S. l.]*, v. 11, n. 3, p. 151–155, 1981. DOI: 10.1007/BF00511253. Disponível em: http://link.springer.com/10.1007/BF00511253. Acesso em: 28 maio. 2020.

CAFFREY, Martin. A comprehensive review of the lipid cubic phase or in meso method for crystallizing membrane and soluble proteins and complexes. **Acta Crystallographica Section F:Structural Biology Communications**, *[S. l.]*, v. 71, n. Pt 1, p. 3–18, 2015. DOI: 10.1107/S2053230X14026843. Disponível em: /pmc/articles/PMC4304740/?report=abstract. Acesso em: 28 ago. 2020.

CARPENTER, Elisabeth P.; BEIS, Konstantinos; CAMERON, Alexander D.; IWATA, So. Overcoming the challenges of membrane protein crystallography. **Current opinion in structural biology**, *[S. l.]*, v. 18, n. 5, p. 581–6, 2008. DOI: 10.1016/j.sbi.2008.07.001. Disponível em: http://www.ncbi.nlm.nih.gov/pubmed/18674618. Acesso em: 11 jul. 2017.

COLCA, Jerry R. et al. Identification of a Mitochondrial Target of Thiazolidinedione Insulin Sensitizers (mTOT)-Relationship to Newly Identified Mitochondrial Pyruvate Carrier

Proteins. **PLoS ONE**, *[S. l.]*, v. 8, n. 5, p. 1–10, 2013. DOI: 10.1371/journal.pone.0061551.

COMPAN, Vincent et al. Monitoring Mitochondrial Pyruvate Carrier Activity in Real Time Using a BRET-Based Biosensor: Investigation of the Warburg Effect. **Molecular Cell**, *[S. l.]*, v. 59, n. 3, p. 491–501, 2015. DOI: 10.1016/j.molcel.2015.06.035. Disponível em: http://linkinghub.elsevier.com/retrieve/pii/S1097276515005298.

DANEV, Radostin; BAUMEISTER, Wolfgang. Cryo-EM single particle analysis with the volta phase plate. **eLife**, *[S. l.]*, v. 5, n. MARCH2016, 2016. DOI: 10.7554/eLife.13046.

DENISOV, I. G.; GRINKOVA, Y. V.; LAZARIDES, A. A.; SLIGAR, S. G. Directed Self-Assembly of Monodisperse Phospholipid Bilayer Nanodiscs with Controlled Size. **Journal of the American Chemical Society**, *[S. l.]*, v. 126, n. 11, p. 3477–3487, 2004. DOI: 10.1021/ja0393574.

DIEKERT, Kerstin; I.P.M. DE KROON, Anton; KISPAL, Gyula; LILL, Roland. Chapter 2 Isolation and subfractionation of mitochondria from the yeast Saccharomyces cerevisiae. *In*: [s.l.] : Academic Press, 2001. v. 65p. 37–51. DOI: 10.1016/S0091-679X(01)65003-9. Disponível em: https://linkinghub.elsevier.com/retrieve/pii/S0091679X01650039. Acesso em: 28 maio. 2020.

DIVAKARUNI, Ajit S. et al. Thiazolidinediones are acute, specific inhibitors of the mitochondrial pyruvate carrier. **Proceedings of the National Academy of Sciences of the United States of America**, *[S. l.]*, v. 110, n. 14, p. 5422–7, 2013. DOI: 10.1073/pnas.1303360110. Disponível em: http://www.pubmedcentral.nih.gov/articlerender.fcgi?artid=3619368&tool=pmcentrez&rendertype=abstract.

DÖRR, Jonas M.; SCHEIDELAAR, Stefan; KOORENGEVEL, Martijn C.; DOMINGUEZ, Juan J.; SCHÄFER, Marre; VAN WALREE, Cornelis A.; KILLIAN, J. Antoinette. **The styrene–maleic acid copolymer: a versatile tool in membrane researchEuropean Biophysics Journal**Springer Verlag, , 2016. DOI: 10.1007/s00249-015-1093-y.

DREW, David et al. A scalable, GFP-based pipeline for membrane protein overexpression screening and purification. **Protein science : a publication of the Protein Society**, *[S. l.]*, v. 14, n. 8, p. 2011–2017, 2005. DOI: 10.1110/ps.051466205. Disponível em: http://eutils.ncbi.nlm.nih.gov/entrez/eutils/elink.fcgi?

dbfrom=pubmed&id=15987891&retmode=ref&cmd=prlinks.

DREW, David; NEWSTEAD, Simon; SONODA, Yo; KIM, Hyun; HEIJNE, Gunnar Von. NIH Public Access. *[S. l.]*, v. 3, n. 5, p. 784–798, 2009. DOI: 10.1038/nprot.2008.44.GFP-based.

FENG, Liang; FROMMER, Wolf B. **Structure and function of SemiSWEET and SWEET sugar transportersTrends in Biochemical Sciences**Elsevier Ltd, , 2015. DOI: 10.1016/j.tibs.2015.05.005.

FERNANDES, L.; CÔRTE-REAL, M.; LOUREIRO, V.; LOUREIRO-DIAS, M. C.; LEÃO, C. Glucose respiration and fermentation in Zygosaccharomyces bailii and Saccharomyces cerevisiae express different sensitivity patterns to ethanol and acetic acid. **Letters in applied microbiology**, *[S. l.]*, v. 25, n. 4, p. 249–253, 1997. DOI: 10.1046/j.1472-765X.1997.00214.x.

FINN, Robert D. et al. Pfam: the protein families database. **Nucleic Acids Research**, *[S. l.]*, v. 42, n. D1, p. D222–D230, 2014. DOI: 10.1093/nar/gkt1223. Disponível em: https://doi.org/10.1093/nar/gkt1223. Acesso em: 31 mar. 2020.

FLOYD, Brendan J. et al. Mitochondrial Protein Interaction Mapping Identifies Regulators of Respiratory Chain Function. **Molecular Cell**, *[S. l.]*, v. 63, n. 4, p. 621–632, 2016. DOI: 10.1016/j.molcel.2016.06.033.

GRAY, Lawrence R.; RAUCKHORST, Adam J.; TAYLOR, Eric B. A method for multiplexed measurement of mitochondrial pyruvate carrier activity. **Journal of Biological Chemistry**, *[S. l.]*, v. 291, n. 14, p. 7409–7417, 2016. DOI: 10.1074/jbc.M115.711663. Disponível em: http://www.jbc.org/cgi/content/long/M115.711663v1. Acesso em: 8 jun. 2016.

HALESTRAP, A. P. The mechanism of the inhibition of the mitochondrial pyruvate transporter by α cyanocinnamate derivatives. **Biochemical Journal**, *[S. l.]*, v. 156, n. 1, p. 181–183, 1976. DOI: 10.1042/bj1560181.

HALESTRAP, A. P.; DENTON, R. M. Specific inhibition of pyruvate transport in rat liver mitochondria and human erythrocytes by alpha-cyano-4-hydroxycinnamate. **The Biochemical journal**, *[S. l.]*, v. 138, n. 2, p. 313–316, 1974. DOI: 10.1042/bj1380313.

HALESTRAP, A.; P. The mitochondrial pyruvate carrier. Kinetics and specificity for substrates and inhibitors. **The Biochemical journal**, *[S. l.]*, v. 148, n. 1, p. 85–96, 1975.

HALESTRAP, Andrew P. The mitochondrial pyruvate carrier. Kinetics and specificity for substrates and inhibitors. **Biochemical Journal**, *[S. l.]*, v. 148, n. 1, p. 85–96, 1975. DOI: 10.1042/bj1480085. Disponível em: https://www.ncbi.nlm.nih.gov/pmc/articles/PMC1165509/pdf/biochemj00558-0098.pdf. Acesso em: 11 jun. 2019.

HALESTRAP, Andrew P. Pyruvate and Ketone-Body Transport across the Mitochondrial Membrane. *[S. l.]*, v. 172, p. 377–387, 1978.

HALESTRAP, Andrew P. The mitochondrial pyruvate carrier: Has it been unearthed at last? **Cell Metabolism**, *[S. l.]*, v. 16, n. 2, p. 141–143, 2012. DOI: 10.1016/j.cmet.2012.07.013.

HERZIG, Sébastien; RAEMY, Etienne; MONTESSUIT, Sylvie; VEUTHEY, J. L. Jean-Luc J. L.; ZAMBONI, Nicola; WESTERMANN, Benedikt; KUNJI, Edmund R. S.; MARTINOU, Jean-Claude J. C. Jean-Claude. Identification and Functional Expression of the Mitochondrial Pyruvate Carrier. **Science**, *[S. l.]*, v. 337, n. 6090, p. 93–96, 2012. DOI: 10.1126/science.1218530. Disponível em: http://www.sciencemag.org/cgi/doi/10.1126/science.1218530.

HILDYARD, John C. W.; ÄMMÄLÄ, Carina; DUKES, Iain D.; THOMSON, Stephen a.; HALESTRAP, Andrew P. Identification and characterisation of a new class of highly specific and potent inhibitors of the mitochondrial pyruvate carrier. **Biochimica et Biophysica Acta - Bioenergetics**, *[S. l.]*, v. 1707, n. 2–3, p. 221–230, 2005. DOI: 10.1016/j.bbabio.2004.12.005.

HORNBECK, Peter V; ZHANG, Bin; MURRAY, Beth; KORNHAUSER, Jon M.; LATHAM, Vaughan; SKRZYPEK, Elzbieta. PhosphoSitePlus, 2014: mutations, PTMs and recalibrations. **Nucleic Acids Research**, *[S. l.]*, v. 43, 2015. DOI: 10.1093/nar/gku1267. Disponível em: http://www.proteinatlas.org/. Acesso em: 28 maio. 2020.

HUTTLIN, Edward L. et al. The BioPlex Network: A Systematic Exploration of the Human Interactome. **Cell**, *[S. l.]*, v. 162, n. 2, p. 425–440, 2015. DOI: 10.1016/j.cell.2015.06.043.

INAGAKI, Sayaka; GHIRLANDO, Rodolfo; GRISSHAMMER, Reinhard. Biophysical Characterization of Membrane Proteins in Nanodiscs. **Methods**, *[S. l.]*, v. 59, n. 3, p. 287–

300, 2013. DOI: 10.1016/j.ymeth.2012.11.006. Disponível em: https://www.ncbi.nlm.nih.gov/pmc/articles/PMC3608844/pdf/nihms426987.pdf. Acesso em: 1 jul. 2019.

ISLAM, Salim T.; ECKFORD, Paul D. W.; JONES, Michelle L.; NUGENT, Timothy; BEAR, Christine E.; VOGEL, Christian; LAM, Joseph S. Proton-dependent gating and proton uptake by Wzx support o-antigen-subunit Antiport across the bacterial inner membrane. **mBio**, *[S. l.]*, v. 4, n. 5, 2013. DOI: 10.1128/mBio.00678-13.

JEŹÉGOU, Adrien et al. Heptahelical protein PQLC2 is a lysosomal cationic amino acid exporter underlying the action of cysteamine in cystinosis therapy. **Proceedings of the National Academy of Sciences of the United States of America**, *[S. l.]*, v. 109, n. 50, p. E3434–E3443, 2012. DOI: 10.1073/pnas.1211198109. Disponível em: www.pnas.org/cgi/doi/10.1073/pnas.1211198109. Acesso em: 17 ago. 2020.

KNOWLES, Timothy J.; FINKA, Rachael; SMITH, Corinne; LIN, Yu-Pin; DAFFORN, Tim; OVERDUIN, Michael. Membrane Proteins Solubilized Intact in Lipid Containing Nanoparticles Bounded by Styrene Maleic Acid Copolymer. **Journal of the American Chemical Society**, *[S. l.]*, v. 131, n. 22, p. 7484–7485, 2009. DOI: 10.1021/ja810046q. Disponível em: https://pubs.acs.org/doi/10.1021/ja810046q. Acesso em: 17 nov. 2019.

KREBS, Hans Adolf; JOHNSON, William Arthur. Acetopyruvic acid (αγ-diketovaleric acid) as an intermediate metabolite in animal tissues. **Biochemical Journal**, *[S. l.]*, v. 31, n. 5, p. 772–779, 1937. DOI: 10.1042/bj0310772. Disponível em: https://www.ncbi.nlm.nih.gov/pmc/articles/PMC1267003/. Acesso em: 13 ago. 2020.

LEE, A. .. Lipid–protein interactions in biological membranes: a structural perspective. **Biochimica et Biophysica Acta (BBA) - Biomembranes**, *[S. l.]*, v. 1612, n. 1, p. 1–40, 2003. DOI: 10.1016/S0005-2736(03)00056-7. Disponível em: https://linkinghub.elsevier.com/retrieve/pii/S0005273603000567. Acesso em: 12 maio. 2020.

LIANG, Lei; LI, Qingguo; HUANG, Liyong; LI, Dawei; LI, Xinxiang. Sirt3 binds to and deacetylates mitochondrial pyruvate carrier 1 to enhance its activity. **Biochemical and Biophysical Research Communications**, *[S. l.]*, v. 468, n. 4, p. 807–812, 2015. DOI: 10.1016/j.bbrc.2015.11.036.

LIVAK, K. J.; SCHMITTGEN, T. D. Analysis of relative gene expression data using real-

time quantitative PCR and. **Methods**, *[S. l.]*, v. 25, p. 402–408, 2001. DOI: 10.1006/meth.2001.1262.

LUNDBY, Alicia et al. Proteomic Analysis of Lysine Acetylation Sites in Rat Tissues Reveals Organ Specificity and Subcellular Patterns. **Cell Reports**, *[S. l.]*, v. 2, n. 2, p. 419–431, 2012. DOI: 10.1016/j.celrep.2012.07.006.

MCCOMMIS, Kyle S.; FINCK, Brian N. Mitochondrial pyruvate transport: a historical perspective and future research directions. **The Biochemical journal**, *[S. l.]*, v. 466, n. 3, p. 443–454, 2015. DOI: doi:10.1042/BJ20141171. Disponível em: http://eutils.ncbi.nlm.nih.gov/entrez/eutils/elink.fcgi?dbfrom=pubmed&id=25748677&retmode=ref&cmd=prlinks%5Cnpapers2://publication/doi/10.1042/BJ20141171.

MEDRANO-SOTO, Arturo; GHAZI, Faezeh; HENDARGO, Kevin J.; MORENO-HAGELSIEB, Gabriel; MYERS, Scott; SAIER, Milton H. Expansion of the transporter-opsin-G protein-coupled receptor superfamily with five new protein families. **PLoS ONE**, *[S. l.]*, v. 15, n. 4, p. e0231085, 2020. DOI: 10.1371/journal.pone.0231085. Disponível em: https://doi.org/10.1371/journal.pone.0231085.t001. Acesso em: 17 ago. 2020.

MILLER, C. A.; MARTINAT, M. A.; HYMAN, L. E. Assessment of aryl hydrocarbon receptor complex interactions using pBEVY plasmids: expressionvectors with bi-directional promoters for use in Saccharomyces cerevisiae. **Nucleic acids research**, *[S. l.]*, v. 26, n. 15, p. 3577–83, 1998. DOI: 10.1093/nar/26.15.3577.

MITRA, Nivedita. Nanodiscs: Membrane Protein Research in Near-Native Conditions. **Materials and Methods**, *[S. l.]*, v. 3, 2013. DOI: 10.13070/mm.en.3.177.

MORRISON, Kerrie ;. et al. Membrane protein extraction and purification using styrene-maleic acid (SMA) copolymer: effect of variations in polymer structure. **Biochemical Journal**, *[S. l.]*, v. 473, n. 23, p. 4349–4360, [s.d.]. DOI: 10.1042/BCJ20160723. Disponível em: https://research.birmingham.ac.uk/portal/files/37050698/Morrison_et_al_Membrane_Protein_Extraction_Biochemical_Journal.pdf. Acesso em: 31 jul. 2019.

NAGAMPALLI, Raghavendra Sashi Krishna et al. Human mitochondrial pyruvate carrier 2 as an autonomous membrane transporter. **Scientific Reports**, *[S. l.]*, v. 8, n. 1, p. 3510, 2018.

DOI: 10.1038/s41598-018-21740-z. Disponível em: http://www.nature.com/articles/s41598-018-21740-z. Acesso em: 17 jul. 2019.

NAŁECZ, M. J. et al. Extraction, partial purification and functional reconstitution of two mitochondrial carriers transporting keto acids: 2-oxoglutarate and pyruvate. **FEBS Letters**, *[S. l.]*, v. 196, n. 2, p. 331–336, 1986. DOI: 10.1016/0014-5793(86)80273-3.

NEWSTEAD, Simon; KIM, Hyun; VON HEIJNE, Gunnar; IWATA, So; DREW, David. High-throughput fluorescent-based optimization of eukaryotic membrane protein overexpression and purification in Saccharomyces cerevisiae. **Proceedings of the National Academy of Sciences of the United States of America**, *[S. l.]*, v. 104, n. 35, p. 13936–13941, 2007. DOI: 10.1073/pnas.0704546104.

OLUWOLE, Abraham Olusegun; DANIELCZAK, Bartholomäus; MEISTER, Annette; BABALOLA, Jonathan Oyebamiji; VARGAS, Carolyn; KELLER, Sandro. Solubilization of Membrane Proteins into Functional Lipid-Bilayer Nanodiscs Using a Diisobutylene/Maleic Acid Copolymer. **Angewandte Chemie International Edition**, *[S. l.]*, v. 56, n. 7, p. 1919–1924, 2017. DOI: 10.1002/anie.201610778. Disponível em: http://www.ncbi.nlm.nih.gov/pubmed/28079955. Acesso em: 16 jul. 2019.

PALMIERI, Ferdinando. The mitochondrial transporter family SLC25: Identification, properties and physiopathology. **Molecular Aspects of Medicine**, *[S. l.]*, v. 34, n. 2–3, p. 465–484, 2013. DOI: 10.1016/j.mam.2012.05.005. Disponível em: https://linkinghub.elsevier.com/retrieve/pii/S0098299712000519.

PALOVCAK, Eugene; WANG, Feng; ZHENG, Shawn Q.; YU, Zanlin; LI, Sam; BETEGON, Miguel; BULKLEY, David; AGARD, David A.; CHENG, Yifan. A simple and robust procedure for preparing graphene-oxide cryo-EM grids. **Journal of Structural Biology**, *[S. l.]*, v. 204, n. 1, p. 80–84, 2018. DOI: 10.1016/j.jsb.2018.07.007. Disponível em: https://linkinghub.elsevier.com/retrieve/pii/S1047847718301655. Acesso em: 31 jul. 2019.

PATTERSON, Jessica N.; COUSTEILS, Katelyn; LOU, Jennifer W.; FOX, Jocelyn E. Manning; MACDONALD, Patrick E.; JOSEPH, Jamie W. Mitochondrial metabolism of pyruvate is essential for regulating glucose-stimulated insulin secretion. **Journal of Biological Chemistry**, *[S. l.]*, v. 289, n. 19, p. 13335–13346, 2014. DOI: 10.1074/jbc.M113.521666.

PEBAY-PEYROULA, Eva; DAHOUT-GONZALEZ, Cécile; KAHN, Richard; TRÉZÉGUET, Véronique; LAUQUIN, Guy J. M. J. M.; BRANDOLIN, Gérard. Structure of mitochondrial ADP/ATP carrier in complex with carboxyatractyloside. **Nature**, *[S. l.]*, v. 426, n. 6962, p. 39–44, 2003. DOI: 10.1038/nature02056.

POLLOCK, Naomi L. et al. SMA-PAGE: A new method to examine complexes of membrane proteins using SMALP nano-encapsulation and native gel electrophoresis. **Biochimica et Biophysica Acta (BBA) - Biomembranes**, *[S. l.]*, v. 1861, n. 8, p. 1437–1445, 2019. DOI: 10.1016/J.BBAMEM.2019.05.011. Disponível em: https://www.sciencedirect.com/science/article/pii/S0005273619301087?via%3Dihub. Acesso em: 13 jul. 2019.

POLLOCK, Naomi L.; LEE, Sarah C.; PATEL, Jaimin H.; GULAMHUSSEIN, Aiman A.; ROTHNIE, Alice J. **Structure and function of membrane proteins encapsulated in a polymer-bound lipid bilayerBiochimica et Biophysica Acta - Biomembranes**Elsevier B.V., , 2018. DOI: 10.1016/j.bbamem.2017.08.012.

POSTIS, Vincent; RAWSON, Shaun; MITCHELL, Jennifer K.; LEE, Sarah C.; PARSLOW, Rosemary A.; DAFFORN, Tim R.; BALDWIN, Stephen A.; MUENCH, Stephen P. The use of SMALPs as a novel membrane protein scaffold for structure study by negative stain electron microscopy. **Biochimica et biophysica acta**, *[S. l.]*, v. 1848, n. 2, p. 496–501, 2015. DOI: 10.1016/j.bbamem.2014.10.018. Disponível em: http://www.ncbi.nlm.nih.gov/pubmed/25450810. Acesso em: 16 jul. 2019.

PUNJANI, Ali; RUBINSTEIN, John L.; FLEET, David J.; BRUBAKER, Marcus A. CryoSPARC: Algorithms for rapid unsupervised cryo-EM structure determination. **Nature Methods**, *[S. l.]*, v. 14, n. 3, p. 290–296, 2017. DOI: 10.1038/nmeth.4169.

RAMPELT, Heike; LAAN, Martin Van Der. Metabolic remodeling: a pyruvate transport affair. *[S. l.]*, p. 1–3, 2015.

SCHELL, John C. C. et al. A Role for the Mitochondrial Pyruvate Carrier as a Repressor of the Warburg Effect and Colon Cancer Cell Growth. **Molecular Cell**, *[S. l.]*, v. 56, n. 3, p. 1–14, 2014. DOI: 10.1016/j.molcel.2014.09.026. Disponível em: http://dx.doi.org/10.1016/j.molcel.2014.09.026.

SCHERES, Sjors H. W. RELION: Implementation of a Bayesian approach to cryo-EM

structure determination. **Journal of Structural Biology**, *[S. l.]*, v. 180, n. 3, p. 519–530, 2012. DOI: 10.1016/j.jsb.2012.09.006.

SEDDON, Annela M.; CURNOW, Paul; BOOTH, Paula J. Membrane proteins, lipids and detergents: Not just a soap opera. **Biochimica et Biophysica Acta - Biomembranes**, *[S. l.]*, v. 1666, n. 1–2, p. 105–117, 2004. DOI: 10.1016/j.bbamem.2004.04.011. Disponível em: https://www.sciencedirect.com/science/article/pii/S0005273604001610?via%3Dihub. Acesso em: 8 jul. 2017.

SHEVCHENKO, Andrej; WILM, Matthias; VORM, Ole; MANN, Matthias. Mass spectrometric sequencing of proteins from silver-stained polyacrylamide gels. **Analytical Chemistry**, *[S. l.]*, v. 68, n. 5, p. 850–858, 1996. DOI: 10.1021/ac950914h.

STROUD, Zoe; HALL, Stephen C. L.; DAFFORN, Tim R. **Purification of membrane proteins free from conventional detergents: SMA, new polymers, new opportunities and new insightsMethods**Academic Press Inc., , 2018. DOI: 10.1016/j.ymeth.2018.03.011.

SWAINSBURY, David J. K.; SCHEIDELAAR, Stefan; VAN GRONDELLE, Rienk; KILLIAN, J. Antoinette; JONES, Michael R. Bacterial reaction centers purified with styrene maleic acid copolymer retain native membrane functional properties and display enhanced stability. **Angewandte Chemie - International Edition**, *[S. l.]*, v. 53, n. 44, p. 11803–11807, 2014. DOI: 10.1002/anie.201406412. Disponível em: http://www.ncbi.nlm.nih.gov/pubmed/25212490. Acesso em: 5 maio. 2020.

TAKEDA, Kojiro; STARZYNSKI, Caroline; MORI, Ayaka; YANAGIDA, Mitsuhiro. The critical glucose concentration for respiration-independent proliferation of fission yeast, Schizosaccharomyces pombe. **Mitochondrion**, *[S. l.]*, v. 22, p. 91–95, 2015. DOI: 10.1016/j.mito.2015.04.003.

TANG, Guang; PENG, Liwei; BALDWIN, Philip R.; MANN, Deepinder S.; JIANG, Wen; REES, Ian; LUDTKE, Steven J. EMAN2: An extensible image processing suite for electron microscopy. **Journal of Structural Biology**, *[S. l.]*, v. 157, n. 1, p. 38–46, 2007. DOI: 10.1016/j.jsb.2006.05.009.

TAVOULARI, Sotiria; THANGARATNARAJAH, Chancievan; MAVRIDOU, Vasiliki; HARBOUR, Michael E.; MARTINOU, Jean-Claude Jean-Claude; KUNJI, Edmund Rs. The yeast mitochondrial pyruvate carrier is a hetero-dimer in its functional state. **The EMBO**

Journal, *[S. l.]*, v. 38, n. 10, 2019. DOI: 10.15252/embj.2018100785. Disponível em: http://www.ncbi.nlm.nih.gov/pubmed/30979775. Acesso em: 2 jun. 2019.

TIMOŃ-GÓMEZ, Alba; PROFT, Markus; PASCUAL-AHUIR, Amparo. Differential regulation of mitochondrial pyruvate carrier genes modulates respiratory capacity and stress tolerance in yeast. **PLoS ONE**, *[S. l.]*, v. 8, n. 11, p. 1–9, 2013. DOI: 10.1371/journal.pone.0079405.

VACANTI, Nathaniel M. M.; DIVAKARUNI, Ajit S. S.; GREEN, Courtney R. R.; PARKER, Seth J. J.; HENRY, Robert R. R.; CIARALDI, Theodore P. P.; MURPHY, Anne N. N.; METALLO, Christian M. M. Regulation of Substrate Utilization by the Mitochondrial Pyruvate Carrier. **Molecular Cell**, *[S. l.]*, v. 56, n. 3, p. 425–435, 2014. DOI: 10.1016/j.molcel.2014.09.024. Disponível em: http://dx.doi.org/10.1016/j.molcel.2014.09.024.

VADVALKAR, Shraddha S.; MATSUZAKI, Satoshi; EYSTER, Craig A.; GIORGIONE, Jennifer R.; BOCKUS, Lee B.; KINTER, Caroline S.; KINTER, Michael; KENNETH, X.; HUMPHRIES, M. Decreased Mitochondrial Pyruvate Transport Activity in the Diabetic Heart ROLE OF MITOCHONDRIAL PYRUVATE CARRIER 2 (MPC2) ACETYLATION *. **NUMBER 11 JOURNAL OF BIOLOGICAL CHEMISTRY**, *[S. l.]*, v. 292, n. 11, p. 4423–4433, 2017. DOI: 10.1074/jbc.M116.753509. Disponível em: https://www.ncbi.nlm.nih.gov/pmc/articles/PMC5377762/pdf/zbc4423.pdf. Acesso em: 7 jun. 2019.

VANDERPERRE, Beno??t; CERMAKOVA, Kristina; ESCOFFIER, Jessica; KABA, Mayis; BENDER, Tom; NEF, Serge; MARTINOU, Jean Claude. MPC1-like is a placental mammal-specific mitochondrial pyruvate carrier subunit expressed in postmeiotic male germ cells. **Journal of Biological Chemistry**, *[S. l.]*, v. 291, n. 32, p. 16448–16461, 2016. a. DOI: 10.1074/jbc.M116.733840.

VANDERPERRE, Benoît; BENDER, Tom; KUNJI, Edmund Rs S.; MARTINOU, Jean-Claude Claude. Mitochondrial pyruvate import and its effects on homeostasis. **Current Opinion in Cell Biology**, *[S. l.]*, v. 33, p. 35–41, 2015. DOI: 10.1016/j.ceb.2014.10.008. Disponível em: https://linkinghub.elsevier.com/retrieve/pii/S0955067414001306. Acesso em: 4 jul. 2019.

VANDERPERRE, Benoît; HERZIG, Sébastien; KRZNAR, Petra; HÖRL, Manuel; AMMAR, Zeinab; MONTESSUIT, Sylvie; PIERREDON, Sandra; ZAMBONI, Nicola; MARTINOU, Jean-Claude. Embryonic Lethality of Mitochondrial Pyruvate Carrier 1 Deficient Mouse Can Be Rescued by a Ketogenic Diet. **PLOS Genetics**, *[S. l.]*, v. 12, n. 5, p. e1006056, 2016. b. DOI: 10.1371/journal.pgen.1006056. Disponível em: https://dx.plos.org/10.1371/journal.pgen.1006056. Acesso em: 28 maio. 2020.

VIGUEIRA, Patrick A. A. et al. Mitochondrial Pyruvate Carrier 2 Hypomorphism in Mice Leads to Defects in Glucose-Stimulated Insulin Secretion. **Cell Reports**, *[S. l.]*, v. 7, n. 6, p. 2042–2053, 2014. DOI: 10.1016/j.celrep.2014.05.017. Disponível em: https://www.sciencedirect.com/science/article/pii/S2211124714003921. Acesso em: 4 jul. 2019.

WHITE, Carl; NIXON, Alex; BRADBURY, Neil A. Determining membrane protein topology using fluorescence protease protection (FPP). **Journal of Visualized Experiments**, *[S. l.]*, v. 2015, n. 98, p. e52509, 2015. DOI: 10.3791/52509.

XU, Yan; TAO, Yuyong; CHEUNG, Lily S.; FAN, Chao; CHEN, Li-Qing; XU, Sophia; PERRY, Kay; FROMMER, Wolf B.; FENG, Liang. Structures of bacterial homologues of SWEET transporters in two distinct conformations. **Nature**, *[S. l.]*, v. 515, n. 7527, p. 448–452, 2014. DOI: 10.1038/nature13670. Disponível em: http://www.nature.com/doifinder/10.1038/nature13670.

YONEDA, Juliana Sakamoto; RIGOS, Carolina Fortes; DE LOURENÇO, Thais Fernanda Aranda Thaís Fernanda Aranda; SEBINELLI, Heitor Gobbi; CIANCAGLINI, Pietro. Na,K-ATPase reconstituted in ternary liposome: The presence of cholesterol affects protein activity and thermal stability. **Archives of Biochemistry and Biophysics**, *[S. l.]*, v. 564, p. 136–141, 2014. DOI: 10.1016/j.abb.2014.09.015.

ZANGARI, Joséphine; PETRELLI, Francesco; MAILLOT, Benoît; MARTINOU, Jean-Claude. The Multifaceted Pyruvate Metabolism: Role of the Mitochondrial Pyruvate Carrier. **Biomolecules**, *[S. l.]*, v. 10, n. 7, p. 1068, 2020. DOI: 10.3390/biom10071068.

ZHENG, Shawn Q.; PALOVCAK, Eugene; ARMACHE, Jean Paul; VERBA, Kliment A.; CHENG, Yifan; AGARD, David A. **MotionCor2: Anisotropic correction of beam-induced motion for improved cryo-electron microscopyNature Methods**Nature Publishing Group, ,

2017. DOI: 10.1038/nmeth.4193. Disponível em: https://www.nature.com/articles/nmeth.4193. Acesso em: 21 jul. 2020.

APPENDIX 1

This thesis contains text and figures adapted from the original article “Human mitochondrial pyruvate carrier 2 as an autonomous membrane transporter”, which I am co-author. The work was published in Scientific Reports, under DOI: https://doi.org/10.1038/s41598-018-21740-z and is licensed under The Creative Commons Attribution 4.0 International License (https://creativecommons.org/licenses/by/4.0/), which allows sharing and adaptation of its contents when properly cited within this thesis.

SPRINGER NATURE

Human mitochondrial pyruvate carrier 2 as an autonomous membrane transporter

Author: Raghavendra Sashi Krishna Nagampalli et al
Publication: Scientific Reports
Publisher: Springer Nature
Date: Feb 22, 2018

Copyright © 2018, Springer Nature

Creative Commons

This is an open access article distributed under the terms of the Creative Commons CC BY license, which permits unrestricted use, distribution, and reproduction in any medium, provided the original work is properly cited.

You are not required to obtain permission to reuse this article.
To request permission for a type of use not listed, please contact Springer Nature

Rights and permissions

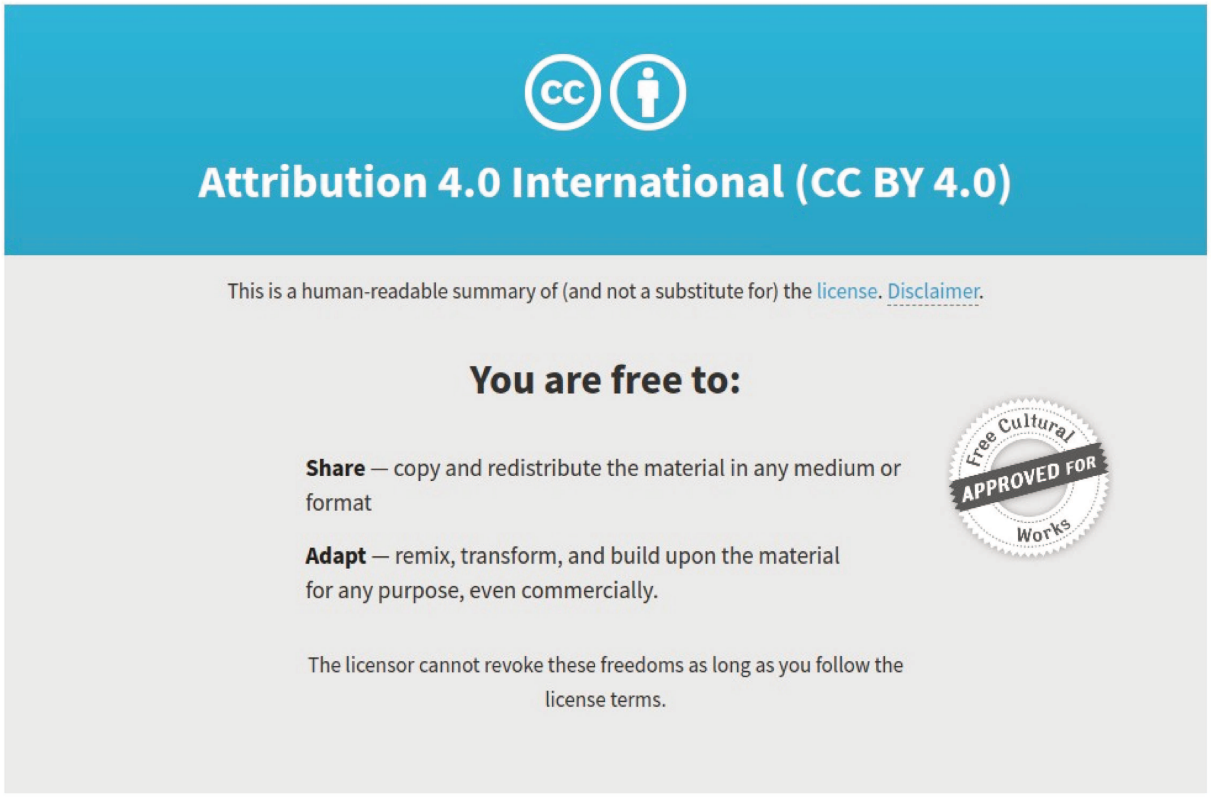

Anexo I

COORDENADORIA DE PÓS-GRADUAÇÃO
INSTITUTO DE BIOLOGIA
Universidade Estadual de Campinas
Caixa Postal 6109. 13083-970, Campinas, SP, Brasil
Fone (19) 3521-6378. email: cpgib@unicamp.br

DECLARAÇÃO

Em observância ao **§5º do Artigo 1º da Informação CCPG-UNICAMP/001/15**, referente a Bioética e Biossegurança, declaro que o conteúdo de minha Tese de Doutorado, intitulada " ***PRODUÇÃO HETERÓLOGA, PURIFICAÇÃO, CARACTERIZAÇÃO FUNCIONAL E PREDIÇÃO ESTRUTURAL DO CARREADOR MITOCONDRIAL DE PIRUVATO HUMANO.*** ", desenvolvida no Programa de Pós-Graduação em Biociências e Tecnologia de Produtos Bioativos do Instituto de Biologia da Unicamp, não versa sobre pesquisa envolvendo seres humanos, animais ou temas afetos a Biossegurança.

Assinatura: _____

Nome do(a) aluno(a): José Edwin Neciosup Quesñay

Assinatura: _____

Nome do(a) orientador(a): Andre Luis Berteli Ambrosio

Data: 5 de Janeiro de 2021

Anexo II

Declaração

As cópias de artigos de minha autoria ou de minha co-autoria, já publicados ou submetidos para publicação em revistas científicas ou anais de congressos sujeitos a arbitragem, que constam da minha Dissertação/Tese de Mestrado/Doutorado, intitulada ***PRODUÇÃO HETERÓLOGA, PURIFICAÇÃO, CARACTERIZAÇÃO FUNCIONAL E PREDIÇÃO ESTRUTURAL DO CARREADOR MITOCONDRIAL DE PIRUVATO HUMANO.*** , não infringem os dispositivos da Lei n.° 9.610/98, nem o direito autoral de qualquer editora.

Campinas, 5 de Janeiro de 2021

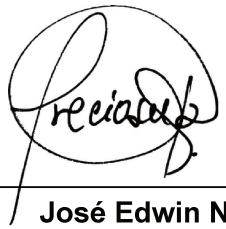

Assinatura : _____

Nome do(a) autor(a): **José Edwin Neciosup Quesñay**

RG n.° G018178-7

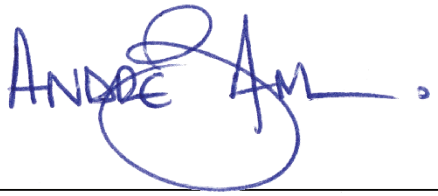

Assinatura : _____

Nome do(a) orientador(a): **Andre Luis Berteli Ambrosio**

RG n.° 23.340.996-8